The *In Vitro* Pharmacological Evaluation of Tetrahydrocannabivarin (THCV) for Intestinal Inflammatory Conditions

A Thesis Submitted to the
College of Graduate Studies and Postdoctoral Studies
in Partial Fulfillment of the Requirements
For the Degree of Master of Science
In the Department of Toxicology
University of Saskatchewan
Saskatoon

By
Jiayi He

PERMISSION TO USE

In presenting this thesis in partial fulfillment of the requirements for a degree of Master of Science from the University of Saskatchewan, I agree that the University Libraries can make it freely available for inspection. I further agree that permission for copying of this thesis in any manner, in whole or in part, for scholarly purposes may be granted by the professors who supervised my thesis work or, in their absence, by the Dean of the College in which my thesis work was done. It is understood that any copying or publication or use of this thesis or parts for any financial gain shall not be allowed without my written permission. It is also understood that due recognition shall be given to me and to the University of Saskatchewan in any scholarly use which may be made of any material in my thesis.

Requests for permission to copy or to make other uses of materials in this thesis in whole or part should be addressed to:

Dean of the College of Pharmacy and Nutrition
110 Science Place
University of Saskatchewan
Saskatoon, Saskatchewan, S7N 5C9
Canada

OR

Dean of the College of Graduate Studies and Research
107 Administration Place
University of Saskatchewan
Saskatoon, Saskatchewan, S7N 5A2
Canada

ABSTRACT

The recreational and medicinal use of *Cannabis* for certain human pathologies has received tremendous attention in recent years. Numerous pre-clinical and clinical findings on the benefits of cannabinoids, the naturally occurring constituents in *Cannabis*, against epilepsy, neuropathic pain, and gastrointestinal (GI) syndromes have allowed many governmental and research sectors to further investigate their therapeutic potential and adverse effects. Currently, several extensively researched cannabinoids such as tetrahydrocannabinol (THC) and cannabidiol (CBD) have shown to possess therapeutic and pharmacological effects in aiding the treatment of various medical conditions. However, due to a desire to enhance our increasing understanding of the physiochemical and pharmacokinetic (PK) characteristics of THC and CBD, research on certain cannabinoids such as tetrahydrocannabivarin (THCV) has not always been the primary focus. Studies on THCV indicated anti-inflammatory effects in *in vitro* cell lines and *in vivo* animal models which compelled us to assess the PK characteristics of THCV. In addition to its PK characteristics, our aim was to evaluate the effects of THCV on how it may affect inflammatory conditions of the GI tract such as inflammatory bowel disease (IBD).

We first investigated THCV's intestinal permeation profile and directly assessed its effects on intestinal barrier integrity with an *in vitro* Transwell system coupled with human epithelial derived cell line comprised of colorectal adenocarcinoma cells (Caco-2). We then examined its interaction with different plasma proteins in human plasma through its relative bound fraction and the unbound fraction in the blood ($f_{u(b)}$) by adopting the 3-solvent extraction plasma protein binding technique. Enzyme kinetic analysis was conducted to better understand the contribution of liver to the first-pass metabolism and systemic clearance of THCV using human liver microsomes (HLM). Its *in vitro* intrinsic clearance ($Cl_{int,u}$) was calculated using the substrate depletion approach and was ranked as to whether it was a low, intermediate or high clearance drug. As a secondary aim, we established a 3-D intestinal organoid (IO) model derived from human inducible pluripotent stem cells (iPSCs) for the preliminary screening of THCV putative anti-inflammatory effects. Collectively, THCV demonstrated limited permeation in the Transwell system with a high degree of non-specific binding to plasticware, relatively higher unbound fraction ($f_{u(b)}$) compared to the literature, and classified as a high clearance drug

indicated by its $Cl_{int,u}$ value. Further, THCV showed promising anti-inflammatory effects by upregulating an anti-inflammatory cytokine in the IO system.

These studies revealed key PK parameters of THCV that is currently unavailable in the literature while the new IO system was capable of upregulating key pro-inflammatory responses upon lipopolysaccharide (LPS) stimulation, which may bridge the gap between traditional *in vitro* cell culture and *in vivo* animal models.

ACKNOWLEDGEMENTS

During my three years of graduate study at the University of Saskatchewan, I learned and benefited greatly from my supervisors, committee members, my colleagues and friends. I would like to sincerely thank my supervisors Dr. Jane Alcorn and Dr. Darrell Mousseau for their academic guidance, generous support, kind understanding and trust for recruiting me to conduct this MSc project. I'm extremely grateful for Dr. Alcorn's guidance during my experimental phases and writing process; her feedback and comments, encouragement and patient support made me become an effective researcher and writer. I am also greatly thankful for Dr. Mousseau's guidance during my research and writing process; his feedback on what to do and think differently and his openness for me to carry out my last panel of experiments in his lab allowed me to become an independent researcher. I would like to thank my committee members, Dr. Lynn Weber and Dr. Robert Laprairie for their helpful suggestions in my research and expertise in each of their graduate courses. I also want to thank my external reader, Dr. Ahmad Al-Dissi in the Department of Veterinary Pathology, WCVM, for his valuable time and comments in my thesis and defense.

I would like to express my utmost gratitude to Deborah Michel and Stephanie Vuong for their help on the mass spectrometry during my research. I also want to thank my colleagues: Dr. Tyler Wenzel, Frank De Silva, Jennifer Le, Alex Cullen for their assistance on my experimental work.

Special thanks are given to my parents and my sister for their encouragement, love and support during my master program. Lastly, I'm sincerely grateful of all my friends for their assistance during my stay in Saskatoon, Canada.

Thanks to the Dr. C.Sisodia graduate scholarship and the Zigurds & Hildegarde Lejins Fund at the University of Saskatchewan for providing the financial support.

TABLE OF CONTENTS

PERMISSION TO USE i

ABSTRACT iii

ACKNOWLEDGEMENTS v

TABLE OF CONTENTS vi

LIST OF TABLES x

LIST OF FIGURES xi

LIST OF ABBREVIATIONS xiii

1. INTRODUCTION 1

2. LITERATURE REVIEW 4

2.1. Cannabis Origins and Historical Applications 4

2.1.1. Δ^9-Tetrahydrocannabinol (THC) 4

2.1.2. Tetrahydrocannabivarin (THCV) 5

2.2. The Endocannabinoid System and its Receptors 6

2.2.1. Overview 6

2.2.2. Distribution of Cannabinoid Receptors and ECS in the Gastrointestinal Tract (GI) 10

2.3. Pharmacological Mechanisms of Cannabinoids 11

2.3.1. Anti-inflammatory Potential 11

2.3.2. Pain Modulation 11

2.3.3. Immunosuppression 12

2.3.4. Insulin Sensitivity Improvement and Potential Intracellular Lipid Level Reduction 13

2.3.5. Pharmacological Effects on Non-CBR_1/non-CBR_2 Molecular Targets 14

2.4. Inflammatory Diseases (Inflammatory Bowel Diseases: IBD) 15
2.4.1. Innate Immune Response 15
2.4.2. Adaptive Immune Response 17
2.4.3. IBD: Diagnosis and Interventions 18
2.4.4. Clinical Serum Biomarkers for IBD Patients 19
2.5. Model Systems to Evaluate the Pharmacology of THCV 20
2.5.1. Intestinal Organoid Model 20
2.5.2. Immune Reaction by Tumor Necrosis F-α and Interferon-γ in Intestinal Organoids 21
2.5.3. Organoid *Versus* Traditional *In Vitro* Models 22
2.5.4. Human Liver Microsomes 23
2.5.4.1. Intrinsic Clearance 24
2.5.4.2. Three-Solvent Plasma Protein Binding Technique 24
2.5.5. Colorectal adenocarcinoma cell (Caco-2) Transwell Model 26
2.6. Rationale 28
2.7. Hypotheses 29
2.8. Objectives 30
3. MATERIALS AND METHODS 31
3.1. Chemicals 31
3.2. Liquid Chromatography–Tandem Mass Spectrometry (LC-MS/MS) Method 32
3.2.1. Instruments and Chromatographic Conditions 32
3.2.2. Preparation of Working Solutions 33
3.2.3. Preparation of Calibration Standards and Quality Control (QC) Samples 33

3.2.4. THCV Method Validation 34
3.3. Three-Solvent Plasma Protein Binding Method 35
3.4. Enzyme Kinetic Studies 36
3.5. Caco-2 Cell Cytotoxicity Assays Using THCV 37
3.6. Caco-2 Cell Permeability Assays Using THCV 38
3.7. Intestinal Organoid Model Establishment 39
3.8. Inflammatory Biomarkers and Quantitation 40
3.8.1. Western Blot 40
3.9. Data and Statistical Analysis 41
4. RESULTS 44
4.1. LC-MS/MS Method Validation for THCV 44
4.2. Linearity of Calibration Curve and Intraday & Interday Accuracy and Precision of Quality Control (QC) Standards in Pooled Human Plasma 48
4.3. Linearity of Calibration Curve and Intraday & Interday Accuracy and Precision of Quality Control (QC) Standards in Hank's Balanced Salt Solution (HBSS) 52
4.4. Determination of the Unbound Fraction of THCV in Human Plasma 56
4.5. *In Vitro* Hepatic Intrinsic Clearance of THCV 60
4.6. THCV Cytotoxicity in Caco-2 Monolayer 66
4.7. Bidirectional Transfer of THCV Across the Caco-2 Polarized Epithelium 68
4.8. Intestinal Organoid Establishment 72
4.9. Preliminary Inflammatory Stimulus Treatment (LPS) in Intestinal Organoids (IOs) 74
5. DISCUSSIONS 82

5.1. Current Knowledge Gaps on Cannabinoids 82
5.2. Three-Solvent Plasma Protein Binding Assay 83
5.3. Substrate Depletion Approach and Linear Extrapolation in the Stability Assay (LESA) 86
5.4. *In Vitro* THCV Permeability Characteristics in Caco-2 Transwell System 88
5.5. Pilot Intestinal Organoid Assays Evaluating the Anti-inflammatory Potential of THCV 92
6. CONCLUSION AND FUTURE WORK 95
7. REFERENCES 98

LIST OF TABLES

Table 4.1 Intraday accuracy and precision in mass spectrometry bioanalytical parameters of THCV in K_2HPO_4 and human liver microsomes (*n* = 6)…….46

Table 4.2 Interday accuracy and precision in mass spectrometry bioanalytical parameters of THCV in K_2HPO_4 and human liver microsomes (*n* = 6)…….47

Table 4.3 Intraday accuracy and precision in mass spectrometry bioanalytical parameters of THCV in pooled human plasma (*n* = 3)……...50

Table 4.4 Interday accuracy and precision in mass spectrometry bioanalytical parameters of THCV in pooled human plasma (*n* = 3)……...51

Table 4.5 Intraday accuracy and precision in mass spectrometry bioanalytical parameters of THCV in Hank's balanced salt solution (HBSS) (*n* = 3)…….54

Table 4.6 Interday accuracy and precision in mass spectrometry bioanalytical parameters of THCV in Hank's balanced salt solution (HBSS) (*n* = 3)…….55

Table 4.7 Intraday recovery of THCV (ng/mL, %) in isooctane, 2-octanol, and acetonitrile following use of the 3-solvent extraction method in pooled human plasma (*n* = 6)…57

Table 4.8 Interday recovery of THCV (ng/mL, %) in isooctane, 2-octanol, and acetonitrile following use of the 3-solvent extraction method in pooled human plasma (*n* = 18)..59

Table 4.9 Linear regression analysis of THCV (1 μM) after 10 minutes of hepatic metabolism in 0.1, 0.2, 0.25, 0.5, and 1.0 mg/mL microsomes (*n* = 2) ……..62

Table 4.10 Caco-2 monolayer assessment by TEER value ($\Omega*cm^2$) at Day 10, 15, 20, and before/after 60 min of THCV permeation at 10 μM (*n* = 6). Mean ± S.D was calculated from six Transwell plates……...69

Table 4.11 Caco-2 monolayer assessment by Lucifer Yellow rejection rate (%) after 0, 15, 30, 45, 60 min of THCV permeation at 10 μM (*n* = 6). Mean ± S.D was calculated from six Transwell plates……..70

Table 4.12 Mass balance of THCV in bidirectional Transwell permeability assays. Data are presented as mean ± S.D of six replicates per experiment for six independent days. Mass balance data were expressed as percentage of total mass quantified in three compartments……..71

LIST OF FIGURES

Figure 2.1 **(1)** Endocannabinoids are produced "on-demand" in response to an action potential in neurons in the post-synaptic terminals: anandamide (AEA) is generated from phospholipase-D (PLD)-mediated hydrolysis of the membrane lipid *N*-arachidonoylphosphatidylethanolamine (NAPE); 2-AG from the diacylglycerol lipase (DAGL)-mediated hydrolysis of the membrane lipid diacylglycerol (DAG); **(2,3)** Anandamide (AEA) and 2-AG diffuse retrogradely towards the pre-synaptic terminals where upon binding, activate the pre-synaptic G-protein-coupled CB_1 receptors. **(4)** AEA and 2-AG enter the post or pre-synaptic nerve terminals where they are catabolized by fatty acid amide hydrolase (FAAH) or monoacylglycerol lipase (MAGL) to yield either arachidonic acid (AA) and ethanolamine (ETA), or arachidonic acid (AA) and glycerol. Schematic was generated using PowerPoint……9

Figure 2.2 Schematic depiction of Caco-2 in a single Transwell……...27

Figure 4.1 Representative LC-MS/MS chromatogram of human liver microsomes spiked with internal standard (CBD-D3 100 ng/mL, 1.76 min) and THCV (1 μM, 1.76 min). Conditions: Agilent 1290 Infinity binary pump coupled with AB Sciex 6500 QTrap triple quadrupole; Agilent Zorbax Eclipse XDB-C18 analytical column (4.6×150 mm., 5 μm); mobile phase A: LCMS-grade water with 0.1% formic acid, mobile phase B: LCMS-grade methanol with 0.1% formic acid…….45

Figure 4.2 Standard curves of THCV during 3 days of plasma protein binding experiments involving the 3-solvent extraction method in pooled human plasma, showing linearity with R^2 values ≥0.98. THCV has 7 standard points, ranging from 0.49-125 ng/mL. Standard curves were weighted $1/y^2$ for improving the regression fit for low standard concentrations. *Plots were generated and modified in MultiQuant™ software…….49

Figure 4.3 Standard curves of THCV during 3 days of Caco-2 permeability assays in Hank's balanced salt solution (HBSS), showing linearity with R^2 values ≥0.98. THCV has 7 standard points, ranging from 0.49-125 ng/mL. Standard curves were weighted $1/y^2$ for improving the regression fit for low standard concentrations. *Plots were generated and modified in MultiQuant™ software……..53

Figure 4.4 A plot of natural log percent remaining of THCV (1 μM) after 10 min of hepatic metabolism in 0.1, 0.2, 0.25, 0.5, and 1.0 mg/mL microsomes (n = 2)……61

Figure 4.5 Linear correlation between $1/Cl_{int}$ and 0.1, 0.2, 0.25, 0.5, 1.0 mg/mL HLM for tetrahydrocannabivarin. Data were fitted by linear regression ($y = 0.0705x + 0.0114$, $R^2 = 0.9875$). The y-axis intercept corresponded to $1/Cl_{int,u}$. Treatments were conducted

in duplicates on three independent days (n = 6). Values were presented as SEM with 95% confidence intervals……..65

Figure 4.6 Cytotoxicity assay in Caco-2 cell cultures treated with 0, 1, 5, 10, 30 μM THCV for 24 h. Data are represented as mean ± S.D. (n = 5). Statistical differences were analyzed using One-way ANOVA, and multiple comparisons were conducted using Tukey's test: $P < 0.0001$……...67

Figure 4.7 Human intestinal organoids generated using the STEMdiff ™ kit……...73

Figure 4.8 Western blot analysis of interleukin-6 (IL-6) in intestinal organoids (1:1000). Samples included eight organoid cell lysates (n = 1). *LPS was added for total duration of 48 hours…….75

Figure 4.9 Western blot analysis of inducible nitric oxide synthase (iNOS) in intestinal organoids (1:1000). Samples included eight organoid cell lysates (n = 1). *LPS was added for total duration of 48 hours…….77

Figure 4.10 Western blot analysis of interleukin-10 (IL-10) in intestinal organoids (1:1000) Samples included nine organoid cell lysates (n = 1). *LPS was added for total duration of 48 hours……...79

Figure 4.11 Western blot analysis of interleukin-10 (IL-10) in intestinal organoids (1:1000) panel **A**. Samples include eight organoid cell lysates (n = 2). *LPS was added for total duration of 48 hours. GAPDH was used for protein normalization. Densitometry analysis of interleukin-10 (IL-10) after 48 hr exposure of LPS (500 ng/mL) and 24 hr of THCV at 3 or 10 μM in intestinal organoids (n = 2) panel **B**. LI-COR Image Studio™ Lite was used for quantitation……...81

LIST OF ABBREVIATION

AA	Arachidonic acid
ABC	ATP-Binding cassette transporters
AEA	Anandamide
AGP	Alpha-Acid glycoprotein
2-AG	2-Arachidonoylglycerol
AKT/PKB	Protein kinase B
ALT	Alanine aminotransferase
ANOVA	One-way analysis of variance
APS	Ammonium persulfate
ASCA	Anti-*Saccharomyces cerevisiae* antibody
AST	Aspartate aminotransferase
ATCC	American Type Culture Collection
B_{reg}	Regulatory B cells
BSA	Bovine serum albumin
Caco-2	Colorectal adenocarcinoma cells
cAMP	Cyclic adenosine monophosphate
CB	Cannabinoid
CBC	Cannabichromene
CBD	Cannabidiol
CBDV	Cannabidivarin
CBG	Cannabigerol

CBGV	Cannabigerovarin
CBGVA	Cannabigerovarinic acid
CBN	Cannabinol
CBR	Cannabinoid receptor
CBR_1	Cannabinoid receptor 1
CBR_2	Cannabinoid receptor 2
CCL3	Chemokine (C-C motif) ligand 3
CD	Crohn's disease
CD45	Intercellular adhesion molecule 1
CHO	Chinese hamster ovary cells
Cl_H	Hepatic clearance
Cl_{int}	Intrinsic clearance
$Cl_{int,u}$	Unbound intrinsic clearance
CNS	Central nervous system
COX-2	Cyclooxygenase-2
CRP	C-reactive protein
CV	Coefficient of variation
CXCL2	Chemokine (C-X-C motif) ligand 1
CYP	Cytochrome P450
DAG	Diacylglycerol
DAGL	Diacylglycerol lipase
DC	Dendritic cells

dH_2O	Deionized water
DIO	Dietary-induced obese
DLD-1	D.L. Dexter colorectal cells
DMEM	Dulbecco's modified Eagle medium
DMSO	Dimethyl sulfoxide
DSS	Dextran sulfate sodium
EC_{50}	Half maximal effective concentration
E. Coli	*Escherichia coli*
ECS	Endocannabinoid system
EFR	Efflux ratio
EGTA	Ethylene glycol tetra-acetic acid
E_{max}	Maximum therapeutic effect
ETA	Ethanolamine
F_a	Bioavailability
FAAH	Fatty acid amide hydrolase
FBS	Fetal bovine serum
FD4	Fluorescein isothiocyanate–dextran
FOXP3	Forkhead box P3
$f_{u(b)}$	Unbound fraction
GABA	Gamma-aminobutyric acid
GAPDH	Glyceraldehyde 3-phosphate dehydrogenase
GBP1	Guanylate binding protein1

GI	Gastrointestinal
GPCR	G-protein coupled receptors
HBSS	Hank's balanced salt solution
HCl	Hydrochloric acid
HEK293	Human embryonic kidney cell
HEPES	4-(2-Hydroxyethyl)-1-piperazineethanesulfonic acid
HHL-5	Human hepatocyte cell line 5
HDL	High-density-lipoprotein
HLMs	Human liver microsomes
HNE	4-hydroxy-2-nonenal
HQC	High quality control
HT29	Human colorectal tumor cells
5-HT_{1A}	5-hydroxytryptamine 1A receptors
IBD	Inflammatory bowel disease
IDO1	Indoleamine2,3-dioxygenase 1
IECs	Intestinal epithelial cells
IFNγ	Interferon gamma
IgG	Immunoglobulin G
IL	Interleukin
IL-1β	Interleukin-1β
IL-4	Interleukin-4
IL-6	Interleukin-6

IL-8	Interleukin-8
IL-10	Interleukin-10
IL-22	Interleukin-22
iLFs	Intestinal lymph follicles
iNOS	Inducible nitric oxide synthase
iPSCs	Induced pluripotent stem cells
K_D	Equilibrium dissociation constant
kDa	Kilodalton
K_{dep}	Substrate depletion rate constant
K_2HPO_4	Dipotassium phosphate
K_m	Michaelis-Menten constant
LC/MS	Liquid chromatography–mass spectrometry
LC-MS/MS	Liquid chromatography–tandem mass spectrometry
LDL	Low-density-lipoprotein
LESA	Linear extrapolation in the stability assay
Lgr5	Mouse leucine-repeat-containing G protein-coupled receptor 5
LLOQ	Lowest limit of detection
LOD	Limit of detection
LOG *P*	Partition coefficient
LPS	Lipopolysaccharide
LQC	Low quality control
LY	Lucifer Yellow CH dipotassium salt

mAmp	Milliapere
MAGL	Monoacylglycerol lipase
MCP-1	Monocyte chemoattractant protein-1
MDCKII	Madin-Darby canine kidney cells
MIPα	Macrophage inflammation protein-α
MIPβ	Macrophage inflammation protein-β
MQC	Medium quality control
$MgCl_2$	Magnesium chloride
MLN	Mesenteric lymph nodes
MPO	Myeloperoxidase
MUC2	Oligomeric mucus gel-forming protein-2
MUC4	Oligomeric mucus gel-forming protein-4
NADPH	Nicotinamide adenine dinucleotide phosphate
NAPE	*N*-Arachidonoylphosphatidylethanolamine
NEAA	Non-essential amino acid
NF-κB	Nuclear factor kappa transcription factors
NO	Nitric oxide
O_2	Oxygen
OA	Oleic acid
OEA	Oleoylethanolamide
OLFM4	Olfactomedin-4
PAMPs	Pathogen-associated molecular pattern

pANCA	Perinuclear antineutrophil cytoplasm antibodies
P_{app}	Apparent permeability coefficient
$P_{eff,man}$	*In vivo* intestinal permeability
PBS	Phosphate buffered saline
PEA	Palmitoylethanolamide
P-gp	P-glycoprotein
PIC	Protease inhibitor cocktail
PLD	Phospholipase-D
P/N	Part number
PNS	Peripheral nervous system
PPARs	Peroxisome proliferator-activated receptors
R^2	Coefficient of determination
RIPA	Radioimmunoprecipitation assay buffer
RLR	Retinoic inducible gene I-like receptor
RRID	Research resource identifier
RSD	Relative standard deviation
SDS	Sodium dodecyl sulfate
STAT	Signal transducer and activator of transcription
TBS	Trisaminomethane-buffered saline
TBST	Trisaminomethane-buffered saline with Tween20
TEER	Transepithelial electrical resistance
TEMED	Tetramethylethylenediamine

TG	Triglyceride
TGF-β	Transforming growth factor-beta
THC	Δ^9-Tetrahydrocannabinol
THCA	Tetrahydrocannabinolic acid
THC-COOH	11-nor-9-carboxy-tetrahydrocannabinol
THCV	Δ^9-Tetrahydrocannabivarin
THCVA	Tetrahydrocannabivaric acid
THCV-COOH	11-nor-9-carboxy-tetrahydrocannabivarin
TNF-α	Tumor necrosis factor-alpha
T_{reg}	Regulatory T cells
TRIS	Trisaminomethane
TRPV	Transient receptor potential cation channels
TWEEN® 20	Polysorbate 20
UDPGA	Uridine diphosphate glucuronic acid
UGTs	Uridine 5'-diphospho-glucuronosyltransferases
V_{max}	Maximum rate of reaction
VLDL	Very-low-density-lipoprotein
11-OH-THC	11-hydroxy-tetrahydrocannabinol
11-OH-THCV	11-hydroxy-tetrahydrocannabivarin

1. INTRODUCTION

Cannabis (*Cannabis sativa*) is one of the oldest cultivated, psychoactive plants [1]. Its leaves and flowering tops contain over 500 distinct compounds and harbor over 100 naturally occurring constituents known as cannabinoids [2]. With legalization of cannabis in Canada following the *Cannabis Act* (October, 2018), the interest in cannabis-related research has grown; however, of the many compounds in cannabis, Δ^9-tetrahydrocannabinol (THC) and cannabidiol (CBD) will potentially remain as the two most studied compounds due to the increased demand for their use in recreational and medicinal research [3]. Their involvement in research has led to the investigation of many other cannabinoids for their possible bioactivity, including tetrahydrocannabivarin (THCV) and cannabidivarin (CBDV) [4]. Research suggests that THCV may attenuate oxidative stress and inflammation in mice [5]. Thus, this finding has allowed consideration of the potential benefits of THCV for inflammatory conditions of the gastrointestinal tract such as inflammatory bowel disease (IBD) in humans.

One of the therapeutic challenges facing the regular use of THC-predominant cannabis is to achieve selective targeting at the site of disease while sparing other body regions such as the cognitive and mood centers of the brain [6]. As THCV is the third most studied cannabinoid, considerable knowledge gaps regarding the basic biological and pharmacological properties of THCV still remain. As with CBD and THC, THCV exhibits highly varied systemic concentration which is the bioavailable, THCV concentration reaching the systemic circulation intact [4,7]. This is, in part, due to low and variable oral bioavailability of cannabinoids, which generally may be attributed to extensive first-pass metabolism; in the blood and urine. The primary metabolite of THCV is 11-nor-9-carboxy-THCV (THCV-COOH), which indicates a significant pre-systemic Phase I metabolism [7,8]. However, the comprehensive interplay between intestinal absorption and liver metabolism has not been fully elucidated. Consequently, a fundamental understanding of the pharmacokinetics of THCV is required for providing essential information on its oral absorption properties.

In my research, I propose to establish an intestinal organoid system to simulate the more dynamic environment seen in humans, thus bridging the gap between traditional *in vitro* and *in*

vivo models, and providing for more potential translation of any experimental outcome. Enzyme kinetic studies using human liver microsomes (HLM) will be conducted to determine the intrinsic clearance (Cl_{int}), which directly measures the maximal efficiency of enzymes to metabolize THCV, and will provide information regarding the extent of first-pass metabolism by the liver and hepatic clearance. Further, a high-throughput screening assay using the immortalized human colorectal adenocarcinoma cell line, Caco-2, that represents a gold-standard, *in vitro* approach will be used for predicting intestinal

permeability of THCV *via* its confluent monolayer. To glean some information regarding THCV distribution processes, plasma protein binding also will be determined using a three-solvent method. Collectively, these experiments will serve as the framework for generating preclinical *in vitro* data for the study of THCV as a treatment option for gastrointestinal inflammatory conditions such as IBD.

2. LITERATURE REVIEW

2.1. Cannabis Origins and Historical Applications

Cannabis (Greek: *kánnabis*; Latin: *cannabis*; both terms referring to hemp) was first described in 2350 B.C [4,9]. Before its psychoactive properties were unravelled, cannabis was widely used for several purposes including textiles, paper, and food sources in ancient Japan and China [10,11]. As a therapeutic agent, it has historical use for nocturnal epilepsy and as an anesthetic in the Indian subcontinents [12]. The use of cannabis in more recent times as an anticonvulsant and anesthetic, appears to rely on particular cultivars (*e.g.* a variety produced by selective breeding) and the relative proportions of bioactive components in each cultivar [13]. Due to the re-emergence of its use in medical therapeutics, an attempt to isolate the active components of cannabis was conducted in the early 20th century; this yielded the first "cannabinoid," named cannabinol (CBN) [14]. The chemical structure of this cannabinoid was discovered in the 1930s, which paved the way for subsequent experiments leading to the isolation of the true psychotropic component of cannabis known as Δ^9-tetrahydrocannabinol [15].

2.1.1. Δ^9-Tetrahydrocannabinol (THC)

Currently, more than 100 cannabinoids have been identified in the cannabis flower [16]. Among these, THC is the major component and has been extensively researched for the psychoactive effects experienced by users; these effects are owing to the action of THC on a family of receptors within the central nervous system (CNS) and peripheral nervous system (PNS) [17]. In the plant, THC mainly exists as a carboxylic precursor known as Δ^9-tetrahydrocannabinolic acid (THCA), which is cyclized by THC synthase. Upon exposure to light or combustion, THCA is decarboxylated, yielding THC within the glandular trichomes of the flowers and leaves. Thus, the genetic profile and the relative level of enzyme expressions of THCA synthase will determine the chemical composition of a particular strain [18,19]. In terms of their physicochemical properties, all cannabinoids are lipophilic. Due to their lipophilicity, one of the challenges that remains is the existence of non-specific binding to glassware and plastics, which requires the use of organic solvents and amber silicate vials or low-bind plastics for minimizing loss, especially during analytical testing procedures [20].

In the past decade, the therapeutic effects of THC have been shown in pre-clinical studies to include the ability to suppress acute nausea and vomiting while more limited clinical evidence indicates use for providing relief for chemotherapy-induced nausea and vomiting [21,22]. Current evidence also suggests that THC may be correlated with certain improvement in multiple sclerosis and epilepsy symptoms including sleep, spasms, and spasticity, but data are lacking regarding its ability in delaying disease progression [23,24]. In addition, one of the more conclusive results indicates a possible dose-dependent effect of THC at modulating pain in human volunteers where an analgesic effect was seen at low doses and a hyperalgesic effect with high doses [25]. These effects may be explained by an increase in sympathetic activity and inhibition of parasympathetic activity induced by THC at low doses and *vice versa* at high doses [26,27].

2.1.2. Tetrahydrocannabivarin (THCV)

THCV is a naturally occurring, *n*-propyl analog of THC and may potentially be a promising phytocannabinoid due to its similarities in chemical structures with THC [4]. It was first detected in cannabis by Gill *et al* and named Δ^9-tetrahydrocannabivarin (Δ^9-THCV) by Merkus in 1971 [28,29]. THCV was found in one of the three fractions isolated with THC being the second fraction and a third heterogenous component that was not further examined; THCV was then purified through chromatography and counter-current distribution from a crude extract of petroleum ether [29]. Although THCV and THC have similar chemical structures, THC possesses psychoactive properties, whereas THCV exhibits non-psychoactive effects both *in vitro* and *in vivo*. This may be partially due to the antagonism on a specific type of receptor, the cannabinoid receptor 1 (CBR_1) in the endocannabinoid system [30]. This distinction allows THCV to have a therapeutic advantage as a non-psychoactive cannabinoid for the management of, for example, clinical obesity and inflammation as reduction in novel biomarkers were seen with THCV in both conditions [5,31].

In terms of THCV synthesis, geranyl-transferase catalyzes a reaction between geranyl pyrophosphate and divarinolic acid forming cannabigerovarinic acid (CBGVA), where CBGVA is then converted to tetrahydrocannabivarin acid (THCVA) by THCV synthase [5,32]. Upon heating, THCVA is decarboxylated into its active component, THCV. This active form of THCVA may

possess therapeutic benefits by mediating anti-inflammatory effects, as demonstrated in cellular models for IBD [5,33].

2.2. The Endocannabinoid System and its Receptors

The endocannabinoid system (ECS) is a primitive, evolutionarily conserved, ubiquitous lipid signalling system present in all vertebrates, and it appears to have crucial regulatory functions within the human body [34]. The ECS is comprised of cannabinoid receptors, endogenous cannabinoids, synthesizing and degrading enzymes as well as other endogenous molecules with "cannabinoid-like" effects such as palmitoylethanolamide (PEA) and oleoylethanolamide (OEA). The principal ECS components include the cannabinoid receptors 1 and 2 (CBR_1 and CBR_2); the CBR ligands anandamide (AEA) and 2-arachidonoylglycerol (2-AG); synthesizing enzymes phospholipase-D (PLD), diacylglycerol lipase (DAGL); and degrading enzymes fatty acid amide hydrolase (FAAH) and monoacylglycerol lipase (MAGL) [35]. The ECS has been implicated in a broad range of physiological processes including neural development, neuropathic pain, inflammation, and immune function [36-38]. Thus, the dysregulation of the ECS may lead to the emergence of various pathophysiological symptoms that subsequently contribute to an array of clinical diseases [34].

2.2.1. Overview

The two primary endogenous activators of the ECS are AEA and 2-AG. AEA is synthesized from PLD-mediated hydrolysis of the lipid *N*-arachidonoylphosphatidylethanolamine (NAPE) whereas 2-AG is generated from DAGL-mediated hydrolysis of the membrane lipid diacylglycerol (DAG) in the post-synaptic terminal (Figure 2.1) [39]. From there, these endocannabinoids along with other phytocannabinoids, including THCV, may bind and activate CBR_1 and CBR_2, which are G-protein coupled receptors (GPCRs) in the pre-synaptic terminal (*e.g.,* the ECS mediates retrograde activation) [40]. This activates a G_i/G_o-dependent cascade that triggers the inhibition of adenylyl cyclase and decreased production of cyclic AMP with similar decreases in protein kinase A [41]. AEA is suggested to be a partial agonist at CBRs with slightly higher affinity at CBR_1 as opposed to CBR_2. 2-AG binds with higher affinity at CBR_1 and

possesses greater efficacy and potency at both receptor subtypes compared to AEA [36,42]. In terms of their pharmacodynamic effects, CBR_1 activation in the CNS may lead to the suppression of release of neurotransmitters such as dopamine, glutamate, acetylcholine, and gamma-aminobutyric acid (GABA) with acute and prolonged durations [40,43]. In contrast, CBR_2 activation is predominantly seen in mast and immune cells, which leads to the inhibition of cytokine release and the inhibition of neutrophil and macrophage infiltration, indicating the important role for CBR_2 in modulating immune functions [44].

Signalling by AEA and 2-AG is terminated by the action of two degrading enzymes: FAAH and MAGL, respectively. FAAH is primarily located in the post-synaptic terminal and preferentially breaks down AEA yielding arachidonic acid (AA) and ethanolamine (ETA). MAGL resides in the pre-synaptic terminal and favours the catabolism of 2-AG, yielding glycerol and AA. Thus, this "on demand" synthesis of endocannabinoids with precise degradation signalling allows biological activities to be tightly controlled both spatially and temporally [45].

Published evidence suggests that THCV may act as a CBR_1 antagonist and CBR_2 agonist both *in vivo* and *in vitro* [30], in contrast with THC which acts as a partial agonist at both receptors [40]. Although its potency (EC_{50}) and efficacy (E_{max}) may differ depending on the route of administration and various parameters in different experiments, the overall effects of THCV on these cannabinoid receptors are fairly conclusive. The suggestion that THCV may block the activation of neuronal CBR_1 resulted from *in vitro* experiments using murine cerebellar slices. The results showed that THCV suppressed CBR_1 inhibition of GABA release from basket-cell interneurons induced by *R*-(+)-WIN55212, a CBR_1 agonist [46]. Secondly, by itself, THCV acts as a CBR_1 antagonist to increase GABA release from these neurons [46]. Further, THCV may also act *via* CBR_2 where its signalling cascades may well represent a complex perspective of the ECS as the pharmacological properties of THCV on this receptor have been documented and can be principally categorized in terms of its anti-inflammatory effects, pain modulation, immunosuppression, and insulin sensitivity [40].

Apart from the well-known cannabinoid receptors, a variety of different cannabinoids were found to act on other molecular targets. These targets include the transient receptor potential channel (TRPV), the 5-hydroxytryptamine-1A ($5\text{-}HT_{1A}$) receptor, the GPR-55, and the nuclear

hormone superfamily known as the peroxisome proliferator-activated receptors (PPARs). Other endocannabinoids such as the palmitoylethanolamide (PEA) and oleoylethanolamide (OEA) do not bind to cannabinoid receptors, but may augment their effects by acting on different PPARs [47]. In addition, the interactions between THCV and some of these non-CBR targets have also recently been documented. Collectively, THCV may have dose-dependent inhibitory effects on mammalian TRPV5 and TRPV6 and upregulated activation *via* 5-HT_{1A} and GPR-55, giving rise to an extra layer of complexity to the current differential effects of cannabinoids [48-50].

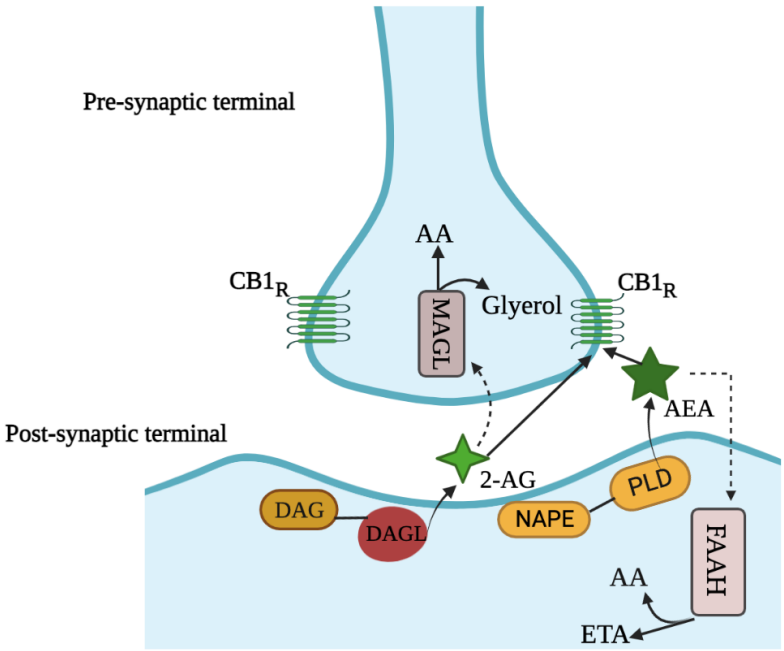

Figure 2.1 (1) Endocannabinoids are produced "on-demand" in response to an action potential in neurons in the post-synaptic terminals: anandamide (AEA) is generated from phospholipase-D (PLD)-mediated hydrolysis of the membrane lipid *N*-arachidonoylphosphatidylethanolamine (NAPE); 2-AG from the diacylglycerol lipase (DAGL)-mediated hydrolysis of the membrane lipid diacylglycerol (DAG); **(2,3)** Anandamide (AEA) and 2-AG diffuse retrogradely towards the pre-synaptic terminals where upon binding, activate the pre-synaptic G-protein-coupled CB_1 receptors. **(4)** AEA and 2-AG enter the post or pre-synaptic nerve terminals where they are catabolized by fatty acid amide hydrolase (FAAH) or monoacylglycerol lipase (MAGL) to yield either arachidonic acid (AA) and ethanolamine (ETA), or arachidonic acid (AA) and glycerol. Schematic was generated using PowerPoint.

2.2.2. Distribution of Cannabinoid Receptors and ECS in the Gastrointestinal Tract (GI)

Most tissues possess a complex ECS comprised of CBR_1 and CBR_2 expressed at different levels. CBR_1 is one of the most highly expressed GPCRs in the CNS and to a lesser extent in the PNS [44]. These receptors are predominantly expressed in neuronal cells in the cerebral cortex, basal ganglia, hippocampus, and cerebellum as well as on the axons of interneurons [43,51]. In addition, CBR_1 are detected in various nonneuronal tissues including the adrenal gland, heart, liver, pancreas, as well as in the neuroendocrine cells of the stomach and submucosal myenteric plexus of the colon [51-53]. Furthermore, GI functions such as fluid secretion and intestinal motility, gastric acid secretion and oesophageal relaxation are largely attributed to CBR_1-mediated function, thus suggesting the upregulation of these proteins during intestinal inflammation [54].

Antibodies to CBR_2 have been utilized for quantifying the distribution of these proteins in the GI tract. These receptors are most highly expressed in the immune system such as the nodular corona of the Peyer's patches, the marginal section of the spleen, and the cortex of the lymph nodes [55]. Under normal conditions, CBR_2 are either absent or weakly expressed in the intestinal epithelium; however, they are increasingly evident in the apical membranes at ulcerative boundaries in IBD [56]. Recently, their expression has been observed in the enteric nervous system of the ileum where expression was detected in the myenteric and submucosal plexus of the enteric ganglia [52]. Most importantly, their presence is detected on all immune cells varying in activation states and cell types. In humans, CBR_2-expression is not consistent across immune cells, with expression being the highest in B lymphocytes > Natural Killer cells > macrophages > polymorphonuclear cells > CD4 helper T cells > CD8 killer T cells [57-58]. In addition, increased CBR_2 expression in derived colonic cell lines such as Caco-2, DLD-1, and HT29 may provide functional relevancy towards IBD [59]. In regards to the endocannabinoids, AEA and 2-AG are produced throughout the GI tract with both lipid precursors, e.g. PLD and DAGL, found in abundance in all sections of the small intestine [35]. FAAH, a degrading enzyme for AEA, is expressed equally across the mucosa of the lower GI tract from the duodenum to the distal colon. MAGL, a degrading enzyme for 2-AG, is found in the enteric neurons and from the epithelium to the muscle layers of the intestinal wall with decreased activity from the duodenum to the distal colon [39,60].

2.3. Pharmacological Mechanisms of Cannabinoids

The current knowledge of THCV function revealed certain mild to strong associations in several chronic diseases such as diabetes, epilepsy and chemotherapy-induced nausea and vomiting. These effects may be attributed to its significant anti-inflammatory potential, pain modulation, immunosuppressing and positive insulin sensitivity effects, which were fairly conclusive in *in vitro* models, but whether these same benefits extend *in vivo* will require further investigation.

2.3.1. Anti-inflammatory Potential

The anti-inflammatory properties of THCV have been documented in the context of specific receptor-mediated effects both *in vitro* and *in vivo* [30]. Although the particular mechanism is unknown, THCV may inhibit stimulated cyclic AMP (cAMP) production in Chinese hamster ovary (CHO) cells transfected with human CBR_2 receptors, whereas no effect is seen in CBR_1 CHO cells and in mouse brain membranes of $CBR_2^{-/-}$ mice [5]. In addition, THCV may downregulate the overexpression of inducible nitric oxide synthase (iNOS), interleukin-1β (IL-1β), and cyclooxygenase-2 (COX-2) proteins stimulated by lipopolysaccharide (LPS) in murine peritoneal macrophages [61]. The reduced nitric oxide (NO) production may be mediated by CBR_2 induction since abolished effects were reported with a CBR_2 antagonist and no effect with rimonabant, a selective CBR_1 antagonist [61]. These findings were in line with previous results that THCV may act on CBR_1 *via* antagonism and as a CBR_2 agonist [40,46]. Collectively, the downregulation of cAMP and nitric oxide *via* CBR_2 activation of THCV may be attributed to the positive findings in pre-clinical studies evaluating the therapeutic outcomes of THCV in mice. Thus, the compelling evidence of CBR_1 inhibition, CBR_2 activation and their effects reported *in vivo* may prompt future human research in the treatment of various inflammatory conditions.

2.3.2. Pain Modulation

Cannabinoids may have potential in pain management after observations made during anticancer and antiretroviral therapies in patients [62,63]. Their analgesic effects are possibly

ascribed to their pharmacodynamic mechanisms *via* CBRs. Although much of the present data indicate that the anti-nociceptive effects of cannabinoids are mediated by CBR_1 receptors, there is emerging evidence to support peripheral interactions *via* CBR_2 [64]. Thus, THCV, as a CBR_2 agonist, remains as one of the top, uninvestigated pain-relieving cannabinoids with minimal psychoactive effects [30,65].

Bolognini *et al* evaluated the analgesic properties of THCV in mice with carrageenan-induced inflammation and formalin tests *via* intra-plantar injection [5]. A single intraperitoneal injection of THCV (0.3 or 1mg·kg^{-1}) was shown to ameliorate carrageenan-induced oedema and thermal hyperalgesia. THCV (0.3 mg·kg^{-1}) injected daily for four days was able to attenuate these effects continuously with sustained induced inflammation (72 hours) with no drug tolerance. In addition, there were two nociceptive periods characterized with the formalin test including a short lasting first phase (0-7 min) and a second, prolonged tonic pain phase (15-60 min). THCV mediated a decrease in pain behaviour during phase two at 1 mg·kg^{-1} and both phases at 5 mg·kg^{-1}. These effects may be attributed to CBR activation and were known to be dose-dependent. This publication provides evidence that THCV may activate mouse CBR_2 *in vivo* and strengthen the rationale for exploring non-psychoactive cannabinoids for the management of inflammatory pain.

2.3.3. Immunosuppression

THCV may modulate oxidative and inflammatory responses as evidenced through studies on ischemia/reperfusion injury. Hepatic ischemia/reperfusion injury is defined as the vascular tissue damage induced by the recirculation of blood following a period of hypoxia [66]. This damage is manifested as a continuum of processes after reperfusion that result in increased ROS production, neutrophil recruitment, and subsequent pro-inflammatory mediators [66]. From previous pharmacological experiments, the activation of CBR_2 by THCV has been associated with the attenuation of inflammation and pain in mice [5,30]. With this evidence, researchers assessed the effects of THCV on human CBR_2 expressed in CHO cells and against hepatic ischemia/reperfusion injury in mice following 1h ischemia and 2, 6, or 24h reperfusion *in vivo* [33]. Pre-treatment with 10 mg·kg^{-1} THCV reduced serum aspartate aminotransferase (AST) and alanine aminotransferase (ALT) levels, which suggests decreased hepatocellular damage.

When combined with SR144528, a CBR_2 antagonist, there were increased peak serum ALT/AST concentrations and upregulated mRNA levels of various pro-inflammatory biomarkers, such as chemokines CCL3, CXCL2, TNF-α, and intercellular adhesion molecule 1 (CD54). In terms of neutrophil infiltration, lipid peroxidation, and apoptotic cell death, there were increased myeloperoxidase (MPO) activity, carbonyl adducts and 4-hydroxy-2-nonenal (HNE), caspase-3/7 activity, and DNA fragmentation. Overall, these findings indicated that THCV may represent a novel therapeutic agent against ischemia/reperfusion injury by modulating oxidative and inflammatory responses.

2.3.4. Insulin Sensitivity Improvement and Potential Intracellular Lipid Level Reduction

Inverse agonists on the CBR_1 may ameliorate type 2 diabetes and dyslipidemia [68]. However, due to the inverse agonism on this receptor, certain compounds such as Rimonabant, were discontinued as a result of adverse psychoactive effects [69]. One cannabinoid, THCV, possesses unique pharmacological action via CBR_1 antagonism and depending on its concentration, as CBR_2 agonist or antagonist [33]. For the first time, an *in vivo* study investigated the effects of THCV in dietary-induced obese (DIO) mice [31]. In DIO mice, 5 and 12.5 mg/kg THCV (Study 1; twice daily oral dosing) were shown to have 8.2% and 13.5% increases in energy expenditure measured by indirect calorimetry when expressed per mouse, and 7.5% and 17.1% increases with respect to kg body weight compared to controls. The % increase was less, yet significant, in mice with once daily dosing (Study 2). In Study 1, THCV exhibited a dose-dependent reduction in insulin concentration 30 min post glucose load with 2.5 and 12.5 mg/kg dose being significant after 1-week treatment. In study 2, fasting glucose was lowered with THCV at the highest dose [31]. Further, *in vitro* assays with normal hepatocytes showed efficient insulin stimulated Akt phosphorylation with no effect from added THCV. Three and 10 μM THCV increased insulin sensitivity *via* Akt activation in HHL-5 hepatocytes treated with 250 μM palmitic acid thus suggesting potential metabolic effects. Most importantly, these positive effects on glucose tolerance and insulin sensitivity were observed without any corresponding significant decrease in body weight. This may be plausible as increase in energy use can lead to beneficial effects with regards to glucose and insulin in the absence of weight loss. Overall, as more *in vivo*

studies using animal models and potential clinical trials involving human participants through oral THCV dosage are warranted, this cannabinoid may serve as a novel agent on obesity-associated metabolic syndromes via neutral antagonism on CBR_1.

With recent evidence suggesting that THCV may improve glucose tolerance, one subsequent study examined the effects of THCV on lipid levels in various *in vitro* and *in vivo* systems [70]. Researchers investigated the potential of THCV to modulate lipid metabolism in HHL-5 cells through an oleic acid (OA)-induced model of hepatosteatosis. THCV mitigated the increase in intracellular lipid levels after 24 h and 48 h of OA exposure. Subsequently, they assessed the lipid profiles of OA-treated cells with addition of THCV at various time points. Upon removal of OA after 24 h, untreated cells were seen with lower triglyceride (TG) levels and the addition of THCV resulted in further decrease in TG levels. After OA exclusion for 2 days, cells exposed to THCV exhibited similar TG levels compared to untreated. Cells quantified at early time points (4, 8, 12, 24, and 48 h) after THCV addition, either alone or with OA after initial 24 h OA incubation, were found to have decreased intracellular TG levels over time, and the highest TG levels were present in groups where OA was present the whole time. Rapid decreases in triglycerides were seen with 5 and 10 μM of THCV in just 4 h, suggesting a fast onset action of THCV in all treatments. Further, for *in vivo* assays, zebrafish larvae were implemented to study THCV effects on lipolysis as larvae are completely dependent on lipid-rich yolk for nutrients. Larvae after 3 to 6 days post fertilization were treated with 5 μM THCV, TG levels were analyzed using AdipoRed post 24, 48, 72 h. THCV reduced AdipoRed staining at 24, 48 h and further reduction was seen at day 3 compared to DMSO controls. Collectively, THCV facilitated lipid mobilization in zebrafish larvae, which was consistent with *in vitro* findings such that it may be a suitable candidate for treating hepatosteatosis.

2.3.5. Pharmacological Effects on Non-CBR_1/non-CBR_2 Molecular Targets

Phytocannabinoids are capable of eliciting diverse effects by acting on non-CBR_1/CBR_2 targets, one of which belongs to the vanilloid subfamily called the transient receptor potential cation channels (TRPV) [42]. More specifically, TRPV 5 and TRPV6 are functionally distinct as they lack temperature sensitivity while being highly calcium selective at the epithelia in kidney

and the gut [71,72]. In HEK293 cells expressing mammalian TRPV5 and TRPV6, THCV exhibited a strong, concentration-dependent inhibition of TRPV5 and TRPV6 with IC_{50} values of 4.8 ± 0.6 μM and 9.4 ± 1.4 μM, respectively, while no significance was reached for CBDV, CBGV, CBC, CBD, and CBG. Overall, this study suggested that THCV, apart from its effects on the cannabinoid receptors, may alter certain physiological processes in humans such as in the kidneys since TRPV5 are highly expressed in the epithelium for facilitating calcium reabsorption in the renal tubules. Thus, this finding adds to the complexity of the pharmacological effects of THCV and must be studied further especially if considered to be added as a constituent for recreational use.

2.4. Inflammatory Diseases (Inflammatory Bowel Diseases: IBD)

IBD is characterized by maladaptive immune responses to antigens of intestinal content leading to chronic inflammation and can be divided into Crohn's disease (CD) and ulcerative colitis [73]. IBD's unclear etiology may be associated with various genetic, cellular, and immunological factors [74]. While CD emergence is triggered from transmural granulomatous inflammation that can be localized throughout the GI tract, the manifestation of ulcerative colitis may be limited to the remitting mucosal inflammation, starting from the proximal colon towards the distal portion of the large intestine, while extending to the rectum [75,76]. Under normal conditions, the immune system modulates low inflammatory reactions to symbiotic bacteria, and only upregulates immune responses when encountering pathogens, thus leading to inflammation [77]. The body has evolved and developed multiple defense mechanisms to protect the intestinal epithelium and these mechanisms may operate synergistically to maintain a healthy intestinal barrier by regulating inflammatory status through innate and adaptive immune responses [78].

2.4.1. Innate Immune Response

The innate immune system comprises the intestinal mucosal and epithelial barriers, natural immune cells, and innate immune molecules [79]. This immunity generates fast, non-specific, and non-memorial responses that secrete a variety of antibodies along with the recruitment of white blood cells and chemokines for combating pathogens [80].

The mucus layer is regarded as the upper barrier of the intestinal epithelium that resembles a mechanical external protection between the intestinal lumen and the lamina propria [81]. Mucus is predominantly composed of three key elements: mucin, a glycoprotein that is encoded by the *MUC2* gene and produced by goblet cells; trefoil factors, a group of protease resistant polypeptides; and secretary immunoglobin A [82]. The primary role of this barrier involves trapping foreign microbes that would otherwise be transferred by peristaltic processes and is mainly dependent on its viscosity due to mucin itself [83]. This process is facilitated by pattern recognition receptors, such as nucleotide oligomerization domain-like receptors, toll-like receptors, retinoic inducible gene I-like receptor (RLR) that identify pathogen-associated molecular pattern (PAMPs) on the surface of pathogens and trigger NF-κB pathways and various antimicrobial agents through epithelial secretions [83-85].

The epithelial barrier is composed of intestinal epithelial cells (IECs) that are connected via desmosomes, adherent junctions, and tight junctions that serve to regulate intestinal permeability [86]. Physiologically, the intestinal epithelium is a polarized epithelium consisting of a single layer of cells separating the external environment from the blood supply in the lamina propria. More specifically, the IECs selectively control the cellular flux and antigen traffic via transcellular transport while limiting paracellular flux through strictly controlled tight junctions [81]. Tight junctions are made up of transmembrane proteins from different families including occludin, claudin, clustered proteins zonulin, and cytosolic proteins cingulin [88]. During active IBD, certain junction proteins and their mRNA expression are significantly reduced allowing the paracellular travel of pathogens thereby activating immune cells and cytokine release [89]. Therefore, it is likely that inflammation may lead to impairment of tight junctions resulting in reduced barrier integrity.

The innate immune cells are divided into macrophages and dendritic cells (DCs). By utilizing proteases and oxygen free radicals, macrophages are capable of degrading pathogens into peptides and lipopolysaccharides [78,90]. These cells are abundant at both sides of the polarized epithelium and can be localized in the intestine after monocyte maturation from the bone marrow [91]. Meanwhile, dendritic cells may act as messengers between innate and adaptive immune systems by modulating local T cell immunity [92]. Specific responses involving mucosal T cells

can be triggered after DCs have reached the inductive sites such as the mesenteric lymph nodes (MLNs), intestinal lymph follicles (iLFs), and Peyer's patches and travel *via* the lymphatic system to activate the effector sites in the lamina propria [93,94]. Lastly, antimicrobial peptides, α-defensins and β-defensins, also contribute to the mucosa by maintaining host immunity and causing microspore formation in the bacterial membranes leading to pathogen degradation [95]. Reduced defensin expression has been observed in IBD patients suggesting impaired innate immunity along with a less coherent acquired immune system [96,97].

2.4.2. Adaptive immune response

The adaptive immune response possesses specificity and immunity memory and is thought to be functioning simultaneously with innate immunity against pathogens. A significant interplay between various cell types was discovered and found to be crucial by modulating excessive inflammation thus achieving homeostasis in the GI tract [78,98]. One of the initial steps in the adaptive response requires the activation of T lymphocytes and the inhibition of T_{reg} cell activity [99]. This process is often mediated by the migration of DC towards the peripheral lymphatic sites where naïve T-lymphocytes are subsequently activated by DC upon antigen recognition [100]. From there, certain gut signalling cues controlled by DCs allow the activated T cells to acquire memory, proliferate, and travel towards the initial antigen binding sites [101]. In the lamina propria, various adhesion molecules complete the integration of T cells via activation of ligands on endothelial cells thereby inducing a systemic response [102]. Traditionally, CD was thought to be mediated by Th1 lymphocytes, whereas ulcerative colitis was more often associated with Th2 activation [103]. However, evidence suggests the involvement of Th9, Th17, and Th22 cells, which indicates a significant overlap between the two pathways in CD and ulcerative colitis [103]. Both Th1 and Th2 can be activated by antigen presence that subsequently trigger different interferons, interleukins, and transcription factors. The Th1 pathway is conducted by the secretion of IL-12, IFNγ, and TNF-α production that further activate a transcription factor known as STAT1. In contrast, IL-4 is mainly responsible for Th2 that leads to the activation of STAT6 and GATA-3 [105-107].

The two important players in attenuating inflammation by suppressing immune response are the B_{reg} and T_{reg} cells. B_{reg} mitigates inflammation by the production of an anti-inflammatory cytokine IL-10 via STAT 3 and IL-1 expression [108]. T_{reg} cells suppress various cells via direct contact and induce IL-10 and TGF-β for maintaining immune tolerance [78]. The function of T_{reg} cells seems to be dependent on a specific surface marker known as Foxp3 where their expression is associated the differentiation of T_{reg} cells, a critical component for modulating immune homeostasis [103]. The reductions in regulatory B and T cells have been found in colonic mucosa and peripheral blood pool of IBD patients, suggesting their roles in IBD pathogenesis [110]. Thus, the imbalance of these cell types may trigger immoderate cytokine and chemokine release leading to inflammation.

2.4.3. IBD: Diagnosis and Interventions

IBD patients exhibit markedly increased levels of pro-inflammatory immune modulators such as TNF-α and INF-γ and various types of interleukins [111]. Due to their abundance in inflamed tissues, these molecules are potentially promising biomarkers for IBD diagnosis and treatments. Currently, IBD intervention incorporates the use of immunosuppressive agents, oral corticosteroids, anti-TNF-α antibodies, and surgery in refractory cases [112].

Capsule endoscopy and biopsies of the GI tract are the two most frequently used techniques in IBD diagnosis [113]. In the first case, a patient swallows a capsule that can take endoscopic images with its wireless camera, which may reveal any localized ulcerations along the GI tract thus identifying the site of inflammation. Biopsies may be implemented to confirm the diagnosis as it is very effective in differentiating the type of inflammation shown in mucosal damage under the microscope [114]. In addition, biomarkers such as anti-granulocyte macrophage colony-stimulating factor, anti-glycoprotein 2, anti-*Saccharomyces cerevisiae* and anti-mannobioside carbohydrate IgG antibodies may also be utilized to determine IBD phenotypes as well as their severity [115].

Many medications involved in IBD interventions possess anti-inflammatory properties. Their mechanism of action is associated with the upregulation of Th2-mediated response and the mitigation of Th1-mediated inflammation. This further initiates the production of anti-

inflammatory cytokines such as IL-4, IL-5, IL-10, and IL-12 while reducing proinflammatory cytokines [116]. With these benefits, limitations do exist in these medications such that the administered drug is delivered to non-specific cells in the body which may result in unexpected side effects and secondary medical conditions [117]. In addition, certain drugs like infliximab can be broken down in the stomach and must be administered *via* IV infusion [118]. Infliximab is a chimeric monoclonal antibody, which reduces TNF-α, and the antibody is made from the recombinant DNA of mouse and humans. However, cases of tuberculosis have been reported in patients soon after their treatments which may be partially due to the suppression of TNF-α [113]. Therefore, with each medication, appropriate delivery system with optimal dosage and dosing interval must be developed and geared towards to each patient.

2.4.4. Clinical Serum Biomarkers for IBD Patients

The diagnosis and subclassification of IBD can be challenging as clinical symptoms may not associate with disease severity such that for example, mucosal lesions are often present in CD patients who may be presenting mild symptoms [120]. Thus, monitoring tests that include many biomarkers can be used in conjunction with endoscopy for IBD diagnosis as the "gold standard assessment" is lacking.

C-reactive protein (CRP) is regarded as one of the most widely used indicators for acute inflammation [121]. This protein is an acute phase reactant produced by the hepatocytes upon inflammation with its expression regulated by pro-inflammatory cytokines such as IL-1, IL-6 and TNF-α [121]. Elevated levels of CRP may identify mucosal active phase from quiescent IBD while having consistent clinical CD symptoms. However, the specificity and sensitivity of CRP is not ideal such that it is not disease specific with cases where normal CRP levels can be found in the serum of active IBD patients [122]. Thus, the combination approach of incorporating addition biomarkers such as α_1-acid glycoprotein and serum amyloid A may be useful for IBD diagnosis and monitoring [123].

Two additional and widely adopted biomarkers are perinuclear antineutrophil cytoplasm antibodies (pANCA) and anti-*Saccharomyces cerevisiae* antibody (ASCA) [124]. pANCA are antibodies that react with lysosomal enzymes of monocytes and neutrophils in the cytoplasm and

possess specificity for UC which targets histone H1 that correlates with immunocytologic preparations of UC patients [125]. Further, additional candidate antigens can be recognized by pANCA such as certain epitopes found in colonic bacteria and mast cells that may support the hypothesis that abnormal immune responses against commensal organisms are often exhibited in IBD patients [126]. ASCA are antibodies against *S. cerevisiae* and have high specificity for CD with lower sensitivity due to the differential expression in various ethnic populations: the prevalence of ASCA is significantly higher in Caucasian CD patients than Asian CD patients [127]. ASCA identifies proteoglycans in the yeast cell wall with various subtypes shared by mycobacteria [125]. The quantification of ASCA in patients may be attributed to impaired immunologic tolerance to specific luminal antigens and not due to increased intestinal permeability as increased antibodies levels to other yeast populations are not apparent [125]. In addition, research shown greater discriminatory ability in IBD diagnosis and sub-classification by pairing pANCA and ASCA with specificity (>90%) and sensitivity (~55%) [128,129]. Although great efforts have been made in IBD management, in the future, it may be plausible to screen markers that separate IBD from non-IBD, active from quiescent IBD, and CD from UC using other optimal approaches.

2.5. Model Systems to Evaluate the Pharmacology of THCV

2.5.1. Intestinal Organoid Model

In 2007, Clevers and colleagues discovered a population of fast-regenerating intestinal stem cells located at the base of the crypts of Lieberkühn expressing high levels of Lgr5 (mouse leucine-rich repeat-containing G protein-coupled receptor 5). The constant division of intestinal stem cells allows the enterocytes to migrate towards the villus tip, thus contributing to the maintenance of the epithelium [130]. This important discovery of Lgr5 stem cells made it possible for the creation of *ex vivo* intestinal organoid cultures, giving rise to a new way of studying intestinal epithelium function.

An intestinal organoid model is defined as a miniature organ with three-dimensional intestinal cellular composition and structure established *in vitro*; it can be derived from either adult multipotent stem cells or induced pluripotent stem cells (iPSCs) [131]. Research is beginning

to deviate from adult stem cells as their differentiation to the intestinal epithelium is rather limited. In contrast, iPSCs were initially derived from embryonic stem cells and are more capable of differentiating into a broader array of tissues [132]. This advantage of iPSCs may provide an accessible platform to study intestinal function in a more physiological relevant context.

According to a specific organoid kit made by STEMCELL Technologies, the selected iPSCs can be instructed to differentiate into a definitive endoderm as well as a mid/hindgut layer. From the mid/hindgut layer, two-dimensional spheroids will detach and further cultured in a matrix, *e.g.* Matrigel, with additional pro-intestinal growth medium. The exogenous growth factors and Matrigel will simulate a proper microenvironment as well as a basement membrane scaffolding that allow the structures of spheroids to resemble their organizations *in vivo*. Eventually, the budded spheroids will grow into three-dimensional intestinal organoids with polarized intestinal epithelium and a surrounding niche factor-producing mesenchyme [133]. A complete intestinal organoid possesses all intestinal cell types including $Lgr5^+$ crypt-based columnar stem cells, transit-amplifying cells, quiescent stem cells, Paneth cells, goblet cells, enteroendocrine cells, and absorptive enterocytes [134]. Thus, the regenerating property of organoids and its closer resemblance to normal intestinal epithelial physiology allow for unrestricted propagations that may increase the screening output leading to an effective integration approach within *ex vivo* systems.

2.5.2. Immune Reaction by Tumor Necrosis Factor-α and Interferon-γ in Intestinal Organoids

TNF-α and IFN-γ are two of the most prominent pro-inflammatory mediators and are upregulated in IBD patients. Their increased production is often induced by macrophages through the detection of foreign antigens in the intestinal lumen, leading to cellular damage at the epithelium through prolonged immune stimulation. In two separate studies, intestinal organoids have been deemed responsive to these cytokines and may serve as a novel platform for investigating mucosal damage in IBD. Onozato *et al* demonstrated the loss of luminal structure, decreased mRNA expression of intestinal biomarkers such as *MUC2* (goblet cells) and *villin1* (enterocytes), increased expression of *LGR5*, *OLFM4* (intestinal stem cells) and caspase-3-

positive cells in organoids treated with 30 ng/mL TNF-α for 96 h [135]. Opposite, yet significant, findings were seen with TNF-α and infliximab, a TNF-α inhibitor at 1 μg/mL. The upregulated expression of *LGR5* and *OLFM4* suggested that the intestinal stem cells may modulate the organoids at the crypt after inflammation to a certain extent.

The signalling mechanism of IFN-γ *via* phosphorylation of STAT1 and gene upregulation in IFN-γ treated intestinal epithelial models have been well evaluated. Workman *et al* aimed to generate intestinal organoids on micro-engineered chips with continuous media flow with the addition of IFN-γ. STAT1 phosphorylation was detected after 1h exposure of IFN-γ from 10–1000 ng/mL [136]. Increased expression in indoleamine2,3-dioxygenase 1 (IDO1) and guanylate binding protein1 (GBP1) were quantified after three-day incubation with 10 ng/mL IFN-γ compared to untreated controls along with upregulation in *PLA2G2A* (Paneth cells) and *MUC4*. Functional barrier studies were conducted by adding 10 μg/mL fluorescein isothiocyanate–dextran (FD4) to the apical chamber and 10 ng/mL of TNF-α and IFN-γ added to the bottom channel for three days. FD4 permeability was assessed over 6 hours with area under the curve (AUC) of FD4 exposed to TNF-α and IFN-γ, and AUC values were significantly increased compared to untreated. MTS assay further confirmed no change in viability between groups suggesting the increased permeability was not due to cell death. The reason for the increased permeability of FD4 was not further investigated in this study, but was demonstrated by other groups such that IFN-γ may disrupt certain cadherin proteins leading to impaired tight junctions.

2.5.3. Organoid *Versus* Traditional *In Vitro* Model

Over the past decade, experimental models have been improved and modified to address the complexity on an area of interest within the human body. To date, *in vitro* cell models have been increasingly adopted for the study of cellular responses and mechanisms in bodily systems [137]. In relation to the intestine, membrane permeability remains as one of the most important parameters for understanding GI absorption [138]. One of the common *in vitro* models involves the use of the immortalized Caco-2 cell line that when confluent expresses various biological and morphological traits of a polarized intestinal epithelium including tight junctions, intestinal enterocytes, and brush-border microvilli [139]. These characteristics facilitate the prediction of drug

intestinal transport by calculating its apparent permeability (P_{app}) over the intestinal barrier by normalizing the pH of the medium, fluid hydrodynamics, and area of the chambers [140]. However, this system may not completely recapitulate the actual intestinal physiology *in vivo* as it comprises only a monolayer of enterocytes. Further, high sensitivity of the cell to chamber media and preparation setup, and high inter-, intra-laboratory variability remain as some of the challenges in Caco-2 models [141].

The mammalian intestinal epithelium is comprised of different cell types with upper and lower barriers that operate coherently to acquire nutrients and modulate immune responses in relation to pathogens. A complete organoid model derived from embryonic stem cells will encompass various cell types known to be present in the epithelium. This suggests that organoids may bridge the gap between traditional *in vitro* cell culture and *in vivo* models. However, certain technical challenges do exist such as imaging and access to its central lumen due to its folded villus domains [142]. One major limitation involving intestinal organoids is the lack of an enteric nervous system and immune cells [143]. Thus, the combination of enteric nerves and immune cells in a co-culture system with intestinal organoids may provide a deeper understanding of the mucosal gut physiology and host-pathogen interactions.

2.5.4. Human Liver Microsomes

Human liver microsomes (HLMs) are subcellular fractions obtained from the endoplasmic reticulum of hepatic cells and are prepared by homogenization along with differential centrifugation [144]. HLMs possess a variety of drug metabolizing enzymes such as cytochrome P450s, epoxide hydrolases, carboxyl esterases, and uridine 5'-diphospho-glucuronosyltransferases (UGTs) which make them a novel *in vitro* system for investigating the metabolic profile of xenobiotics. More specifically, the examination of phase I oxidation and phase II glucuronidation can be more closely evaluated by adding different cofactors such as NADPH and UDPGA, respectively [145]. Microsomes are purchased at relatively low costs and can be stored at -80°C for a substantial period with minimal loss of enzymatic activities [146]. In addition, microsomes from similar as well as different species are commercially available and are often well-standardized. Pooled HLMs are subcellular fractions accumulated from different human subjects varying in

numbers (5, 10, 50, 200 subjects), that are conventionally used within *in vitro* studies for minimizing inter-individual variations resulting from differential enzymatic activities [147]. One of the major limitations of using HLMs is the potential higher biotransformation rates due to the enrichment of CYPs and UGTs in the microsomal fraction compared to the *in vivo* physiological state [148]. Therefore, certain equations exist to promote the most optimal *in vitro-in vivo* extrapolation of PK parameters in humans. Some other drawbacks include different incubation conditions, varying pH of the medium, ionic strength, and types of organic solvents that may collectively affect the enzyme activity measurements in HLM studies [148].

2.5.4.1. Intrinsic Clearance

Intrinsic clearance (Cl_{int}) is the ability of an organ to permanently remove drug from the blood in the absence of physiological considerations such as blood flow and protein binding [149]. Cl_{int} is a variable that directly measures the efficacy of enzymes for metabolizing substrates, thus influencing hepatic clearance (Cl_H), a primary pharmacokinetic parameter [150]. Thus, the determination of Cl_{int} will elucidate the relative contribution of enzymes of an organ to xenobiotic metabolism *in vivo*. However, the Cl_{int} may not be a true value as non-specific binding to microsomal membranes is seen with many lipophilic compounds. Nonspecific binding results in a reduction in free drug concentration that is available for interactions with enzymes in the endoplasmic reticulum leading to an underestimation of Cl_{int} [151]. The 'true' Cl_{int} is defined as the value exhibited in the absence of microsome binding known as the unbound intrinsic clearance ($Cl_{int,u}$). In 2005, a method (linear extrapolation in the stability assay, LESA) was established to allow for the direct determination of $Cl_{int,u}$ without calculating the unbound fraction of the drug ($f_{u(b)}$) [152]. This involved extrapolating from *in vitro* metabolic studies conducted with different quantities of microsomal proteins and may yield a more accurate metabolic profile for xenobiotics.

2.5.4.2. Three-Solvent Plasma Protein Binding Technique

The unbound fraction in the blood is a pharmacokinetic parameter that indicates the ability of a drug to bind to plasma proteins such as albumin, $alpha_1$ acid glycoprotein, and

lipoprotein. This parameter is dependent on the amount of protein available dictated by the number of binding sites/per protein and total protein content (i.e. nP term) and the proteins' affinity for binding through the equilibrium dissociation constant, K_D [153]. The unbound fraction, $f_{u(b)}$ relates the unbound plasma concentration of a drug to the total plasma drug concentration comprised of both bound and unbound drug [140]. The unbound fraction has critical importance as it reflects the availability of the unbound drug concentration, which elicits the pharmacological effects [155]. Over the years, various techniques have been introduced and optimized for quantifying the unbound fraction such as equilibrium dialysis and ultrafiltration. However, certain methods that are high-throughput but require long duration to reach equilibrium may be problematic for unstable compounds and increased error in measuring $f_{u(b)}$ may occur as a result of the volume shift in the device due to the Donnan effect, which is a phenomenon of unequal distribution in charged ions on both sides of the semi-permeable membrane due to an unequal electrical charge of impermeable ions collected on the opposite side [152,156]. One recent procedure referred to as the three-solvent extraction technique was developed for quantifying the binding of lipophilic compounds such as pyrethroids where three organic solvents are added in specific order for calculating the $f_{u(b)}$ [157]. Briefly, isooctane is first added to the drug of interest in plasma to remove the unbound portion as plasma proteins are insoluble in the mixture. The remaining plasma will then be mixed with 2-octanol to remove the bound portion to lipoprotein, with acetonitrile being added in the end to remove the bound portion to albumin. This extraction procedure collectively would then have measured the unbound drug concentration and the total drug plasma concentration yielding the unbound fraction. Although this technique is fairly new, the selection of the organic solvents was based on published procedures thus suggesting its validity especially with the investigation of highly lipophilic compounds that exhibit extensive non-specific binding to devices used in traditional methods.

2.5.5. Colorectal adenocarcinoma cell (Caco-2) Transwell model

Although Caco-2 cell culture model may not be suitable for recapitulating the dynamic vasculature of the human intestine *in vivo*, the Transwell apparatus in which Caco-2 cells are seeded provides a unique, functional barrier that allows for the study of drug permeability as well as the identification of inducers or inhibitors on certain transporters [141]. Cells at an optimal density are plated on the membrane of Transwell inserts and are set to grow for 21 days. Over this time course, Caco-2 cells are able to form a polarized epithelium where an apical-basal symmetry is established with distinct structures such as the microvilli expressed apically and the formation of tight junctions that laterally connect the colorectal cells while restricting paracellular flux [158]. Thus, the apical chamber of the inserts with seeded cells will represent the lumen of the intestine where the basal chamber is indicative of the lamina propria shown below. With this design, the Transwell using Caco-2 is routinely used for modelling the permeability of compounds in two-dimension, and whether they can be substrates for certain efflux or uptake transporters may also be evaluated based on the flux ratio with regards to either direction.

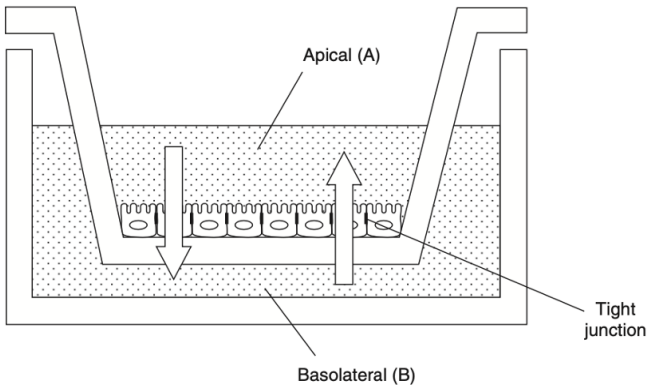

Figure 2.2 Schematic depiction of Caco-2 in a single Transwell insert [141].

2.6. Rationale

The use of *Cannabis* in the treatment of certain human pathologies has received tremendous attention in recent years. Various pre-clinical and clinical findings on the benefits of cannabinoids in epilepsy, neuropathic pain, and GI syndromes have allowed many governmental and research sectors to further investigate their therapeutic potential, constituent compositions, and adverse effects.

The evidence on the effectiveness of THCV as an anti-inflammatory agent and a pain modulator in *in vitro* and *in vivo* systems encourage additional research for human applications. Currently, the pharmacokinetic data of THCV indicated a reduced bioavailability and a potential, good epithelial absorption profile in the intestine. This finding supports its potential for regulating biological activity at the intestinal epithelium. IBD is a clinically important condition that may benefit from the anti-inflammatory effect of THCV as inflammation is often initially present that triggers the patients' immune responses and exacerbate their symptoms [98]. The use of intestinal organoids may offer a robust and valid platform to study the pharmacology of THCV in intestinal inflammation. Further, THCV may be an alternative treatment due to its non-psychoactive properties, which may possibly achieve selective targeting at the site of disease while sparing other bodily regions such as the brain. Therefore, experimental data on assessing the PK characteristics of THCV through GI absorption, metabolic stability, and unbound fraction in the blood are essential to validate the potential significant effects of this cannabinoid.

2.7. Hypotheses

1. THCV has a low unbound fraction ($f_{u(b)}$) in the blood.
2. THCV downregulates the expression of certain inflammatory biomarkers (IL-6 and iNOS) in the intestinal organoid system.
3. THCV exhibits relatively high permeability across a Caco-2 cell monolayer with predicted apparent permeability coefficient (P_{app}) of $\geq 1.0 \times 10^{-6}$ cm s^{-1} and efflux ratios (EFR) close to 1.0.
4. THCV (μM) exhibits an Cl_{int} value consistent with intermediate to high clearance compounds.

2.8. Objectives

1. To modify and partially validate an existing liquid chromatography with tandem mass spectrometry (LC-MS/MS) analytical method to include THCV.
2. To evaluate through *in vitro* screening of THCV for its essential PK characteristics of gastrointestinal absorption (Caco-2 cell model), metabolic stability (liver microsomes and substrate depletion approach), and plasma protein binding (three-solvent procedure).
3. To establish an intestinal organoid screening system derived from inducible human pluripotent stem cells (iPSCs) and a commercially available intestinal organoid kit.
4. To evaluate the anti-inflammatory effects of THCV on intestinal epithelial barrier integrity against inflammatory stimulus such as lipopolysaccharide (LPS) in the organoid system.

3. MATERIALS AND METHODS

3.1. Chemicals

Tetrahydrocannabivarin (THCV), cannabidiol-D3 (CBD-D3, internal standard), NADPH were obtained from Cerilliant Corporation and Sigma-Aldrich Canada Ltd (Oakville, ON). Dipotassium phosphate (K_2HPO_4) powder and sucrose were purchased from Thermo Scientific (Toronto, ON). Magnesium chloride ($MgCl_2$) solution was obtained from Bioshop Canada Inc (Burlington, ON). Purified deionized water was acquired through the MilliQ Synthesis (Millipore, Bedford, MA) Water Purification system. Human liver microsomes (HLM) were purchased from XenoTech, LLC (Lenexa, KS). Borosilicate culture tubes (10/75 mm), Pasteur pipets (5.75 ”), low retention SureOne plastic pipette tips (P1000, P200, P10), and other chemicals such as Optima LC/MS grade acetonitrile, methanol (MeOH), isooctane, and 2-Octanol were acquired from Thermo Scientific Inc. Captiva EMR-Lipid, 96-well plate, 96-deep well collection plate, 2 mL amber HPLC vials, blue vial caps, glass vial inserts with flat bottom were obtained from (Agilent Technologies, USA).

Dulbecco’s modified Eagle medium (DMEM) high glucose, HEPES, MEM-Non-essential amino acid (NEAA), fetal bovine serum (FBS), Trypsin 2.5% with no phenol red, versene, trypan blue and Lucifer Yellow CH dipotassium salt (LY) were purchased from Sigma-Aldrich (St. Louis, MO). Hank’s balanced salt solution (HBSS), phosphate buffered saline (PBS) were acquired from Hyclone laboratories Inc. Human colorectal adenocarcinoma Caco-2 (HTB37™) cell line and dimethyl sulfoxide (DMSO, 99.5% purity) were obtained from American Type Culture Collection (ATCC, Manassas, VA). Transwell permeable supports, polyester membrane pore size 0.4 μm, diameter 6.5 mm (24-well plates) were purchased from Corning Inc., while LoBind microcentrifuge tubes (1.5, 2.0, 5 mL) were purchased from Eppendorf Canada (Mississauga, ON).

UCSD086i-6-3 iPSCs was purchased from WiCell Research Institute Inc (WI, USA). STEMdiff™ intestinal organoid kit, growth medium and mTeSR™1 was purchased from STEMCELL Technologies (Vancouver, BC). Corning® Matrigel® growth factor reduced (GFR) basement membrane matrix (phenol red-free) was obtained from Corning® Inc (New York, NY).

Nunclon® Delta surface treated 24-well, flat-bottom tissue culture plates were purchased from Sigma-Aldrich. Bio-Plex Pro™ human cytokine 27-plex assay were purchased from Bio-Rad Laboratories Inc (CA, USA).

For reagents used for Western Blotting, 30% Acrylamide/bis solution 29:1, tetramethylethylenediamine (TEMED) and Tris (trisaminomethane) were purchased from Bio-Rad (CA, USA). Bovine serum albumin (BSA), ammonium persulfate (APS), and Tween® (Polysorbate) 20 were obtained from Sigma-Aldrich (Oakville, ON). Sodium dodecyl sulfate (SDS) micropellets and glycine were purchased from Fisher Bioreagents ™ (MA, USA). RIPA buffer (10X) and TNF-α (#3707, Rabbit, 1:1000) were purchased from Cell Signalling Technology (MA, USA). Protease inhibitor cocktail (PIC), lipopolysaccharide (#L2630, *E.coli*, 1 mg/mL) and inducible nitric oxide synthase (#482728, Rabbit, 1:1000) antibodies were obtained from Sigma-Aldrich. Interleukin-6 (#P620, Rabbit, 1:1000) and IL-10 (#PA5-85660, Mouse, 1:1000) polyclonal antibodies were purchased from ThermoFisher Scientific (Toronto, ON). IRDye® 800CW anti-Rabbit IgG and anti-Mouse IgG secondary antibodies (RRID: P/N 925-32219, P/N 925-32210, Goat, 1:2000) were obtained from LI-COR Biosciences (NE, USA).

3.2. Liquid Chromatography–Tandem Mass Spectrometry (LC-MS/MS) Method

A detailed and reliable LC-MS/MS method for the quantitative determination of THCV in HBSS within the Caco-2 cell matrix was established in our lab. Hence, a partial method validation was conducted to allow for the quantitative determination of THCV for the permeability assay. Method validation was further conducted for THCV in K_2HPO_4, $MgCl_2$, and heat inactivated pooled human liver microsomes for the enzyme kinetics studies.

3.2.1. Instruments and Chromatographic Conditions

All samples including cell lysates were analyzed using AB Sciex 6500 QTrap triple quadrupole (Sciex, Canada) coupled with Agilent 1290 Infinity binary pump (Agilent Technologies, USA). Liquid chromatography was conducted using the Agilent Zorbax Eclipse XDB-C18 analytical column (4.6×150 mm, 5 μm) with a C-18 guard column (Agilent, USA). Nitrogen served as the curtain gas, nebulizer gas, and collision gas on the MS. The mobile phases

consisted of A (LC-MS grade water with 0.1 mM ammonium formate) and B (LC-MS grade MeOH with 0.1mM ammonium formate). The analytes were eluted under isocratic mode consisting of 20:80 mobile phase A:B with a flow rate of 700 µL/min, while the column temperature was maintained at 30°C, the autosampler at 4°C and the injection volume was 5 µL. Electrospray ionization mass spectrum (ESI-MS) were acquired in the positive (ES+) and then negative (ESI-) ion mode. The Turbo Ion source operated at 600°C with IonSpray voltage of 5500 V. Other MS conditions were: curtain gas, 50 psi; nebulizer gas, 70 psi; heater gas, 60 psi, entrance potential and collision activated dissociation at 10 psi respectively. THCV was identified by the retention time (~1.7 min), multiple reaction monitoring with transitions of 287.24 *m*/*z* for precursor ions at Q1 and 165.20 *m*/*z* for product ions at Q3, and collision energy of 31 V. Integration of the chromatographic peaks was performed through Analyst® Software (Sciex, Canada). The relative concentrations of THCV were expressed as the peak area ratios of the analyte to internal standard for Transwell and enzyme kinetic assays, and the ratios were converted to micro-molar concentration according to the calibration curve.

3.2.2. Preparation of Working Solutions

Primary stock solutions (1 mg/mL) of THCV and CBD-D3 (100 µg/mL) were dissolved in MeOH by Cerilliant Corporation. THCV (1 mg/mL) was diluted with MeOH to produce working standards: 9.77, 39.06, 78.125, 156.25, 312.5, 625, 1250, 2500 ng/mL and Quality Controls of 28 (low quality control) (LQC), 1012 (middle quality control) (MQC), and 2024 (high quality control) (HQC) ng/mL to a total volume of 1000 µL per standard. 10-fold dilution was conducted for CBD-D3 to a concentration of 10 µg/mL which was further diluted to 100 ng/mL per use. 1 mL of 100 ng/mL CBD-D3 was yielded by adding 10 µL of 10 µg/mL CBD-D3 to 990 µL of methanol.

3.2.3. Preparation of Calibration Standards and Quality Control (QC) Samples

Calibration standards were prepared by spiking 10 µL of each working standard in sequential order to 190 µL of matrices in HEPES for Caco-2 permeability assays, pooled human plasma for plasma protein binding, and inactivated human liver microsomes for metabolic

stability assays in K_2HPO_4 and $MgCl_2$ to final concentrations of 0.49, 1.97, 3.91, 7.81, 15.6, 31.25, 62.5, 125, 1.4 (LQC), 50.6 (MQC), 101.2 (HQC) ng/mL. By volume, K_2HPO_4 accounted for 167.37 µL, 20.58 µL of HLM, and 2.05 µL of $MgCl_2$ per 190 µL of matrix. Protein precipitation solutions were made in bulk by adding 163.93 µL of 100 ng/mL CBD-D3 and 9.84 mL of LC-MS grade acetonitrile. 610 µL cold protein precipitation solution was added to each calibration standards and QC samples (1.64 ng/mL CBD final concentration calibration standards and QC samples). Each sample was vortexed for 30 seconds and centrifuged at 14000 rpm for 5 min at 4°C (5804 R, Eppendorf, Mississauga, ON). Samples were transferred to an Agilent Captiva EMR-Lipid 96-well plate and filtered using vacuum. 700 µL of supernatant were added to borosilicate culture tubes and were dried using ThermoLyne Dri-Bath with filtered air at 37°C. The residue was reconstituted with 200 µL of mobile phase and vortex-mixed for 30 s. The reconstituted samples were transferred to amber HPLC vials with flat bottom inserts using glass Pasteur pipettes and placed in the autosampler.

3.2.4. THCV Method Validation

Partial LC-MS/MS method validation procedures were conducted following the FDA guidelines [159]. Selectivity was evaluated by analyzing pooled human liver microsomes (HLM), human liver specimens in K_2HPO_4 and $MgCl_2$, whose preparations were added with internal standard (100 ng/mL CBD-D3) to quantify the presence of any endogenous compounds with similar retention times as THCV.

The sensitivity of the method was assessed by the determination of the lowest limit of quantification (LLOQ) and the limit of detection (LOD). LLOQ was the lowest concentration of the analyte in the standard curve that yielded optimal accuracy and precision. LOD was determined as the lowest detectable concentration with a signal to noise ratio of three. Accuracy (%) was calculated as [(mean measured concentration/nominal concentration)*100] with acceptable limits at ± 15% except at LLOQ, where it should not surpass ± 20%. Precision (%) was defined as [(relative standard deviation (RSD)/ mean measured concentration) *100] with ± 15% of the coefficient of variation (CV) except for LLOQ, where it should not surpass ± 20% of CV. The intra-day accuracy and precision were assessed by analyzing six replicates of quality

control samples (LQC, MQC, HQC) on a single day. The inter-day accuracy and precision were assessed from the same QC samples for three different days.

The linearity of the method was determined by analyzing a six-point calibration curve on several different days. The ratios of the analyte peak areas and the internal standard were plotted against the analyte nominal concentrations. A linear least-squares regression analysis using $1/y^2$ as weighting factor was adopted to determine slope, intercept and coefficient of determination (r^2) to demonstrate linearity of the method. A coefficient of determination (r^2) value of >0.98 would be deemed acceptable according to the FDA guidelines. In terms of stability, short term stability (bench top), processed sample stability and autosampler stability were previously determined in our lab. No drastic change in known analyte concentrations was found during sampling and storage. Although matrix effect studies were not conducted, the calculated concentrations of THCV standards were consistent with the nominal concentrations in the calibration curve and no additional peaks were present in the chromatogram other than THCV and CBD-D which had similar elution time (1.76 min).

3.3. Three-Solvent Plasma Protein Binding Method

The binding of THCV was quantified by a three-step organic solvent extraction procedure. THCV (low, mid, high) working standards were diluted with LC-MS grade MeOH using the primary THCV stock (1 mg/mL) yielding concentrations of 600, 1000, 10000 ng/mL. 190 µL of blank human pooled plasma was spiked with 10 µL of THCV (low, mid, high) working standards in a total volume of 200 µL where each concentration was conducted in six replicates yielding final concentrations of 30, 50, 500 ng/mL. Low retention SureOne plastic pipette tips and Eppendorf LoBind microcentrifuge tubes were used to avoid THCV adherence to plastic. The samples were covered with aluminum foil and incubated for 24 h in an orbital shaker (185 rpm) at 37°C. Preparation of organic solvents mixed with CBD-D3 internal standard involved adding 196.8 µL of 100 ng/ml of CBD-D3 to each solvent (isooctane, 2-Octanol, acetonitrile) to a total volume of 12 mL and vortex mixed for 30 s. Mobile phase A and B were prepared as described above (See section 3.2.1) and mixed together with 11.63 mL of mobile phase B and 3.37 ml of mobile phase A. Following the incubation, 610 µL of isooctane with internal standard were

vortexed for 30 s with each sample in dry ice and centrifuged for 3 min at 5000 rpm. 500 µL of the isooctane layer was transferred to borosilicate glass tubes for each sample, dried using ThermoLyne Dri-Bath and reconstituted with 200 µL of mobile phase A+B. The remaining plasma in dry ice was next mixed with 610 µL of 2-Octanol with internal standard, vortexed for 30 s, and centrifuged for 3 min at 5000 rpm. 500 µL of the 2-Octanol layer was transferred to borosilicate glass tubes, dried using ThermoLyne Dri-Bath and reconstituted with 200 µL of mobile phase A+B. The final plasma portion in dry ice was mixed with 610 µL of acetonitrile with internal standard, vortexed for 30 s, and centrifuged for 3 min at 5000 rpm. Lastly, 500 µL of the acetonitrile layer was transferred to borosilicate glass tubes, dried using ThermoLyne Dri-Bath and reconstituted with 200 µL of mobile phase A+B. Finally, all samples reconstituted with 200 µL mobile phase A+B in borosilicate glass tubes were vortex mixed for 30 s and transferred to amber HPLC amber vials with inserts for LC-MS/MS analysis. The absolute recovery of THCV was determined as the amount of THCV extracted relative to the final concentration of working standards (low, mid, high) mixed in 190 µL of blank human pooled plasma.

3.4. Enzyme Kinetic Studies

Enzyme kinetic analysis was performed using pooled HLM; Pooled human liver (pool of 50) microsomes were from mixed gender subjects purchased from XenoTech, LLC. Metabolic profiles and stability of THCV was evaluated through the determination of intrinsic clearance (Cl_{int}) in HLM. Cl_{int} (a variable that directly measures the efficacy of enzymes for metabolizing substrates) was quantified using the substrate depletion approach where the consumption of substrate is monitored as a function of time [152].

The incubation mixture in 2.0 mL LoBind tubes were comprised of (at their final concentrations): microsomes (0.1, 0.2, 0.25, 0.5, 1.0 mg/mL) in 150 µL aliquots thawed slowly on ice, 2 mM $MgCl_2$, and 50 mM K_2HPO_4 buffer (adjusted with HCl to pH 7.4). THCV concentration (1µM) was incubated in HLM with total incubation volumes of 1.5 mL in all treatments with different microsomal concentrations. Before the reaction, all constituents, excluding NADPH, were preincubated in uncapped tubes with exposure to air at 37°C for 5 min in a shaking water bath. Reactions were initiated by the addition of NADPH (final concentration

1 mM) and kept in the bath for the remainder of the experiment. At multiple incubation time points (0-60 min) at 0, 2, 4, 6, 10, 15, 30, 60 min intervals, aliquots of (50 µL) incubations were withdrawn for all treatments and combined with 500 µL cold internal standard (1.64 ng/mL cannabidiol) in acetonitrile (19.7 mL, final volume of 20 mL) that were previously prepared for each time point and placed in ice thus terminating the reactions. Actual acetonitrile volume was optimized depending on the number of microsomal incubations involved per experiment. Further, all mixtures were centrifuged at 10,000×g for 10 min in an Eppendorf microcentrifuge (Model 5417C, Brinkmann Instruments, Westbury, NY). 200 µL of supernatant were taken in duplicates for all incubations and placed in amber HPLC inserts and vials (Agilent Technologies, USA). Lastly, incubations were later injected onto the Agilent Zorbax Eclipse XDB-C18 analytical column (4.6×150 mm I.D., 5 µm particle size) for LC-MS/MS analysis of THCV. Incubations with no NADPH cofactor, heated microsomes (45°C for 30 min) with THCV, and normal microsomes without THCV were used as negative controls.

3.5 Caco-2 Cell Cyto-toxicity Assays Using THCV

The highest final concentration of THCV was determined that ensured minimal cytotoxicity effects on Caco-2 cells and was further adopted for the permeability assay. Caco-2 cells (see culture conditions below) were seeded at a density of 1×10^5 cells/well in 24-well plates for 24 hours. THCV working concentrations (100, 500, 1000, 3000 µM) were diluted with LC-MS grade MeOH using the primary THCV stock (1 mg/mL). 10 µL of THCV working concentrations were added in five replicates into each well containing 1 mL of media for an additional 24 hours to achieve final THCV concentrations (1, 5, 10, 30 µM). THCV stocks were prepared from the previous day at concentrations of 100 to 3000 µM to account for the organic solvent, methanol. 10 µL of 100% methanol was added as vehicle control in four replicates. On the second day, 1 mL of DMEM containing 2% FBS and 1% NEAA was refreshed into each well before adding THCV. Upon collection, media was removed and 400 µL of TrypLE was added to each well for cell detachment for 15-20 min. The mixtures were washed over the bottom of the well several times to remove weakly attached cells and transferred to microcentrifuge tubes. In each microcentrifuge tube, 20 µL of cell suspension was mixed with 20µL of trypan blue and 10

μL resultant solution was added to one chamber of the cell counting slide. Each sample was counted in both chambers using the BioRad TC20 automated cell counter. Cell viability in percent was recorded for each well.

3.6 Caco-2 Cell Permeability Assays Using THCV

The Caco-2 cell line was used as an *in vitro* model to simulate the intestinal epithelium for investigating the permeation of THCV. Caco-2 cells with passage number 20-30 were grown in DMEM containing 10% FBS and 1% NEAA in conditions of 95% O_2 and 5% CO_2 at 37°C. Cells were sub-cultured using 2.5% trypsin, versene for cellular detachment and seeded in 24-well Transwell plates with permeable supports (polyester membrane pore size 0.4 μm, insert diameter 6.5 mm) at a density of 1×10^4 cells/well once they reached 70-90% confluency. DMEM was replaced three times per week in all compartments and was incorporated in experiments after 21 days in culture.

On the day of the experiment, cells in both compartments were washed with HBSS with 20 mM HEPES. Initial TEER measurements were measured using a Millicell-ERS Volt-ohm meter after the monolayer was equilibrated for 15 min at 37°C. THCV with a final concentration of 10 μM was added to apical (200 μL) or basal (600 μL) compartments with fresh replacements of HBSS+HEPES. At various incubation times (0, 15, 30, 45, 60 min) full volume of both compartments was removed and stored in LoBind microcentrifuge tubes and placed at -80°C until further LC-MS/MS analysis. After sample collection, cells were washed in HBSS before the assessment of post TEER. Lucifer Yellow, a marker for paracellular flux, in HBSS at a concentration of 0.1mg/mL was added to the apical compartment of each insert for 60 min. After 60 min, all permeable inserts were transferred to an empty plate and LY was aspirated, the fluorescence level of the basal compartment was determined using the Biotek Synergy HT microplate reader with adjusted excitation wavelength of 485 nm and 535 nm for emission. TEER evaluations and LY assays were implemented as parameters for assessing the integrity of the monolayer barrier throughout the experiment. After microplate reading, the emptied inserts were placed back onto the original plate in the same order. 200 μL of 10% ACN was added to each inserts for lysing the cells at room temperature for 1 h, cell lysates were then collected. The

600 µL of HEPES in the basal compartment for each well that were subjected to the microplate reader were also collected for mass balance calculations. In Transwell plates with no seeded Caco-2, THCV permeation and sample collection up to 60 min was similar as previously described. Plate with no cells did not undergo LY assay but 200 µL of 10% ACN was added to each insert for mimicking cell lysing procedure at room temperature for 1 h and 600 µL of HEPES in the basal compartment was collected for each well. Following quantitative analysis using LC-MS/MS, apparent permeability coefficients (P_{app}) and efflux ratios (EFR) were determined using established equations (see Data Analysis) that allow for subsequent predictions of *in vivo* intestinal permeability ($P_{eff,man}$) and bioavailability (F_a) of THCV [140].

3.7. Intestinal Organoid Model Establishment

The following methodology was adopted and summarized from STEMdiff ™ intestinal organoid manual. Human induced pluripotent stem cells (iPSCs), UCSD086i-6-3 derived from skin fibroblast, were cultured in complete mTeSR™1 medium in tissue culture-treated 6-well plates or T-75 flasks coated with Matrigel®. They were ready for passage when the colonies exhibited dense centres compared to their edges, which usually takes place after 5 days with enzyme-free passage reagent. Passaged cells were then plated onto 24-well plates coated with Matrigel® and differentiation to definitive endoderm was performed using specific medium after cell confluency was assessed after 24 hours. Each bottle of Matrigel® (5 mL) was aliquoted using a specific dilution factor stated in its certificate of analysis. 342 µL was aliquoted for each Matrigel® bottle in our lab. For coating, one aliquot of Matrigel® was mixed with 25 mL of DMEM, and 1 mL of Matrigel® with DMEM was added to each well in a TC-treated 6-well plate. 1 mL of volume was evenly distributed and covered each well before stem cell passage. From Day 4-9, cells were differentiated to mid/hindgut layers resembling spheroids with daily media change. Spheroid suspension were added to a new 24-well plate for counting. Cell aggregates ≥ 75 µm in diameter promised good yields for yielding intestinal organoids. Subsequently, Matrigel® was added with spheroids in tubes and were transferred onto a Nunclon® Delta surface treated 24-well tissue forming domes. After approximately seven to ten days, spheroids were passaged forming intestinal organoids. However, multiple passages were required for establishing

long-term organoids in relation to their density, size, and morphology for optimal results. Cryo-preservation of intestinal organoids were performed after passage four or approximately 7-8 weeks.

3.8. Inflammatory Biomarkers and Quantitation

Inflammatory biomarkers were predominantly quantified in terms of cytokine recruitment. In the first preliminary experiment using intestinal organoids, lipopolysaccharide (LPS, 50, 500 ng/mL), LPS with fluorescent conjugate (50 ng/mL), tumor necrosis alpha (TNFα, 10, 50 ng/mL) and interferon gamma (IFNγ, 10, 50 ng/mL) were added to the media for 48 hours to simulate chronic inflammation with two untreated wells and three wells with added sterile water in a 12-well plate. After 48 hours, the supernatant from all wells was collected and RIPA lysis agent was added to the Matrigel with the organoids before collection. Formalin was added in the well with fluorescent LPS and stored at 4°C. Lowry assay was conducted to determine the total protein level in samples before proceeding with Western Blot. TNF-α, IL-6, IL-10, and iNOS were quantitated by their corresponding primary and secondary antibodies derived from mouse or rabbit.

3.8.1. Western Blot

Gels were made prior to experimentation using the Mini-PROTEAN® Tetra Cell Casting Module (Bio-Rad, CA, USA). Four, 10-well, 1 mm gels were made at once with two layers: the resolving gel and the stacking gel. To make four gels, components in the resolving gel were poured first into the casting stands including 4.7 mL of dH_2O, 5 mL of buffer A (90.9 g of Tris-base, 2 g of SDS, pH 8.8 with HCl in 500 mL of dH_2O), 10 mL of 30% Acryl-Bis, 200 µL of 10% SDS, 100 µL of 10% APS, and 20 µL of TEMED. Components in the stacking gel were poured after the resolving gel solidified including 6 mL of dH_2O, 2.5 mL of buffer C (30.3g of Tris-base, 2 g of SDS, pH 6.8 with HCl in 500 mL of dH_2O), 1.4 mL of 30% Acryl-Bis, 100 µL of 10% SDS, 50 µL of 10% APS, and 10 µL of TEMED. Once solidified, each gel was wrapped in wetted paper towel, plastic ceramic wrap, and stored in fridge at 4°C.

For protein extraction, intestinal organoids were lysed in 300 µL of RIPA buffer (1X) with PIC (1X) and denatured using dry bath at 100°C for 5 min. For each sample, 0.5 µg/µL of protein was loaded and separated on 15% SDS PAGE gels in 1X running buffer (10X: 30.3 g Tris-base, 144 g glycine, 10 g SDS in 1L of deionized water) at 50 constant Volts for 30 min and at 180 Volts for additional 60 min using the POWER PAC 200 (Bio-Rad, CA, USA). Gels were transferred on to nitrocellulose/filter paper sandwich (Thermo Scientific, Toronto, ON) in transfer buffer (12 g Tris-base, 57.6 g glycine, 150 mg SDS, 800 mL MeOH). Gels were further submerged in electrophoresis tanks (Bio-Rad) at 230 constant mAmps for 90 minutes. Membranes were washed in 1X TBS (10X: 30 g Tris-base, 80 g NaCl in 1L of deionized water at pH 7.4) with 500 µL Tween20 (TBST) for 30 min; membranes were blocked in 5% BSA in 50 mL of 1X TBST for 60 min. Membranes were probed with primary antibodies such as IL-6 (Thermo Scientific) and iNOS (Sigma-Aldrich) in dilution of 1:1000 in 5% BSA in TBST overnight at 4°C. Next morning, membranes were washed in TBST for 30 min and probed with LI-COR IRDye® 800CW Goat anti-Rabbit IgG secondary antibody (1:2000) in 5% skim milk with TBST for 60 min under aluminum foil. Membranes were imaged on LI-COR Odyssey® Infrared Imaging System.

3.9. Data and Statistical Analysis

Substrate depletion rate constant (k_{dep}) and Cl_{int} involved in the hepatic microsomal studies were estimated using previously established methods by Obach and Reed-Hangen and Giuliano *et al* [152,160]. Similar methodology was adopted and modified from our previous lab member, Chaojie Lin [161]. The THCV/internal standard (CBD-D3) peak area was determined and standardized to the ratio obtained at time, t=0, which shows the substrate remaining at 100%. A graph of natural log showing THCV percentage remaining versus time was established for calculating the substrate depletion rate constant (k_{dep}), which is determined as the slope of each linear line at each THCV concentration. The K_m and $k_{dep([S] \rightarrow 0)}$ were calculated by plotting k_{dep} versus all initial THCV concentrations through nonlinear least squares regression using Prism 8.3.0 (GraphPad Prism, San Diego, CA, USA) with Eq 3.1 showed below:

$$k_{dep} = k_{dep([S]\rightarrow 0)} \text{ X } (1 - \frac{[S]}{[S] + K_m})$$

(Eq 3.1)

where k_{dep} is the apparent depletion rate constant following first-order kinetics, $k_{dep([S] \rightarrow 0)}$ is the theoretical maximum depletion rate constant at an infinitesimally low substrate concentration, [S] is the THCV concentration and the Michaelis-Menten constant, K_m. The intrinsic clearance (Cl_{int}) or the intrinsic clearance at infinitesimally low substrate concentration ($Cl_{int,\ app([S]=0)}$) was calculated by dividing $k_{dep([S] \rightarrow 0)}$ with various microsomal protein concentrations. V_{max}, the maximum rate of reaction catalyzed by microsomes was calculated as a product of $k_{dep([S] \rightarrow 0)}$ and K_m. Further, the intrinsic clearance (Cl_{int}) was also calculated as the Dose/AUC_∞ where Dose is the initial quantity of THCV in the microsomal mixture (unit of mol/mg microsomal protein), and AUC_∞ is the area under the curve (concentration versus time) extrapolated to infinity (unit of Molar (mol/L) · h). The unit for Cl_{int} is l/h/mg protein and conversion for μL/min/mg is often adopted for *in vitro* comparison of stability assays. Subsequently, using the LESA model where plotting the reciprocal of Cl_{int} (same THCV concentration) versus different microsomal concentrations (*M*) may result in a straight-line intersecting at the y-intercept with $1/Cl_{int}$ with *K'* denoting a proportionality constant (Eq 3.2).

$$\frac{1}{\mathrm{Cl_{int}}} = \frac{1}{\mathrm{Cl_{int}}} + \frac{K'}{\mathrm{Cl_{int}}} \text{ X M}$$

(Eq 3.2)

With respect to the Caco-2 and organoid models, the comparison of means between two or multiple groups was conducted using Prism 8.3.0 with statistical tests such as the independent Student's *t* test and one-way analysis of variance (ANOVA) paired with Tukey's test for parametric data. Data was expressed as mean ± SD with level of significance at $p < 0.05$.

For the Caco-2 permeability assay, the apparent permeability coefficient (P_{app}) can be determined following the LC-MS/MS analysis of the permeability samples. P_{app} is defined as the compound's permeation rate or flux through the Caco-2 monolayer in cm/s [162]. dQ/dt is needed

for calculating P_{app} which is the apparent steady-state permeation rate (μM/s) in the basal chamber determined from the linear portion of the drug permeation vs time profile. Further, the surface area of the inserts (cm^2) as well as the initial concentration (μM) in the donor chamber are also required (Eq 3.3). Lastly, the $P_{app(B\rightarrow A)}$ over $P_{app(A\rightarrow B)}$ is calculated as the efflux ratio (Eq 3.4) shown below.

$$P_{app}(cm/sec) = \frac{dQ}{dt} \text{ X } \frac{1}{C_{\substack{initial \\ donor}} \text{ X } A} \qquad \text{(Eq 3.3)}$$

$$\frac{P_{app(B\rightarrow A)}}{P_{app(A\rightarrow B)}} \qquad \text{(Eq 3.4)}$$

4. RESULTS

4.1. LC-MS/MS Method Validation for THCV

A LC-MS/MS method was previously developed and validated for the quantitative determination of THCV in HLM for ensuring the specific detection and quantitation in THCV concentration presented in each sample. Figure 4.1 displays an LC-MS/MS chromatogram where THCV was found in incubations consisting of human liver microsomes (HLM), $MgCl_2$, and K_2HPO_4 at room temperature for 1 h. LC-MS/MS analysis showed THCV's retention time at 1.76 min with symmetrical peak shape and internal standard, CBD-D3, exhibiting a similar elution time. Table 4.1 and Table 4.2 summarized the intraday and interday accuracy and precision of quality control standards of THCV in microsomal mixtures. The intraday accuracy for quality control levels except LLOQ (Day 2: 115.1%, Day 3: 116.7%) and MQC (Day 3: 112.5%) were < 10% with an intraday accuracy range of 90.5% to 116.7%. The intraday precision except for LLOQ (Day 1: 12.3%, Day 3: 16.9%) were < 10% with an intraday precision range of 2.5%. to 16.9%. The interday precision and accuracy for all quality controls (LLOQ, LQC, MQC, HQC) were < 10% with an interday precision range of 4.7% to 5.3% and interday accuracy range of 96.3% to 100.8%. The linear range of the calibration curve was from 1.96 ng/mL to 500 ng/mL with an average coefficient of determination (R^2) of 0.9981 over three days.

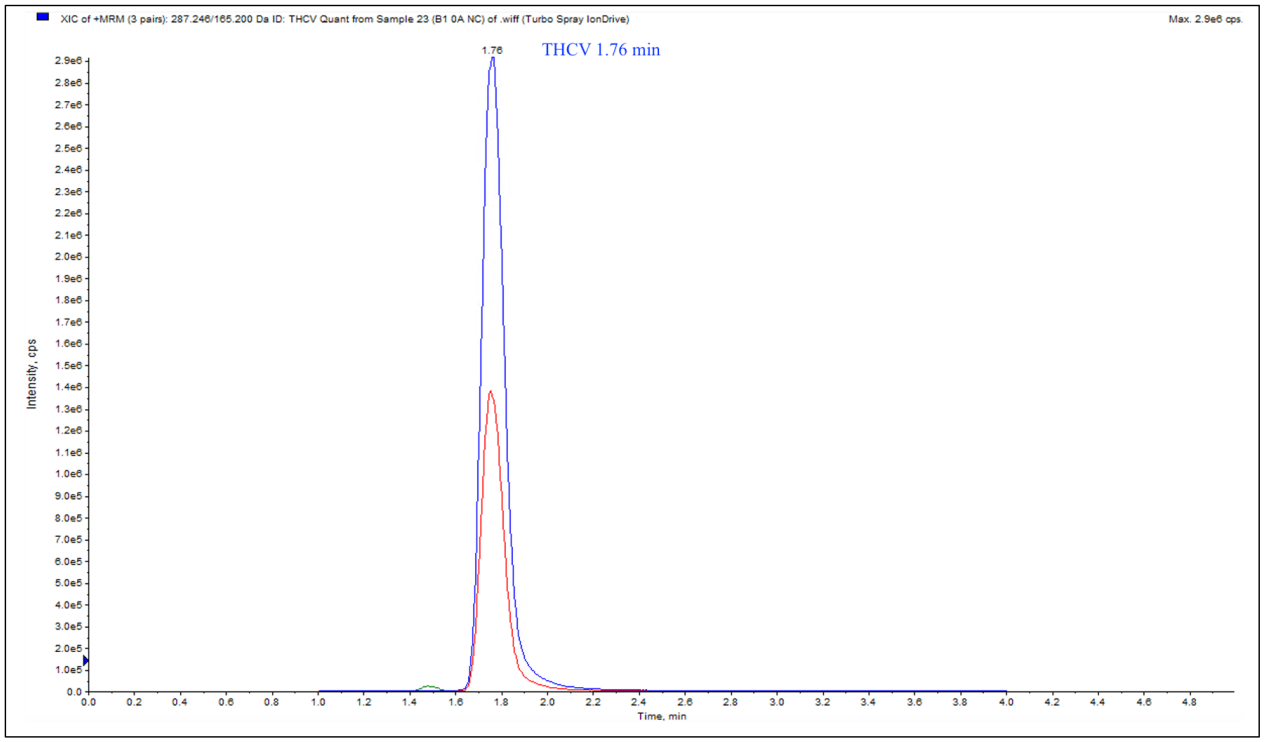

Figure 4.1 Representative LC-MS/MS chromatogram of human liver microsomes spiked with internal standard (CBD-D3 100 ng/mL, 1.76 min) and THCV (1 µM, 1.76 min). Conditions: Agilent 1290 Infinity binary pump coupled with AB Sciex 6500 QTrap triple quadrupole; Agilent Zorbax Eclipse XDB-C18 analytical column (4.6×150 mm., 5 µm); mobile phase A: LCMS-grade water with 0.1% formic acid, mobile phase B: LCMS-grade methanol with 0.1% formic acid

Table 4.1 Intraday accuracy and precision in mass spectrometry bioanalytical parameters of THCV in K_2HPO_4 and human liver microsomes (n = 6)

QC levels	**Precision (%)**	**Accuracy (%)**
LLOQ		
Day 1	12.3	101.3
Day 2	5.7	115.1
Day 3	16.9	116.7
LQC		
Day 1	4.5	90.5
Day 2	5.8	109.8
Day 3	7.7	105.4
MQC		
Day 1	5.8	101.6
Day 2	2.7	104.1
Day 3	3.7	112.5
HQC		
Day 1	5.4	107.3
Day 2	3.2	106.2
Day 3	2.5	108.9

Accuracy = 100 $[Analyte]_{measured}/[Analyte]_{nominal}$

Precision = 100 S.D./$[Analyte]_{measured, average}$

* LLOQ for THCV is 1.96 ng/mL; LQC for THCV is 5.0 ng/mL; MQC is 175 ng/mL and HQC is 375 ng/mL

Table 4.2 Interday accuracy and precision in mass spectrometry bioanalytical parameters of THCV in K_2HPO_4 and human liver microsomes (n = 6)

QC levels	**Precision (%)**	**Accuracy (%)**
LLOQ	5.3	97.5
LQC	4.7	96.3
MQC	6.1	99.2
HQC	4.8	100.8

Accuracy = 100 $[Analyte]_{measured}/[Analyte]_{nominal}$

Precision = 100 S.D./$[Analyte]_{measured, average}$

* LLOQ for THCV is 1.96 ng/mL; LQC for THCV is 5.0 ng/mL; MQC is 175 ng/mL and HQC is 375 ng/mL

4.2. Linearity of Calibration Curve and Intraday & Interday Accuracy and Precision of Quality Control (QC) Standards in Pooled Human Plasma

Bioanalytical parameters involving linearity of calibration curve, intraday and interday accuracy and precision of quality control (QC) standards were conducted in pooled human plasma to ensure the specific detection and quantitation of THCV concentration for plasma protein binding experiments involving the 3-solvent extraction method using isooctane, 2-Octanol, and acetonitrile. Standard curves prepared in pooled human plasma with THCV concentrations ranged from 0.49-125 ng/mL showed linearity ($R^2 \geq 0.98$) during the 3 days of independent experiments (Figure 4.2). THCV slopes displayed consistency with an average of 0.1350 ± 0.048. All standard curve points have passed the acceptable criteria for accuracy.

Table 4.3 and Table 4.4 summarize the intraday and interday accuracy and precision of quality control standards of THCV in pooled human plasma. The intraday accuracy for all quality control levels were within 10% with an intraday accuracy range of 97.6% to 109%. The intraday precision except for LLOQ (Day 1: 13.2%) were < 10% with an intraday precision range of 3.6%. to 13.2%. The interday precision and accuracy for all quality controls (LLOQ, LQC, MQC, HQC) were < 10% with an interday precision range of 3.9% to 7% and interday accuracy range of 97.5% to 108.1%.

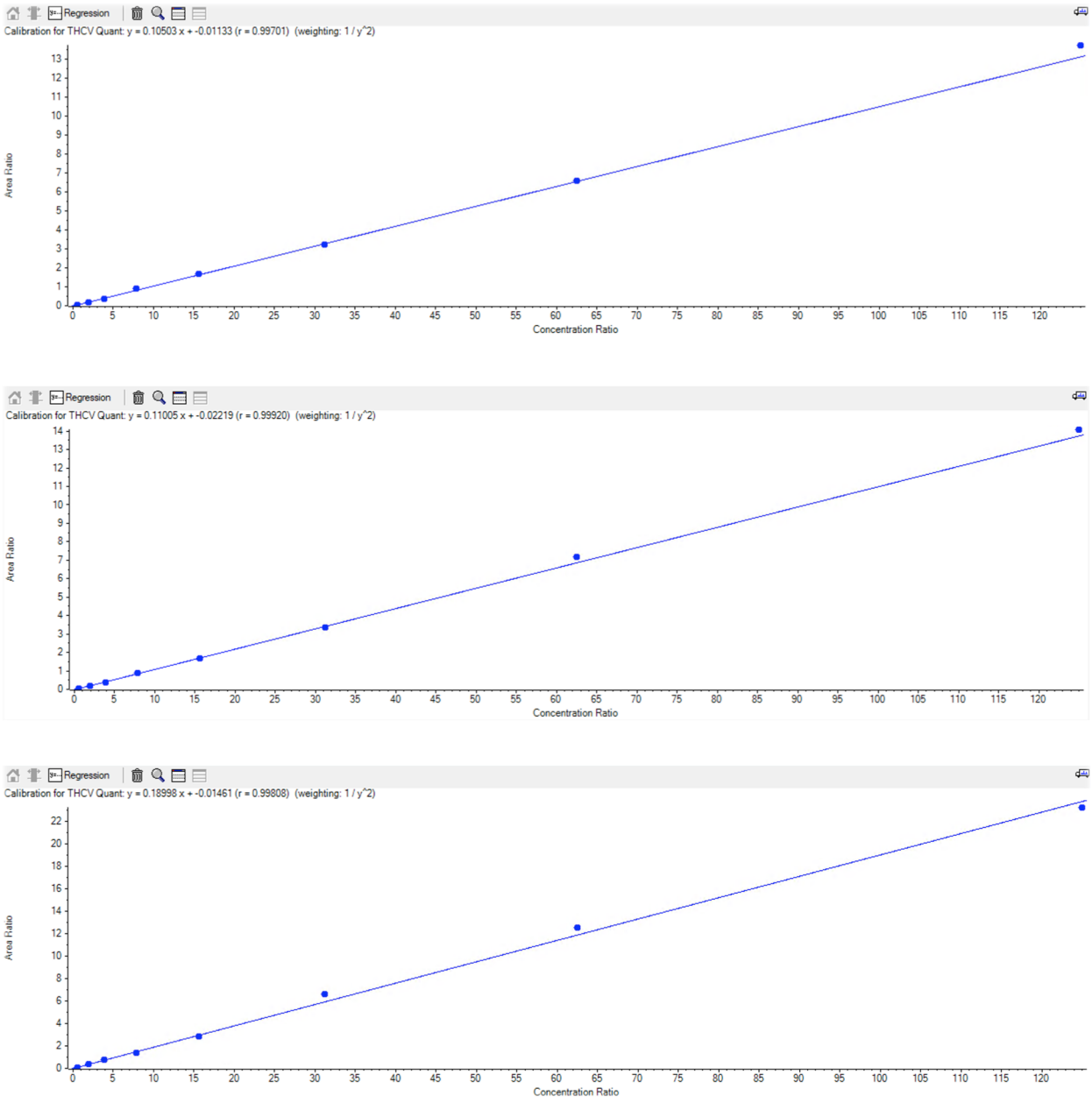

Figure 4.2 Standard curves of THCV during 3 days of plasma protein binding experiments involving the 3-solvent extraction method in pooled human plasma, showing linearity with R^2 values ≥0.98. THCV has 7 standard points, ranging from 0.49-125 ng/mL. Standard curves were weighted $1/y^2$ for improving the regression fit for low standard concentrations. *Plots were generated and modified in MultiQuant™ software.

Table 4.3 Intraday accuracy and precision in mass spectrometry bioanalytical parameters of THCV in pooled human plasma (n = 3)

QC levels	**Precision (%)**	**Accuracy (%)**
LLOQ		
Day 1	13.2	109.0
Day 2	8.9	101.2
Day 3	9.3	108.9
LQC		
Day 1	7.4	107.6
Day 2	4.9	101.4
Day 3	6.1	102.3
MQC		
Day 1	3.8	100.3
Day 2	4.1	97.6
Day 3	6.5	105.2
HQC		
Day 1	4.4	106.7
Day 2	5.8	108.2
Day 3	3.6	103.5

Accuracy = 100 $[\text{Analyte}]_{\text{measured}}/[\text{Analyte}]_{\text{nominal}}$

Precision = 100 S.D./$[\text{Analyte}]_{\text{measured, average}}$

* LLOQ for THCV is 0.49 ng/mL; LQC for THCV is 1.4 ng/mL; MQC is 50.6 ng/mL and HQC is 101.2 ng/mL

Table 4.4 Interday accuracy and precision in mass spectrometry bioanalytical parameters of THCV in pooled human plasma (n = 3)

QC levels	**Precision (%)**	**Accuracy (%)**
LLOQ	3.9	97.5
LQC	4.8	98.8
MQC	5.5	105.5
HQC	7.0	108.1

Accuracy = 100 $[\text{Analyte}]_{\text{measured}}/[\text{Analyte}]_{\text{nominal}}$

Precision = 100 S.D./$[\text{Analyte}]_{\text{measured, average}}$

* LLOQ for THCV is 0.49 ng/mL; LQC for THCV is 1.4 ng/mL; MQC is 50.6 ng/mL and HQC is 101.2 ng/mL

4.3. Linearity of Calibration Curve and Intraday & Interday Accuracy and Precision of Quality Control (QC) Standards in Hank's Balanced Salt Solution (HBSS)

Bioanalytical parameters involving linearity of calibration curve as well as intraday and interday accuracy and precision of quality control (QC) standards were conducted in Hank's balanced salt solution (HBSS) to ensure the specific detection and quantitation of THCV concentration in Caco-2 permeability assays. Standard curves prepared in HBSS with THCV concentrations ranged from 0.49-125 ng/mL showed linearity ($R^2 \geq 0.98$) during 3 occasions of independent experiments (Figure 4.3). THCV slopes displayed consistency with an average of 0.1553 ± 0.007. All standard curve points passed the acceptable criteria for accuracy.

Table 4.5 and Table 4.6 summarized the intraday and interday accuracy and precision of quality control standards of THCV in HBSS. The intraday accuracy for quality control levels except LLOQ (Day 1: 110.4%, Day 2: 111.3%) and HQC (Day 1: 112.1%) were < 10% with an intraday accuracy range of 98.4% to 112.1%. The intraday precision for quality control standards were < 10% with an intraday precision range of 1.6%. to 9.2%. The interday precision and accuracy for all quality controls (LLOQ, LQC, MQC, HQC) were < 10% with an interday precision range of 3.2% to 8.1% and interday accuracy range of 93.6% to 107.7%.

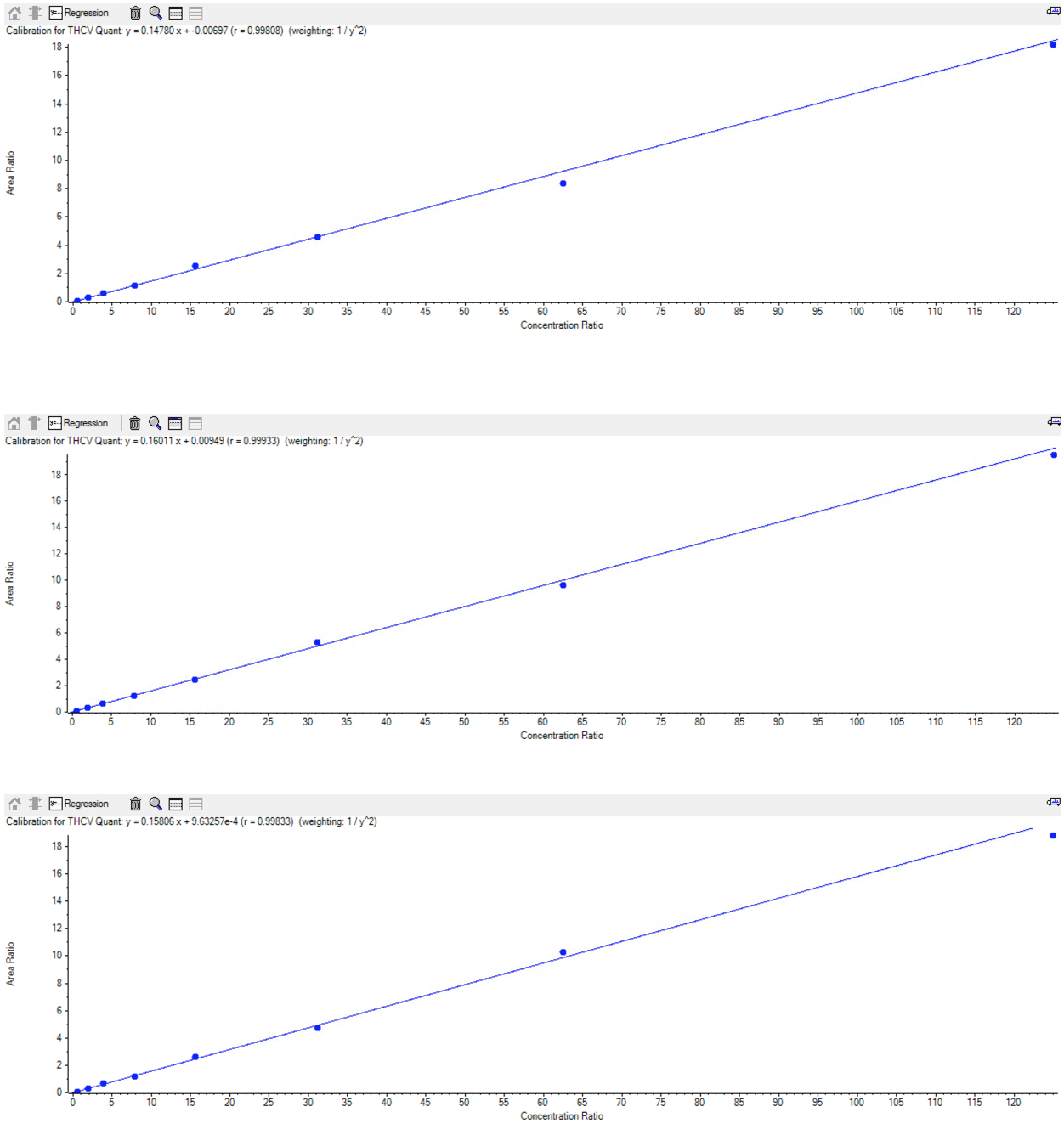

Figure 4.3 Standard curves of THCV during 3 days of Caco-2 permeability assays in Hank's balanced salt solution (HBSS), showing linearity with R^2 values ≥0.98. THCV has 7 standard points, ranging from 0.49-125 ng/mL. Standard curves were weighted $1/y^2$ for improving the regression fit for low standard concentrations. *Plots were generated and modified in MultiQuant™ software.

Table 4.5 Intraday accuracy and precision in mass spectrometry bioanalytical parameters of THCV in Hank's balanced salt solution (HBSS) (n = 3)

QC levels	**Precision (%)**	**Accuracy (%)**
LLOQ		
Day 1	8.1	110.4
Day 2	7.3	111.3
Day 3	9.2	107.0
LQC		
Day 1	6.9	109.1
Day 2	5.1	108.2
Day 3	3.7	105.8
MQC		
Day 1	1.6	99.0
Day 2	3.3	98.4
Day 3	2.8	103.5
HQC		
Day 1	3.6	112.1
Day 2	1.9	103.8
Day 3	3.1	105.6

Accuracy = 100 $[\text{Analyte}]_{\text{measured}}/[\text{Analyte}]_{\text{nominal}}$

Precision = 100 S.D./$[\text{Analyte}]_{\text{measured, average}}$

* LLOQ for THCV is 0.49 ng/mL; LQC for THCV is 1.4 ng/mL; MQC is 50.6 ng/mL and HQC is 101.2 ng/mL

Table 4.6 Interday accuracy and precision in mass spectrometry bioanalytical parameters of THCV in Hank's balanced salt solution (HBSS) (n = 3)

QC levels	**Precision (%)**	**Accuracy (%)**
LLOQ	6.3	93.6
LQC	3.9	103.9
MQC	8.1	107.7
HQC	3.2	99.2

Accuracy = 100 $[Analyte]_{measured}/[Analyte]_{nominal}$

Precision = 100 S.D./$[Analyte]_{measured, average}$

* LLOQ for THCV is 0.49 ng/mL; LQC for THCV is 1.4 ng/mL; MQC is 50.6 ng/mL and HQC is 101.2 ng/mL

4.4. Determination of the Unbound Fraction of THCV in Human Plasma

The 3-solvent extraction method uses liquid-liquid extraction with 3 different solvents to quantify the unbound, lipoprotein bound, and remaining plasma protein bound fractions with serial additions of isooctane, 2-octanol, and acetonitrile, respectively. The relative extent of THCV binding to protein albumin and lipoprotein fractions in human plasma was presented in Table 4.7 and 4.8 for intraday and interday recovery. The 3-solvent extraction technique was repeated over three days in replicates of six at 30, 50, and 500 ng/mL of THCV to yield congruent values thus validating the reproducibility and reliability of the method.

For intraday recovery of THCV (Table 4.7), the percentages of unbound THCV, associated with lipoproteins, and remaining proteins in human plasma at 30 ng/mL were approximately 6.2%, 2.8%, and 90.9%, respectively. The percentages of unbound THCV, associated with lipoproteins, and remaining proteins in human plasma at 50 ng/mL were approximately 9.6%, 4.3%, and 85.5%, respectively. The percentages of unbound THCV, associated with lipoproteins, and remaining proteins at 500 ng/mL were 10.8%, 11.3%, and 74.8% respectively. There was an increased percent recovery in lipoprotein and decreased percent recovery in the remaining plasma fraction moving from 30 to 500 ng/mL of THCV. In addition, the highest THCV concentration at 500 ng/mL involved was calculated to be equal to 1.7 μM which indicated that saturation of binding was unlikely to be achieved. One caveat was that 42 ng/mL of THCV was not detected compared to the total theoretical concentration of THCV at 500 ng/mL.

Table 4.7 Intraday recovery of THCV (ng/mL, %) in isooctane, 2-octanol, and acetonitrile following use of the 3-solvent extraction method in pooled human plasma (n = 6).

Drug	Theoretical Concentration (ng/mL)	Free Cannabinoid Isooctane Concentration (mean ± SD; ng/mL)	Lipoprotein-Cannabinoid 2-Octanol Concentration (mean ± SD; ng/mL)	Protein-Cannabinoid Acetonitrile Concentration (mean ± SD; ng/mL)	Total Observed Concentration (mean ± SD; ng/mL)
THCV	30	1.85 ± 0.8 (6.2%)	0.85 ± 0.3 (2.8%)	27.26 ± 1.9 (90.9%)	29.96 ± 0.4
	50	4.78 ± 0.9 (9.6%)	2.13 ± 0.6 (4.3%)	42.77 ± 2.7 (85.5%)	49.68 ± 1.9
	500	54.22 ± 4.6 (10.8%)	56.52 ± 8.3 (11.3%)	374.08 ± 4.1 (74.8%)	457.82 ± 18.3

For interday recovery of THCV (Table 4.8), pooled from 18 replicates of THCV samples at each standard concentration (30, 50, 500 ng/mL), the percentages of unbound THCV, associated with lipoproteins, and remaining proteins in human plasma at 30 ng/mL were approximately 8.2%, 2.5%, and 89.3%, respectively. The percentages of unbound THCV, associated with lipoproteins, and remaining proteins in human plasma at 50 ng/mL were approximately 10.9%, 6.1%, and 83.0%, respectively. The percentages of unbound THCV, associated with lipoproteins, and remaining proteins at 500 ng/mL were 12.4%, 10.8%, and 76.8% respectively. Overall, the average unbound fraction ($f_{u(b)}$) of THCV calculated from the 18 replicates at each THCV concentration was found to be 10.5% or 0.105. The interday results also showed increased percent recovery in lipoprotein and decreased precent recovery in the remaining plasma fraction moving from 30 to 500 ng/mL of THCV. In summary, the total of unbound THCV, bound to lipoprotein and in the remaining plasm proteins was very close to the nominal concentration, suggesting high recovery of this cannabinoid can be obtained through the 3-solvent extraction procedure.

Table 4.8 Interday recovery of THCV (ng/mL, %) in isooctane, 2-octanol, and acetonitrile following use of the 3-solvent extraction method in pooled human plasma (n = 18).

Drug	Theoretical Concentration (ng/mL)	Free Cannabinoid Isooctane Concentration (mean ± SD; ng/mL)	Lipoprotein-Cannabinoid 2-Octanol Concentration (mean ± SD; ng/mL)	Protein-Cannabinoid Acetonitrile Concentration (mean ± SD; ng/mL)	Total Observed Concentration (mean ± SD; ng/mL)
THCV	30	2.37 ± 0.9 (8.2%)	0.72 ± 0.4 (2.5%)	25.83 ± 2.4 (89.3%)	28.92 ± 1.7
	50	5.21 ± 1.1 (10.9%)	2.92 ± 0.5 (6.1%)	39.68 ± 3.8 (83.0%)	47.81 ± 3.5
	500	58.68 ± 3.4 (12.4%)	51.11 ± 7.9 (10.8%)	363.46 ± 5.3 (76.8%)	473.25 ± 12.6

4.5. *In Vitro* Hepatic Intrinsic Clearance of THCV

The hepatic intrinsic clearance of THCV was determined using the substrate depletion approach. One THCV concentration was incubated with different concentrations of liver microsomes for a total of 60 min. Figure 4.4 showed the natural log percent remaining of THCV (1 μM) in 0.1, 0.2, 0.25, 0.5, and 1.0 mg/mL HLM. In 10 min of metabolism, THCV depletion was the greatest in 1.0 mg/mL HLM with k_{dep} of 0.237 and the least in 0.1 mg/mL HLM with k_{dep} of 0.142. Variation did remain in replicates within treatments; however, correlations were exhibited for each treatment as shown by the R^2 values ranging from 0.95-0.98 (Table 4.9). Control incubations with heated microsomes, without microsomes and no NADPH showed no substrate depletion over time.

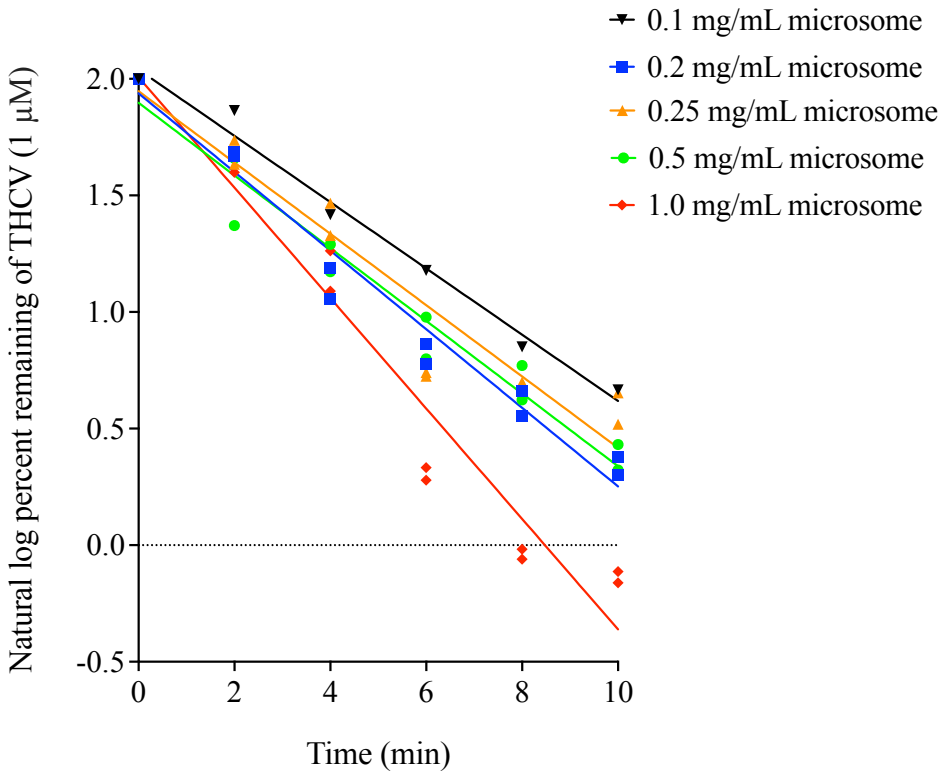

Figure 4.4 A plot of natural log percent remaining of THCV (1 µM) after 10 min of hepatic metabolism in 0.1, 0.2, 0.25, 0.5, and 1.0 mg/mL microsomes (n = 2).

Table 4.9 Linear regression analysis of THCV (1 μM) after 10 minutes of hepatic metabolism in 0.1, 0.2, 0.25, 0.5, and 1.0 mg/mL microsomes (n = 2).

Microsomal proteins (mg/mL)	**Linear regression parameters**		
	Equation	k_{dep}	R^2
0.1	y = -0.1421x + 2.040	-0.1421	0.9784
0.2	y = -0.1686x + 1.938	-0.1686	0.9709
0.25	y = -0.1530x + 1.947	-0.1530	0.9523
0.5	y = -0.1559x + 1.898	-0.1559	0.9622
1.0	y = -0.2369x + 2.007	-0.2369	0.9547

The linear extrapolation in the stability assay (LESA) model enables the direct calculation of *in vitro* intrinsic clearance Cl_{int} in the absence of the unbound fraction of the drug. The *in vitro* Cl_{int} of THCV was determined collectively in five different concentrations (0.1, 0.2, 0.25, 0.5, 1.0 mg/mL) of pooled HLMs (Figure 4.5). In the LESA model, when $1/Cl_{int}$ (min*mg/µL) was graphed against the HLM concentrations (mg/mL), $1/Cl_{int,u}$ was interpolated as the y-intercept from the linear regression analysis. Figure 4.5 showed that $1/Cl_{int}$ of THCV was directly proportional to the microsomal concentrations with coefficient of determination (R^2) of 0.9875. The $Cl_{int,u}$ of THCV was calculated as 1/y-intercept which yielded a value of 87.7 µL/min/mg.

In terms of the calculations, after LC-MS/MS analysis, the THCV/internal standard (CBD-D3) peak area was determined and standardized to the ratio obtained at time, t = 0, which equaled to 100%. Each percentage value was converted a numeric unit (100% = 1) and subjected to AUC_{∞} analysis. The tail end of the AUC was calculated by the last numeric value/slope (k_{dep}) and was added to the total. Cl_{int} was calculated as Dose/AUC with the dose (finite) converted from micromole to mol and normalized with each microsomal concentration (changing) in mg/mL. Currently, Cl_{int} possessed a unit of mL/h/mg protein with $1/Cl_{int}$ being h*mg/mL. Then, algebraically, multiplied by 60 to convert hour (h) to min and divided by 1000 to convert millilitre (mL) to microlitre (µL) so that $1/Cl_{int}$ became min*mg/µL and Cl_{int} was in µL/min/mg.

Traditionally, the substrate depletion rate constant (k_{dep}) would be calculated using the substrate depletion approach by adopting a range of THCV concentrations (1-500 µM) in one microsomal concentration (0.5 mg/mL). Hence, one k_{dep} value would be quantified for each THCV concentration used per experiment. When plotting the *in vitro* depletion rate constants (k_{dep}) against THCV concentrations (µM), a graph that resembled an exponential decay would be expected as k_{dep} decreases with higher THCV concentrations since microsomal concentration is finite. However, the highest final THCV concentration that could be used in the experiment was 35 µM due to solubility limits. A THCV concentration range capped at 35 µM using this approach would identify only the beginning portion of an exponential decay curve. Given this limitation as well as the desire to understand an unbound intrinsic clearance, the LESA method

was favoured over the substrate depletion approach as described in Section 3.9 of the methods section for calculating the unbound intrinsic clearance ($Cl_{int,u}$) of THCV.

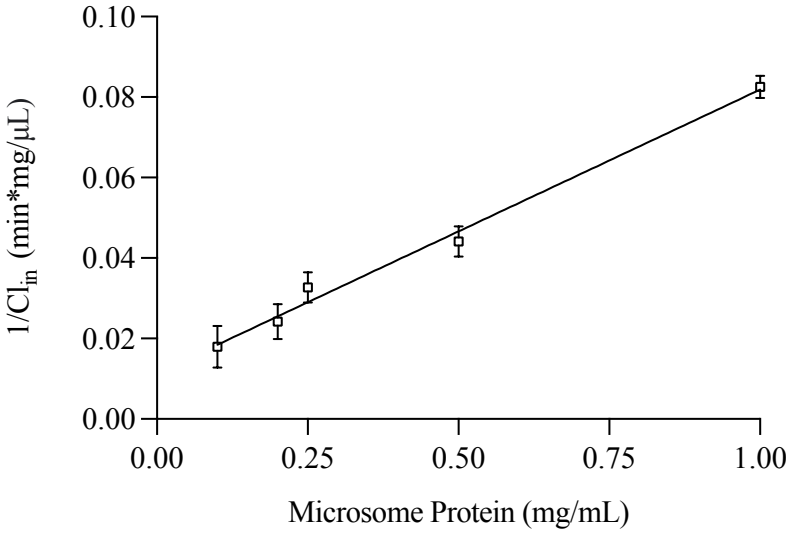

Figure 4.5. Linear correlation between $1/Cl_{int}$ and 0.1, 0.2, 0.25, 0.5, 1.0 mg/mL HLM for tetrahydrocannabivarin. Data were fitted by linear regression ($y = 0.0705x + 0.0114$, $R^2 = 0.9875$). The y-axis intercept corresponded to $1/Cl_{int,u}$. Treatments were conducted in duplicates on three independent days ($n = 6$). Values were presented as SEM with 95% confidence intervals.

4.6. THCV Cytotoxicity in Caco-2 Monolayer

The cytotoxicity of THCV was assessed in Caco-2 monolayers at four concentrations (1, 5, 10, 30 μM) with 1% MeOH as the vehicle control to identify a nontoxic concentration for subsequent Caco-2 permeation assays. 1% organic solvent exhibited a high cell viability of 97.8% ± 1.4. The highest final THCV concentration at 10 μM showed relatively high cell viability of 90.5% ± 3.8. There was a statistically significant decrease ($P < 0.0001$) in cell viability to 25.6% ± 6.8 at 30 μM of THCV (Figure 4.6). Thus, highest non-cytotoxic THCV concentration adopted for Caco-2 permeability assays at 10 μM.

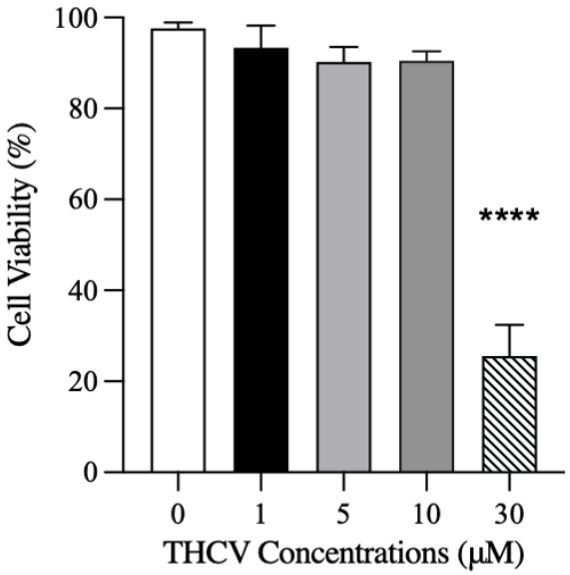

Figure 4.6 Cytotoxicity assay in Caco-2 cell cultures treated with 0, 1, 5, 10, 30 μM THCV for 24 h. Data are represented as mean ± S.D. (n = 5). Statistical differences were analyzed using One-way ANOVA, and multiple comparisons were conducted using Tukey's test: $P < 0.0001$.

4.7. Bidirectional Transfer of THCV Across the Caco-2 Polarized Epithelium

To evaluate the functional barrier integrity across the 21-day period, and before/after permeability experiment, we assessed the transepithelial electrical resistance (TEER, $\Omega*cm^2$), a hallmark for measuring the dynamic integrity of tight junctions, and Lucifer Yellow rejection rate (%), a marker for paracellular flux across the Caco-2 monolayer. According to the literature, Caco-2 TEER values are expected to increase subsequentially post seeding and values above 300 $\Omega*cm^2$ in Transwell plates are deemed appropriate to proceed with experiments. Table 4.10 showed TEER values at Day 10, 15, 20, and before/after permeability assays with THCV (10 μM) for 60 min on six independent days. On Day 21 before experiment, 500.71 ± 20.91 $\Omega*cm^2$ were recorded in inserts from apical to basal direction, and 516.63 ± 22.18 $\Omega*cm^2$ from basal to apical. After experiment, non-significant decreases ($P > 0.05$) were seen in both directions with 481.02 ± 18.43 $\Omega*cm^2$ from apical to basal, and 475.19 ± 21.45 $\Omega*cm^2$ from basal to apical. In addition, average Lucifer Yellow rejection after 0, 15, 30, 45, 60 min of THCV permeation from apical to basal at 10 μM ($n = 1$) was 99.32 ± 0.011 and basal to apical was 99.36 ± 0.016 with no significant difference with respect to either direction (Table 4.11). This finding also validated that final concentration of THCV at 10 μM was non-cytotoxic.

The bidirectional Transwell assays were conducted for investigating the permeability profile of THCV. The mass balance of THCV was calculated as THCV was not quantifiable in the receiver compartment going from apical to basolateral (Table 4.12). It was noted that ~29% of THCV was trapped intracellularly when THCV was added from A → B and ~12 % when added from B → A. Overall, less than ~2% of THCV was detected in the receiver chamber suggesting limited THCV permeation in the Transwell system. In addition, ~12% of THCV was detected intracellularly going from B → A and ~4% from A → B in the absence of Caco-2 suggesting the non-specific binding of THCV to plasticwares.

Table 4.10 Caco-2 monolayer assessment by TEER value ($\Omega*cm^2$) at Day 10, 15, 20, and before/after 60 min of THCV permeation at 10 μM (n = 6). Mean ± S.D was calculated from six Transwell plates.

Time of TEER Measurement	**Transepithelial Electrical Resistance (TEER, $\Omega*cm^2$)**	
	Directional Flux of THCV	
	Apical to Basolateral (Row B)	**Basolateral to Apical (Row C)**
Day 10	249.6 ± 22.83	260.5 ± 19.25
Day 15	343.9 ± 17.31	359.3 ± 15.34
Day 20	464.3 ± 15.82	483.8 ± 18.93
Day 21 Before Experiment	500.7 ± 20.91	516.6 ± 22.18
Day 21 After Experiment	481.0 ± 18.43	475.2 ± 21.45

Table 4.11 Caco-2 monolayer assessment by Lucifer Yellow rejection rate (%) after 0, 15, 30, 45, 60 min of THCV permeation at 10 μM (n = 6). Mean ± S.D was calculated from six Transwells.

THCV Permeation (min)	**Mean ± S.D. Lucifer Yellow Rejection Rates (%)**	
	Directional Flux of THCV	
	Apical to Basolateral (Row B)	**Basolateral to Apical (Row C)**
0	99.4 ± 0.007	99.2 ± 0.005
15	98.9 ± 0.015	99.2 ± 0.003
30	99.5 ± 0.006	99.8 ± 0.002
45	99.8 ± 0.003	99.5 ± 0.004
60	99.0 ± 0.024	99.2 ± 0.008

Table 4.12 Mass balance of THCV in bidirectional Transwell permeability assays. Data are presented as mean ± S.D of six replicates per experiment for six independent days. Mass balance data were expressed as percentage of total mass quantified in three compartments.

Caco-2	Compartments	**Mean ± S.D. Mass Balance of THCV (%)**	
		Apical to Basolateral	**Basolateral to Apical**
THCV (n = 6)	Receiver	0	0.4 ± 0.03
	Donor	29.5 ± 8.28	62.9 ± 11.74
	Cell lysates	29.2 ± 11.07	11.9 ± 4.75
No Caco-2			
THCV (n = 6)	Receiver	0.6 ± 0.05	1.8 ± 0.02
	Donor	31.6 ± 3.76	52.0 ± 9.23
	Mock Cell lysates	17.6 ± 1.78	21.6 ± 2.45

4.8. Intestinal Organoid Establishment

Intestinal organoids (IOs) cultured using the STEMdiff ™ kit showed distinct border with epithelial cells and luminal space (Figure 4.7). Image was captured 12 days after the first passage (Magnification: 4X). Preliminary intestinal organoids experiments were conducted using IO with passage number > 5 to evaluate the anti-inflammatory effects of THCV following lipopolysaccharide stimulation.

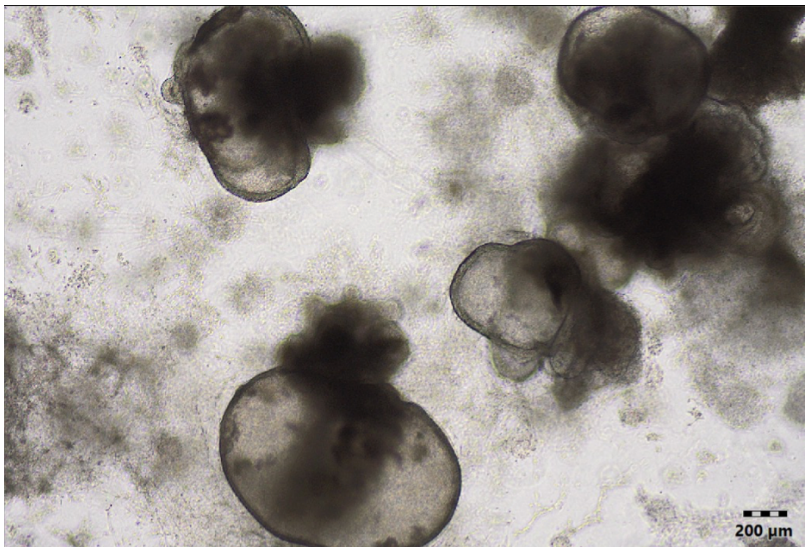

Figure 4.7 Human intestinal organoids generated using the STEMdiff ™ intestinal organoid kit.

4.9. Preliminary Inflammatory Stimulus Treatment (LPS) in Intestinal Organoids (IOs)

Preliminary western blots were conducted to assess the potential inflammatory response in intestinal organoids (IOs) stimulated by lipopolysaccharide (LPS, 500 ng/mL) for 48 hr to simulate chronic inflammation *in vivo*. In Figure 4.8, there was increased interleukin-6 (IL-6) expression, a proinflammatory cytokine (26 kDA), after 48 hr exposure to LPS and THCV at 10 μM (n = 1). IL-6 protein was also detected when THCV (10 μM) was added 6 and 24 hr after LPS stimulation. Relatively weaker IL-6 expression was seen in samples treated with lower THCV concentration (5 μM) following LPS. Meanwhile, no IL-6 was present in controls. This finding showed that IOs were able to mount a proinflammatory response as indicated by enhanced expression of IL-6 when exposed to LPS.

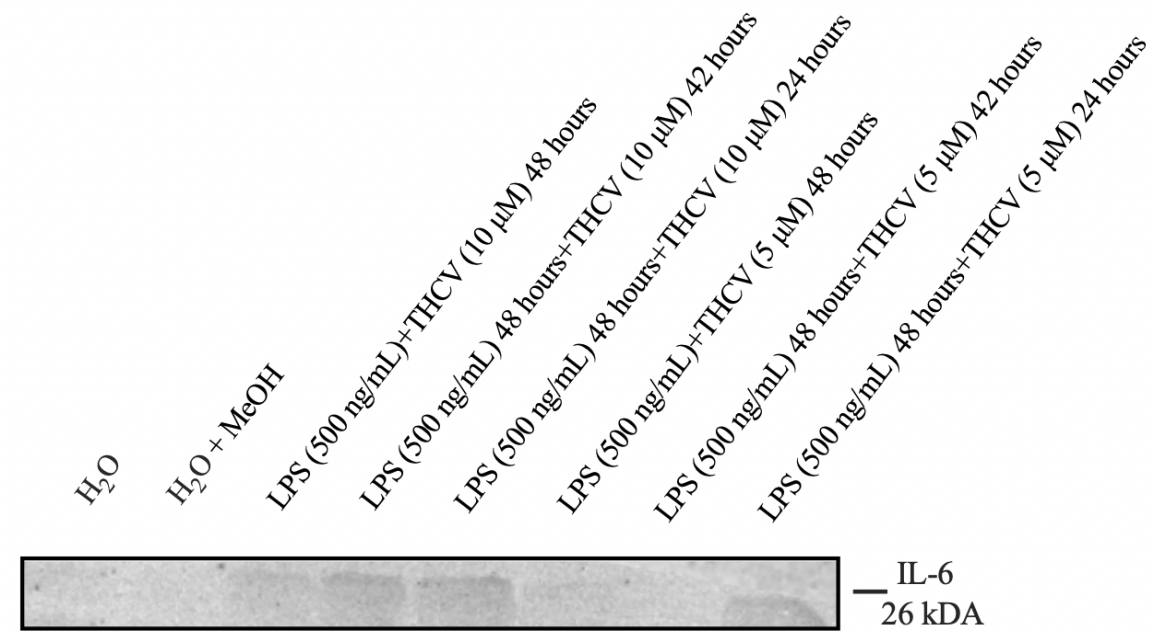

Figure 4.8 Western blot analysis of interleukin-6 (IL-6) in intestinal organoids (1:1000). Samples included eight organoid cell lysates (n = 1). *LPS was added for total duration of 48 hours.

To further ensure the effectiveness of LPS stimulation in intestinal organoids (IOs), inducible nitric oxide synthase (iNOS), a reactive oxygen species for oxidative stress following inflammation, was probed in eight organoid cell lysates (n = 1). There was increased iNOS expression at 130 kDa when solely treated with LPS (500 ng/mL) with no expression in control (Figure 4.9). Consistent iNOS expression was detected after 48 hr exposure to LPS and THCV at two concentrations (5, 10 μM). iNOS was also detected when THCV (5, 10 μM) was added 6 and 24 hr post LPS stimulation. Although the attenuation of iNOS by THCV was ambiguous, the decreased iNOS expression was captured following 48 hr exposure to both LPS and THCV (10 μM).

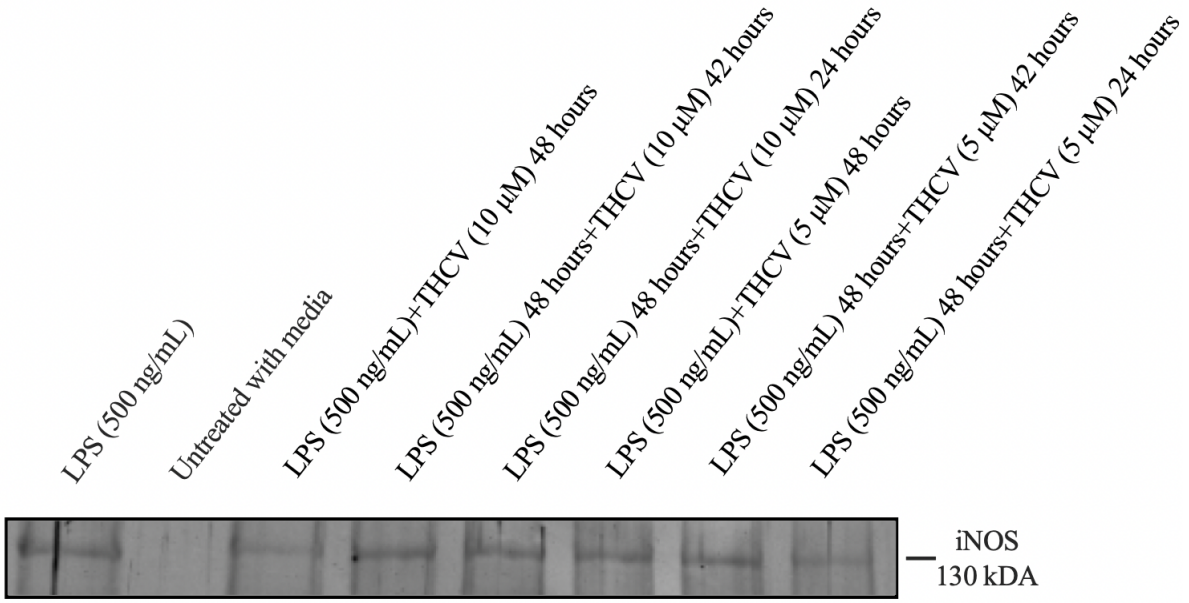

Figure 4.9 Western blot analysis of inducible nitric oxide synthase (iNOS) in intestinal organoids (1:1000). Samples included eight organoid cell lysates (n = 1). *LPS was added for total duration of 48 hours.

To evaluate the potential anti-inflammatory effects of THCV in intestinal organoids after LPS stimulation (500 ng/mL), Interleukin-10 (IL-10), an anti-inflammatory cytokine was probed in nine organoid cell lysates (n = 1). There was increased IL-10 expression at 18.6 kDa after 48 hr exposure to both LPS and THCV at 3 and 10 μM (Figure 4.10). IL-10 proteins were detected after 48 hr exposure of LPS and 24 hr exposure of THCV at 3 and 10 μM. No IL-10 was found in control treatments solely with THCV at 3, 5, 10 μM after 48 hr.

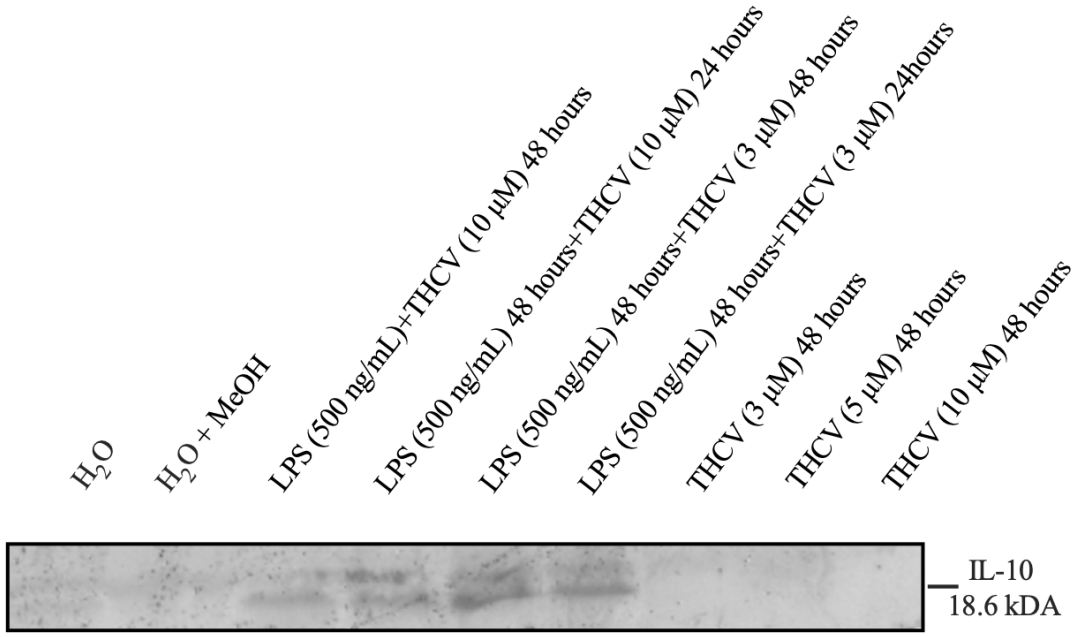

Figure 4.10 Western blot analysis of interleukin-10 (IL-10) in intestinal organoids (1:1000). Samples include nine organoid cell lysates (n = 1). *LPS was added for total duration of 48 hours.

The anti-inflammatory effects of THCV was reassessed in intestinal organoids after LPS stimulation (500 ng/mL). Interleukin-10 (IL-10) was probed in eight cell lysates (n = 2) in a complete experiment with positive, negative, and vehicle (MeOH) controls (Figure 4.11A). Relatively strong IL-10 expression was detected in IOs after 48 hr exposure of LPS and MeOH. IL-10 proteins were also found after 48 hr LPS-treated and 24 hr THCV treated samples at 3 and 10 μM. Contrary to Figure 4.10, basal IL-10 levels was seen in untreated with media and THCV (3, 10 μM) solely treated samples after 48 hr.

Densitometry quantitation of Western blots (Figure 4.11 B) confirmed the interleukin-10 (IL-10) signal following LPS stimulation in intestinal organoids. Relatively strong IL-10 expression was detected in IOs after 48 hr exposure of LPS and MeOH with mean 3.48 x 10^5 units compared to vehicle control in MeOH (Figure 4.11 B). IL-10 expression with mean 2.01 x 10^5 and 2.16 x 10^5 units was detected after 48 hr LPS-treated and 24 hr THCV treated samples at 3 and 10 μM respectively. Relatively lower IL-10 expression was quantified for THCV (3, 10 μM) solely treated samples after 48 hr with mean 1.14 x 10^5 and 1.21 x 10^5 units. Collectively, these preliminary findings may indicate that THCV possess certain anti-inflammatory effects *via* IL-10 secretion in intestinal organoids both by itself and following LPS treatment.

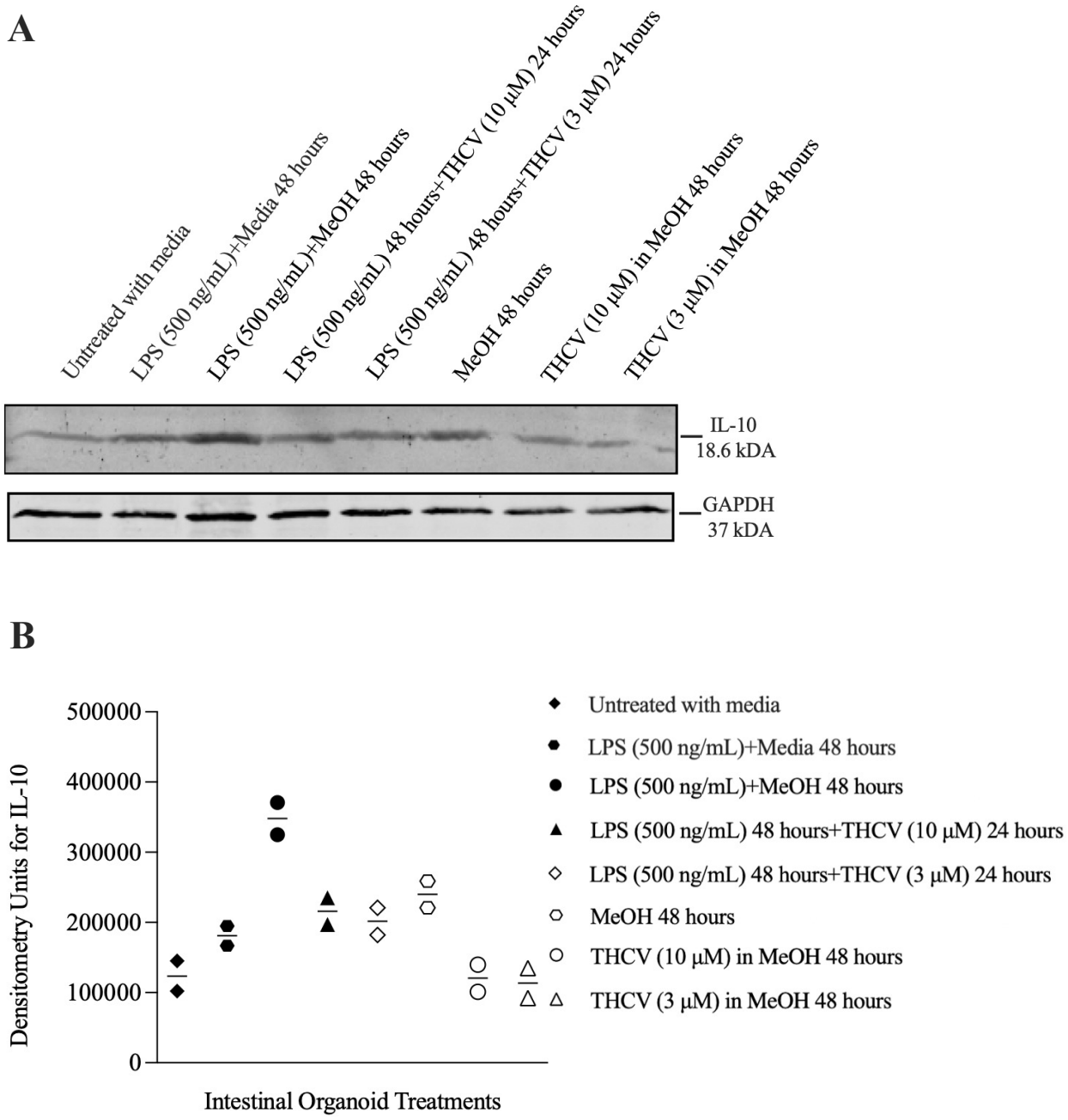

Figure 4.11 Western blot analysis of interleukin-10 (IL-10) in intestinal organoids (1:1000) panel **A**. Samples include eight organoid cell lysates (n = 2). *LPS was added for total duration of 48 hours. GAPDH was used for protein normalization. Densitometry analysis of interleukin-10 (IL-10) after 48 hr exposure of LPS (500 ng/mL) and 24 hr of THCV at 3 or 10 μM in intestinal organoids (n = 2) panel **B**. LI-COR Image Studio™ Lite was used for quantitation.

5. DISCUSSION

The primary aim of this project was to conduct *in vitro* pharmacokinetic screening of THCV for its essential PK characteristics of GI absorption, plasma protein binding, metabolic stability using the Caco-2 Transwell system, 3-solvent extraction plasma protein binding method and the substrate depletion approach in HLM for hepatic metabolic stability, respectively. The *in vitro* PK characterization of THCV (e.g. absorption, metabolism) using human based cells and tissues is crucial to understand THCV absorption and disposition characteristics *in vivo* without the need to utilize *in vivo* preclinical models which may translate poorly to human. Moreover, a secondary aim was to establish a 3D intestinal organoid system derived from human iPSCs that can be used for screening compounds such as THCV for potential anti-inflammatory effects.

5.1. Current Knowledge Gaps on Cannabinoids

The interest in using cannabis as a potential alternative treatment for alleviating patient symptoms with inflammatory bowel disease (IBD) has been growing following the legalization of cannabis through the *Cannabis* Act. Its therapeutic benefits in pre-clinical and clinical post-cancer treatments have been documented by Health Canada [63]. Currently, there is inadequate scientific evidence in evaluating the efficacy of *Cannabis* in clinical studies due, in part, to a lack of understanding of the pharmacokinetics of phytocannabinoids, the naturally occurring constituents found in *Cannabis*. The term 'pharmacokinetics' relates to the absorption, distribution, metabolism, and excretion (ADME) phases of a compound through the body; this area of research is important as ADME processes affect the total body exposure (as indicated by AUC), a critical metric which determines a compound's safety and efficacy. Moreover, due to the available pharmacokinetic data predominantly based on THC and CBD (the top two phytocannabinoids by abundance), research that focuses on less known cannabinoids, such as THCV and CBDV, has been neglected to an extent. This is critical as THCV is available in *Cannabis* products and has been accessible to the general public over the age of 19 years while with reportedly, a third of youth in Canada has tried *Cannabis* at the age of 15 [163]. Thus, detailed research on the PK characteristics of THCV is needed to ensure the safe consumption of

Cannabis recreationally and to facilitate any translational findings from *in vitro* to *in vivo* settings for therapeutic purposes.

To investigate the knowledge gaps of less researched cannabinoids, I conducted an *in vitro* pharmacological evaluation of THCV using humanized *in vitro* model systems. To understand THCV intestinal permeation characteristics, we used the gold-standard intestinal assay, *i.e.* Caco-2 cells grown on Transwells. Unbound fraction ($f_{u(b)}$) and unbound intrinsic clearance ($Cl_{int,u}$) were determined using the three-solvent extraction method and the substrate depletion and linear extrapolation in stability assay (LESA), respectively. Lastly, a 3-D intestinal organoid system was established to assess the effects of THCV in mitigating an inflammatory response following stimulation of inflammation by addition of LPS to organoid cultures.

5.2. Three-Solvent Plasma Protein Binding Assay

The unbound fraction ($f_{u(b)}$) in the blood is a pharmacokinetic (PK) parameter that indicates the ability of a drug to bind to plasma proteins such as albumin, alpha1 acid glycoprotein, and lipoprotein. This PK parameter relates the unbound plasma concentration of a drug to the total plasma drug concentration comprised of both bound and unbound drug. The unbound fraction has critical importance as it reflects the availability of the unbound drug concentration, which elicits the pharmacological effects. Cannabinoids are categorized as high extraction ratio drugs where changes in the $f_{u(b)}$ following oral administration will affect the total steady plasma concentration through the changes of unbound fraction, intrinsic clearance, and blood flow affecting the oral bioavailability while the unbound steady state concentration remain unchanged [164]. Thus, failure to consider the relationship between bound and unbound drug concentrations may result in erroneous bias in interpreting total drug concentrations generated from pharmaceutical analytical assays or when trying to understand the impact of disease or individual variability in response to a given dosage amount.

Equilibrium dialysis, ultrafiltration, and ultracentrifugation are the three most commonly used techniques for the determination of the unbound fraction ($f_{u(b)}$) (*i.e.* the fraction of total compound not bound to plasma proteins) [165]. Despite the versatility of these methods, equilibrium dialysis and ultrafiltration have disadvantages such as drug adsorption to the dialysis membrane and

potential volume shift due to the Donnan effect which is a phenomenon of unequal distribution in charged ions on both sides of the semi-permeable membrane due to an unequal electrical charge of impermeable ions collected on the opposite side [152,156]. Further, rigorous sampling procedures are involved in ultracentrifugation to extract each layer, especially the middle portion of free drug as it may sediment to the bottom with longer wait times [166]. Collectively, with these limitations, a new 3-solvent extraction technique was introduced for evaluating the plasma protein binding profile of THC and CBD, and this method was further applied to the evaluation of the $f_{u(b)}$ of THCV [167].

The total observed THCV concentration, calculated as the sum of the cannabinoid concentrations obtained from the three fractions, was congruent to the total theoretical cannabinoid concentrations for THCV. This showed that the three-solvent extraction method allowed for high recovery while displaying limited non-specific binding (*e.g.* to plastics). This alternative technique not only enabled the distinct separation of bound THCV in other plasma proteins, such as albumin and to lipoproteins, but evaluated the free fraction of THCV that was isolated first from isooctane. On the contrary, predominant plasma protein bind assays primarily assess the total and free concentration of cannabinoids with the difference then provides the bound fraction, which do not necessarily translate to the appropriate *in vitro* conditions compared to the three-solvent extraction where each unbound and bound fraction was calculated and was added to the total which had clear criteria of 100% or congruent with the initial cannabinoid concentration added in the system [153].

According to this extraction method, the unbound fraction of THCV at each standard concentration (30, 50, 500 ng/mL) was 8.2%, 10.9% and 12.4%, respectively, with an average unbound fraction ($f_{u(b)}$) of THCV of 10.5%. Interestingly, the results showed that as THCV concentration increased from 30 to 500 ng/mL, the percent bound THCV to lipoprotein (2.5 to 10.8%) increased while, bound THCV to other plasma proteins (89.3 to 76.8%) decreased where data was consistently displayed in intraday and interday experiments. This was odd as regardless of *in vitro* or *in vivo* settings, albumin accounts for 50-60% of plasma proteins and should expect interaction with THCV where opposite pattern was found. It was unclear whether THCV can display saturable binding to albumin or other proteins at higher concentrations. However, certain drugs such as propranolol showed saturable binding to α_1-Acid glycoprotein (AGP) at high

concentrations (2500 ng/mL) [168]. Thus, more studies on the interaction of THCV with other proteins are needed. In addition, the drying process of 2-octanol was integral for obtaining the THCV bound to lipoprotein, where more than twelve hours of drying time was needed due to its high viscosity. The protracted drying time could lead to the degradation of cannabinoids. However, this reasoning was questionable as all replicates across each standard were subjected to similar drying times and if this assumption were valid, we would see more THCV degradation and decreased bound fraction to lipoproteins. Therefore, the characteristics of lipoproteins and their major classes may play a role for the data. Klausner (1975) evaluated the plasma protein binding of THC where it showed around 60% was bound to lipoproteins [169]. Although this finding was not recent, there was clear evidence of THC partitioning across very-low-density-lipoprotein (VLDL), low-density-lipoprotein (LDL), and high-density-lipoprotein (HDL) at 11%, 34% and 18%. The majority of THC was bound to LDL as they are the predominant lipoproteins in plasma. Since research showed that binding to lipoproteins can occur primarily *via* low-affinity, non-specific hydrophobic bonds, it was likely the partitioning and binding of THC in the lipid core of lipoproteins was reversible. Due to the long drying time of 2-octanol used in this experiment, it was likely that THCV was bound to these major classes of lipoproteins after reaching equilibrium with the drug, protein to drug-protein complex. Because the accumulative bound THCV was quantified in lipoproteins as opposed to their individual classes, it was reasonable to think that when unbound THCV was already extracted using isooctane, the remaining THCV may re-equilibrate and had the tendency of more binding to lipoproteins as opposed to albumin. Note that although the binding pattern was clear between the three fractions, there was 5% loss in THCV recovery at high concentration (500 ng/mL). Assuming 100% THCV recovery, its $f_{u(b)}$ would likely remain the same as the unbound fraction is independent of its total concentration and the drastic increase in albumin binding is unlikely with merely 5% increase in THCV recovery.

5.3. Substrate Depletion Approach and Linear Extrapolation in the Stability Assay (LESA)

The microsomal stability assay is routinely used for categorizing compounds according to their metabolic stability. Due to the high lipophilicity of many cannabinoids, it is suspected that THCV may exhibit non-specific binding to the lipid-protein matrix of the microsomal membrane [152]. Such nonspecific interactions can lead to a reduction in THCV free concentration and decreased interaction with microsomal drug-metabolizing P450 enzymes. Intrinsic clearance (Cl_{int}) is a parameter that directly measures the efficacy of enzymes for metabolizing substrates, and is a key physiological determinant of hepatic clearance (Cl_H). Consequently, determination of Cl_{int} is important for the ranking of compounds' metabolic stability in *in vitro* drug metabolism and to identify whether a compound can be classified as high, intermediate or low clearance. Thus, if the non-specific binding in microsomal assay systems is not addressed, an underestimation of Cl_{int} is inevitable due to the depletion of unbound THCV [152]. $Cl_{int,u}$, termed the unbound intrinsic clearance is the "true" Cl_{int} of a drug in the absence of microsomal binding and remains as the endpoint in this study.

The substrate depletion approach was utilized in each stability assay, where the consumption of the parent drug was tracked over time. It is a rapid, time efficient technique as no additional method validation in LC-MS/MS is needed other than the substrate as opposed to the product formation approach that was traditionally adopted and characterized by the metabolite production in different substrate concentrations requiring various analytical validations and availability of purified metabolite. A concentration-time curve was reported in Figure 4.4 that showed the natural log percentage remaining of THCV (1 μM) following NADPH-dependent reaction in HLMs. The rapid consumption of one THCV concentration (1 μM) in five microsomal concentrations indicated that this low micromolar concentration was unlikely to cause saturated binding in stability assays. This plot further excluded one of the limitations for stability assays adopting the substrate depletion approach which was inaccuracy may increase if sufficient turnover of the substrate was less than 20% [170]. In this study, THCV turnover was greater than 50% across all microsomal concentrations in under 10 min of P450 enzyme-

mediated metabolism, which yielded more accurate estimation of $Cl_{int,u}$ for THCV. Consistent linear depletion profiles after natural log conversion indicated that limited inactivation and inhibition of the enzymes were present in HLM [171]. A clinical study focused on assessing THCV as a marker for the ingestion of *Cannabis* revealed that THCV can be metabolized by human hepatocytes to THCV-COOH *via* Phase I metabolism and was excreted in urine where THCV-COOH-glucuronide was not quantified [172]. Thus, the metabolic stability assays confirmed that THCV can indeed undergo Phase I metabolism catalyzed by NADPH. It was suspected that THCV can be metabolized to 11-OH-THCV first *via* Phase I following similar pathways as THC. Note that the microsomal stability assays did not contain the necessary cofactors to support Phase II metabolism.

The direct evaluation of $Cl_{int,u}$ for THCV was calculated in the absence of THCV unbound fraction ($f_{u(b)}$) using a new method called the linear extrapolation in the stability assay (LESA). The unbound fraction of a drug, and consequently $Cl_{int,u}$ can be determined by three different extraction techniques used traditionally such as equilibrium dialysis, ultrafiltration, and ultracentrifugation with each having limitations that predominantly related to the high lipophilicity of cannabinoids and their non-specific binding to plasticwares which can affect the overall recovery of cannabinoids [173]. Thus, the LESA model was favored and led to the determination of *in vitro* unbound intrinsic clearance of THCV, which was 87.7 µL/min/mg. According to the Cl_{int} classification bands derived from Houston (1994) using the well-stirred model, compounds with *in vitro* Cl_{int} >47.0 µL/min/mg are perceived as high clearance drugs in humans [174]. In a study assessing the enzyme kinetics of THC through the substrate depletion in HLM, Cl_{int} of THC was found to be 435.3 ± 217.0 µL/min/mg [175]. The significant variation in S.D. was likely due to the saturation of CYP2C9 as nonlinear depletion was seen in THC. The intrinsic clearance of CBD was investigated in a separate study in HLM. Cl_{int} for CBD was found to be at approximately 460.6 µL/min/mg [176]. However, the Cl_{int} value was calculated according to Zientek *et al* (2016) where $Cl_{int} = k_{dep}$ x (µL of incubation)/(mg protein) which most likely lead to overestimation of Cl_{int} [177]. Although the intrinsic clearance of THCV was relatively smaller compared to THC and CBD in the literature, their direct comparison should not be warranted as the "true" unbound intrinsic clearance was calculated for

THCV and the $f_{u(b)}$ of THC and CBD were used for their calculation of Cl_{int}. Overall, the stability assay using LESA provided confidence in the experimental data where $Cl_{int,u}$ was linearly extrapolated from different Cl_{int} values across five microsomal concentrations for THCV.

5.4. *In Vitro* THCV Permeability Characteristics in Caco-2 Transwell System

The cytotoxic effects of THCV in Caco-2 cells has not been conducted previously in the literature which led to the objective of finding the optimal THCV concentration that would exhibit non-cytotoxic effects in Caco-2 cells to allow the assessment of THCV permeability using the Caco-2 permeability assay model. The endpoint for these experiments was cell viability (%) calculated using Trypan Blue which is a hydrophilic dye that can permeate into non-intact membrane of dead cells [178]. Due to the concentration of THCV stock (1 mg/mL) available by Cerilliant, the highest final THCV concentration exposed to Caco-2 was 30 μM in 1% MeOH to minimize the effect of organic solvent on cells. Although limited data on THCV and THC toxicity in cell culture is available, my result showing the significant decrease in Caco-2 cell viability at 30 μM was consistent in a finding involving anandamide (AEA), an endocannabinoid, in Caco-2 with decreased cell viability at 30 μM where AEA cytotoxic effects were CBR independent but rather through mitochondrial functions *via* oxidative stress [179]. The cyto-toxic effects of THCV may be attributed to programmed cell death, as cannabinoids have been shown to inhibit cell growth and induce apoptosis in tumour cells such as lung adenocarcinomas, breast carcinomas, and neuroblastomas [180,181]. In addition, the research on the effects of cannabidiol (CBD) in Caco-2 was more apparent. A study showed a concentration-dependent cyto-toxic activity of CBD in three cell lines including Caco-2 as well as anti-inflammatory effects through IL-8 reduction only at low concentration (114 μg/mL) [182]. Thus, it was likely that THCV exhibited a concentration-dependent cytotoxic effect in Caco-2 at 30 μM. Lastly, with regards to THC, significant cellular accumulation of THC was found in MDCKII cells [183]. It was unknown whether THCV can accumulate in Caco-2 at this point and whether any THCV retained in cells may induce apoptosis, which in my subsequent experiments indicated otherwise.

Drug permeability at the intestinal epithelium is one of the most important factors for determining oral drug absorption. In recent years, numerous *in vitro* experimental techniques have been developed for evaluating the intestinal permeability of compounds due to the rapid increase in synthesis and testing of constituents for potential therapeutic activity as pharmaceuticals. The culturing of human epithelial cell lines such as Caco-2 has emerged and remained as the gold-standard, *in vitro* drug screening approach for assessing intestinal drug permeability [184]. Caco-2 cultured on Transwell inserts allows evaluation of the bidirectional permeation of compounds as Caco-2 cells can produce a functional barrier through formation of a polarized epithelium with distinct apical and basal domains. Tight-junction proteins between adjacent cells control the paracellular flux of hydrophilic solutes while maintaining monolayer integrity [185]. Thus, with these attributes, the Caco-2 Transwell system was involved in predicting the *in vitro* permeability characteristics of THCV.

Prior to the permeability experiment, the TEER values (Ω*cm^2) were recorded for three weeks across Day 10, 15 and 20 with steady increases up to 460 Ω*cm^2 in both directions. According to the literature, Caco-2 TEER values >250 Ω*cm^2 measured in Millicell-ERS Volt-ohm meter was deemed appropriate to proceed with permeability assays at Day 21 [186]. The drop in TEER values after the permeability assay compared to before experiment on Day 21 was likely due to the use of HBSS in contrast to DMEM supplemented with FBS used in the culturing period from Day 1 to 20. Although HBSS is commonly used in these assays as an isotonic buffer with glucose as the primary carbohydrate for cells, their short-term deprivation of FBS seemed to induce an effect that influenced the TEER values post-experiment [187]. After 60 min of THCV permeation (10 μM), Lucifer Yellow (LY) was added to all apical Transwell inserts to evaluate the monolayer integrity. The results showed that the Caco-2 monolayer had high LY rejection of approximately 99% regardless of permeation time intervals and either direction from apical to basal and basal to apical compartments. This finding indicated that the Caco-2 cells had formed a functional barrier and that THCV permeability occurred transcellularly. Currently, it is unknown whether THCV is a substrate for efflux or uptake transporters due to limited PK data. THCV has a molecular weight of 286.4 g/mol and a partition coefficient (log *P*) value of 6.08 [188], an

indicator for lipophilicity, it was postulated that THCV may predominantly undergo passive diffusion across the lipid bilayer of Caco-2. However, research indicated that certain cannabinoids such as THC and its metabolite, THC-COOH are substrates for efflux transporters in the ATP-binding cassette (ABC) superfamily such as the P-glycoprotein (P-gp) which are apically expressed in the Caco-2 monolayer and mediate the transport of compounds into the apical compartment or to the intestinal lumen *in vivo* [183,189]. This increased luminal secretion may limit the bioavailability of orally administered drugs and serve as a detoxifying mechanism in the body [190]. Overall, THCV transcellular permeation likely involves passive diffusion but the involvement of uptake or efflux transporters cannot be ruled out.

The results of the Caco-2 permeability experiment of THCV were very peculiar. When initially added to the apical or basal side, only a small amount of THCV permeated into the receiver (< 1%). When THCV was added to the apical side, close to 30% of THCV remained in this compartment. When THCV was added in the basal side, close to 63% of THCV remained in this compartment. Because THCV was not quantifiable in the receiver space, its efflux ratio could not be calculated. Therefore, we assessed the mass balance of THCV and incorporated another component where Caco-2 cells were lysed and subjected to LC-MS/MS analysis. We found that an additional 30% of THCV was trapped intracellularly when THCV was added to the apical side, while 12% of THCV accumulated within cells when THCV was added to the basal side. This data indicated that THCV showed extensive cellular accumulation in Caco-2 cells as well as nonspecific binding to the cell culture and Transwell plate plastics. One study demonstrated that THC and its active and inactive metabolites, 11-OH-THC and THC-COOH, respectively demonstrated 80%, 70%, and 40% accumulation within MDCKII cells grown on Transwells, respectively [183]. THCV is a highly lipophilic molecule (log *P*, 6.08) with low aqueous solubility of 0.0089 mg/mL [188,191]. According to the Biopharmaceutical Classification System (BCS) for Class II drugs with low aqueous solubility and high permeability, the steady increase in log *P* values greater than 4.0 may not necessarily predict a drug's relative increase in permeability as its low aqueous solubility may induce slower partitioning rate from the lipophilic bilayer of Caco-2 cells to the extracellular space (HBSS) [192,193]. Since low organic solvent

(MeOH) final concentration (1%) and THCV stock solution (1 mg/mL) were used, small volume of 2 and 6 μL of 1000 μM THCV working stock was added to with respect to either side, the low volume of solvent may not facilitate THCV release in HBSS. Thus, the physiochemical nature of THCV may explain the findings above as when added on the apical side, it was likely that THCV was intracellular trapped initially and slowly released into the HBSS after 1 hr. Less THCV was found with less cellular accumulation in the apical side when THCV was added in basal as Caco-2 was seeded on the opposite side of where THCV was administered. The difference in surface area between the 24-well bottom and membrane insert could also affect THCV recovery as the wells had surface area of 2.08 cm^2 compared to 0.33 cm^2 in inserts. Overall, the proportional loss of THCV would be greater when added from the basal side due to larger surface area for non-specific binding and apically seeded Caco-2 cells [194]. Thus, THCV may be categorized in a class where its permeability profile could not be accurately evaluated in the Caco-2 Transwell system.

Cannabinoids have extensive non-specific binding to cell culture plasticwares made of polymer plastics, such as polystyrene, polycarbonate and polyester which are highly hydrophobic molecules [195]. Cannabinoids such as THCV is non-polar and lipophilic where it can adhere to plastic tubes and membrane inserts of Transwells through hydrophobic interaction [195]. Thus, we evaluated the non-specific binding of THCV in Transwells with no Caco-2 cells and collected the samples as mock cell lysates. 10% acetonitrile, a water miscible organic solvent was added to release bound THCV from the inserts [196]. The result was congruent with previous finding where limited THCV has permeated into the receiver (< 2%) when initially added to the apical or basal side. When THCV was added to the apical side, close to 30% of THCV remained in this compartment. When THCV was added in the basal side, close to 52% of THCV remained in this compartment. This 20% difference was likely due to same final concentration of THCV (10 μM) added in different compartments where the total HBSS volume in basal was three times greater (600 μL) than in the apical (200 μL). Despite the low aqueous solubility of THCV, the larger volume in the basal compartment may further facilitated the THCV release from MeOH and into HBSS. Close to 18% and 22% of THCV was trapped in inserts when THCV was added to the apical and basal side respectively. Thus, regardless of where THCV was added initially as the

donor, it was able to permeate into the inserts, pore size (0.4 μm) but not into the receiver. This indicated that in the absence of Caco-2 and its intracellular trapping of this cannabinoid, THCV showed non-specific binding to polyester Transwell inserts which added another layer of complexity for the study of cannabinoids through *in vitro* Caco-2 permeability experiments.

5.5. Pilot Intestinal Organoid Assays Evaluating the Anti-inflammatory Potential of THCV

The 3D intestinal organoid (IO) model was established to evaluate the anti-inflammatory potential of THCV. Lipopolysaccharide (LPS, 500 ng/mL) was used as an inflammatory stimulus in the IO system. LPS is a major component of Gram-negative bacterial cell walls and is commonly used to initiate inflammatory responses in *in vitro* assays [197]. Extensive research have shown that LPS can induce inflammation in macrophages through the secretion of pro-inflammatory cytokines such as interleukin-6 (IL-6) and inducible nitric oxide synthase (iNOS) [198,199]. Due to the lack of macrophages in the IO system, the screening of IL-6 and iNOS was appropriate as they can be secreted by various cell types such as endothelial cells, and intestinal epithelial cells, a group that is native in the IOs [200,201]. Thus, IL-6 and iNOS protein expression were evaluated using Western blots to confirm an inflammatory response by IOs and whether THCV can attenuate the expression of these proteins. Additionally, IL-10, an anti-inflammatory cytokine, was screened in IOs.

IL-6 expression was upregulated in IOs treated with LPS. This is consistent with the literature both *in vitro* and *in vivo*. Research has shown that LPS is a known ligand on the Toll-like receptors which are constitutively expressed in human intestinal crypts [202,203]. A study showed that IL-6 was detected post 1, 2, and 4 hr post *Salmonella* infection in crypt-derived mouse intestinal organoids involving the upregulation of nuclear factor-κB pathways [204]. As well, IL-6 levels are drastically elevated in patients with CD and this cytokine triggers the hepatic production of C-reactive proteins, a serum biomarker for CD [205,206]. IL-6 expression was relatively the greatest when THCV was added 24 hr post LPS stimulation where in contrast, it was downregulated when THCV was co-administered with LPS at Time 0. Limited IL-6

secretion was detected in IOs following LPS when a lower THCV concentration (5 μM) but not higher THCV concentration (10 μM) was added indicating potential inhibition of the pro-inflammatory cytokine, IL-6. iNOS expression also was upregulated in IOs treated with LPS and THCV in all treatments relatively to the control with no iNOS. Consistent with the trend of IL-6, the decreased iNOS expression was detected in IOs when THCV was co-administered with LPS at Time 0. In one study, decreased iNOS expression was found with THCV following LPS stimulation in murine peritoneal macrophages [61]. The downregulation of this protein is important as it is highly expressed at mucosal surface in ulcerative colitis patients [207]. Collectively, the inflammatory stimulus, LPS, was capable of upregulating IL-6 and iNOS in the intestinal organoid model, both of which are clinical biomarkers for Crohn's and ulcerative colitis in IBD [208]. Thus, IOs derived using human iPSCs can be used to model pathophysiological conditions and potential therapeutic effects of desired compounds.

The upregulation of IL-10, an anti-inflammatory cytokine was detected in all treatments including controls (untreated with media). There was basal IL-10 expression in untreated IOs with media. This was plausible as *in vivo*, the intestines occupy the largest pool of IL-10-producing macrophages in the event of stimuli such as exogenous microbial factors and endogenous bile acids thus maintaining gut homeostasis [209,210]. However, basal IL-10 proteins in intestinal organoids was unlikely to be secreted by macrophages as IOs do not possess additional immune cells [211]. Research showed that intestinal epithelial cells (IECs) such as the enterocytes possess intrinsic expression of IL-10 where its inhibition in IECs can induce increased IFN-γ production and extensive apoptosis at the epithelium [212]. The enterocytes in IOs were likely the reason for IL-10 detection in untreated media. It was interesting to note that there was an unknown interaction of THCV with IOs as IL-10 was detected when treated solely with THCV without LPS. Increased IL-10 levels were seen in treatments after 48 h exposure of LPS and 24 h of THCV at either 3 or 10 μM. This indicated that THCV potentially possess anti-inflammatory effects post LPS treatment *via* IL-10. The strongest relative IL-10 expression was found in IOs treated for 48 h with both LPS and 1% methanol. One study showed that a methanol extract of the root in *Lilium lancifolium* had anti-inflammatory effects on LPS-stimulated murine

macrophage cell line (Raw264.7) with reduced expression of iNOS and cyclooxygenase-2 (COX-2) *via* downregulated NF-κB signaling components [213]. Methanol extract was also found to reduce mucosal damage, edema, and tissue myeloperoxidase (MPO) accumulation in dextran sulfate sodium (DSS)-induced colitis model in mice [214]. Currently with THCV, it possessed preliminary evidence of reduced proinflammatory (IL-6) and increased anti-inflammatory (IL-10) mediators in intestinal organoids after LPS. Attenuation of iNOS by THCV was less apparent as only one treatment demonstrated the predicted pattern.

6. CONCLUSION AND FUTURE WORK

The aim of the project primarily was to conduct *in vitro* pharmacokinetic screening of tetrahydrocannabivarin (THCV) for its essential (PK) characteristics. Caco-2 Transwell system, a gold-standard *in vitro* permeability assay was conducted to assess the permeation profile of THCV. The 3-solvent extraction technique was used to understand the plasma protein binding of THCV *via* the unbound fraction ($f_{u(b)}$). The metabolic stability of THCV was completed through the substrate depletion approach in human liver microsomes (HLM) for evaluating its hepatic Phase I metabolism. The *in vitro* PK characterization of this cannabinoid (e.g. absorption, metabolism) using human based cells and tissues is crucial for understanding the absorption and disposition characteristics of THCV *in vivo* without the use of *in vivo* preclinical models which have poor translational outcomes in humans. Moreover, a secondary aim was to establish a 3D intestinal organoid system derived from human iPSCs that can be used for screening in compounds such as THCV for potential anti-inflammatory effects.

For my first objective, THCV (10 μM) was added with respect to apical and basal side in the Transwell system with Caco-2 cells. THCV permeation was limited throughout the experiment (1 hr) as the majority of THCV remained in the compartment in which it was initially added. A significant proportion of THCV (~20%) was non-specifically bound to the polyester membrane inserts with no Caco-2 cells. Due to the non-linear permeation profile and the cellular accumulation of THCV, we were unable to calculate the apparent permeability coefficient (P_{app}) as well as the efflux ratio of THCV. These results indicated that the Caco-2 Transwell system was not suitable for the study of THCV permeability *in vitro*.

For my second objective, the three-solvent extraction technique was adopted to combat the non-specific binding of cannabinoids seen in traditional methods while yielding the unbound and bound fractions of THCV. The unbound fraction of THCV was found to be 10.5% with the preference of binding to lipoproteins with higher THCV concentrations (500 ng/mL). The total observed concentration was congruent to the total theoretical cannabinoid concentrations for THCV which indicated that the three-solvent extraction method allowed for high recovery of this compound.

For my third objective, the linear extrapolation in stability assay (LESA) through substrate depletion was used to evaluate the unbound intrinsic clearance ($Cl_{int,u}$) without the need to incorporate the unbound fraction. According to the Cl_{int} classification bands derived from Houston (1994), compounds with *in vitro* Cl_{int} >47.0 µL/min/mg are perceived as high clearance drugs in humans [174]. Thus, THCV is a high clearance compound with $Cl_{int,u}$ of 87.7 µL/min/mg.

For my last objective, the 3D intestinal organoid (IO) model derived from human iPSCs was established in our lab as an *in vitro* human screening platform for compounds such as THCV for its anti-inflammatory effects. In a series of preliminary experiments after lipopolysaccharide (LPS) stimulation, intestinal organoids prepared as cell lysates had increased expression of interleukin-6 (IL-6), a proinflammatory cytokine, and inducible nitric oxide synthase (iNOS), a biomarker for oxidative stress. Although there was decreased expression of IL-6 and iNOS in certain treatments following the addition of THCV, its overall attenuation of proinflammatory signals *via* the downregulation of IL-6 and iNOS showed mild association in these pilot studies. However, the expression of interleukin-10 (IL-10), an anti-inflammatory cytokine was consistently detected in THCV treated IOs after LPS. Relatively stronger IL-10 expression was found in these samples compared to untreated control and samples with only THCV, both of which had basal IL-10 expression. Thus, THCV may possess certain anti-inflammatory effects *via* the upregulation of IL-10. Overall, the intestinal organoid model may represent a more comprehensive tool for *in vitro* screening of desired compounds as shown from my work, that IOs were capable of upregulating key proinflammatory pathways which are native in the intestinal mucosa *in vivo* upon inflammatory damage.

This current research is critical in paving the way for future work through the umbrella of translational PK research for cannabinoids. Due to the various panel of experiments and the associated techniques in this project, future PK related research will proceed in multiple directions.

It was found and validated in my work that THCV can undergo Phase I hepatic metabolism through the cytochrome P450 enzymes. However, no THCV metabolites have been quantified *via* Phase II glucuronidation. It is suspected that THCV may yield THCV-COOH-glucuronide in similar way as THC *via* Phase II metabolism. This can be conducted efficiently as

the metabolic stability assay with substrate depletion and LESA approach have been established. One simple adjustment can be made by adding the cofactor, uridine 5'-diphospho-glucuronosyltransferases (UGTs) that catalyzes Phase II metabolism in human liver microsomes [215]. Furthermore, reaction phenotyping studies (*i.e.* P450 expression systems, chemical or antibody inhibition studies, and correlation analysis) can be conducted to identify the P450 enzymes involved in the hepatic metabolism of THCV [216]. Finally, the extrahepatic metabolism, in particular intestinal metabolism, of THCV can be evaluated to understand the contribution of the intestine to oral bioavailability, and other tissues to overall systemic clearance [217].

In terms of the *in vitro* permeability assay, the Caco-2 Transwell system was unsuitable for the study of THCV permeation. One technique *via Ex Vivo* diffusion chamber could be adopted where purchased or donated human intestinal tissues are used and mounted as epithelial sheets between two chambers filled with oxygenated buffer [218]. The general purpose and rationale of this technique is similar to the Transwell model. However, the use of actual intestinal tissue may reveal new findings that were not seen in our previous model.

There are many questions left unanswered with regards to the organoid experiments as this realm of research is fairly recent. In the future, immunostaining for various intestinal biomarkers should be conducted first in IOs to ensure that they possess various intestinal cell types. Further, any compounds taken orally will reach the intestinal lumen before permeating from the mucosa to the serosa which is very difficult to simulate in intestinal organoids *in vitro*. Although technique such as microinjection into the lumen of IOs does exist, its cost vs benefit is not ideal for many research facilities. Thus, efficient and more cost friendly methods should be made available in the near future for addressing this difficulty.

Although THCV does not account for the majority of cannabinoids in *Cannabis*, the amount of THC:CBD content has been steadily increasing *via* recreational use [219]. Therefore, the additional pharmacokinetic information of THCV must be carefully evaluated to ensure safe consumption of *Cannabis* in all age demographics and for all purposes, whether recreational or medicinal.

7. REFERENCES

1. Russo EB. History of cannabis and its preparations in saga, science, and sobriquet. *Chem Biodivers*. 2007 Aug 1;4(8):1614–48.

2. Dewey WL. Cannabinoid pharmacology. *Pharmacol Rev*. 1986 Jun 1;38(2):151 LP – 178.

3. Boggs DL, Peckham A, Boggs AA, Ranganathan M. Delta-9-tetrahydrocannabinol and cannabidiol: Separating the chemicals from the "weed," a pharmacodynamic discussion. *Ment Heal Clin*. 2016 Nov 3;6(6):277–84.

4. Ligresti A, De Petrocellis L, Di Marzo V. From Phytocannabinoids to Cannabinoid Receptors and Endocannabinoids: Pleiotropic Physiological and Pathological Roles Through Complex Pharmacology. *Physiol Rev*. 2016 Sep 14;96(4):1593–659.

5. Bolognini D, Costa B, Maione S, Comelli F, Marini P, Di Marzo V, et al. The plant cannabinoid Delta9-tetrahydrocannabivarin can decrease signs of inflammation and inflammatory pain in mice. *Br J Pharmacol*. 2010 Jun;160(3):677–87.

6. Miller LK, Devi LA. The highs and lows of cannabinoid receptor expression in disease: mechanisms and their therapeutic implications. *Pharmacol Rev*. 2011/07/13. 2011 Sep;63(3):461–70.

7. Scheidweiler KB, Newmeyer MN, Barnes AJ, Huestis MA. Quantification of cannabinoids and their free and glucuronide metabolites in whole blood by disposable pipette extraction and liquid chromatography-tandem mass spectrometry. *J Chromatogr A*. 2016;1453:34–42.

8. Huestis MA. Human cannabinoid pharmacokinetics. *Chem Biodivers*. 2007 Aug;4(8):1770–804.

9. Pollio A. The name of cannabis: A short guide for nonbotanists. *Cannabis cannabinoid Res*. 2016 Oct 1;1(1):234–8.

10. Miyaji T, Nagasawa M, Yamaguchi T, Tsutani K. Tackling the pharmaceutical frontier: Regulation of cannabinoid-based medicines in Postwar Japan. *Cannabis cannabinoid Res*. 2016 Jan 1;1(1):31–7.

11. Li H-L. An archaeological and historical account of cannabis in China. *Econ Bot*. 1974 Jun 23;28(4):437–48.

12. Ayonrinde OA. Cannabis and psychosis: Revisiting a nineteenth century study of "Indian Hemp and Insanity" in colonial British India. *Psychol Med*. 2020 May;50(7):1164—1172.

13. Boggs DL, Nguyen JD, Morgenson D, Taffe MA, Ranganathan M. Clinical and preclinical evidence for functional interactions of cannabidiol and Δ(9)-tetrahydrocannabinol. *Neuropsychopharmacology*. 2017/09/06. 2018 Jan;43(1):142–54.

14. Cahn RS. 326. Cannabis indica resin. Part IV. The synthesis of some 2 : 2-dimethyldibenzopyrans, and confirmation of the structure of cannabinol. *J Chem Soc*. 1933;(0):1400–5.

15. Loewe S, Adams R. Structure-activity relationship (SAR) and pharmacological peculiarities of new synthetic congeners of tetrahydrocannabinol. *Fed Proc*. 1947;6(1):352.

16. Russo EB. Taming THC: Potential cannabis synergy and phytocannabinoid-terpenoid entourage effects. *Br J Pharmacol*. 2011 Aug;163(7):1344–64.

17. Atakan Z. Cannabis, a complex plant: Different compounds and different effects on individuals. *Ther Adv Psychopharmacol*. 2012 Dec;2(6):241–54.

18. Sharma P, Murthy P, Bharath MMS. Chemistry, metabolism, and toxicology of cannabis: clinical implications. *Iran J Psychiatry*. 2012;7(4):149–56.

19. Zager JJ, Lange I, Srividya N, Smith A, Lange BM. Gene networks underlying cannabinoid and terpenoid accumulation in cannabis. *Plant Physiol*. 2019/05/28. 2019 Aug;180(4):1877–97.

20. Console-Bram L, Marcu J, Abood ME. Cannabinoid receptors: nomenclature and pharmacological principles. *Prog Neuropsychopharmacol Biol Psychiatry*. 2012/02/28. 2012 Jul 2;38(1):4–15.

21. Sutton IR, Daeninck P. Cannabinoids in the management of intractable chemotherapy-induced nausea and vomiting and cancer-related pain. *J Support Oncol*. 2006;4(10):531–5.

22. Ekert H, Waters KD, Jurk IH, Mobilia J, Loughnan P. Amelioration of cancer chemotherapy-induced nausea and vomiting by delta-9-tetrahydrocannabinol. *Med J Aust*. 1979 Dec 1;2(12):657–9.

23. Ungerleider JT, Andyrsiak T, Fairbanks L, Ellison GW, Myers LW. Delta-9-THC in the treatment of spasticity associated with multiple sclerosis. *Adv Alcohol Subst Abuse*. 1988 Feb 5;7(1):39–50.

24. Sastre-Garriga J, Vila C, Clissold S, Montalban X. THC and CBD oromucosal spray (Sativex®) in the management of spasticity associated with multiple sclerosis. *Expert Rev Neurother*. 2011 May 1;11(5):627–37.

25. Wallace M.D. M, Schulteis Ph.D. G, Atkinson M.D. JH, Wolfson M.A. T, Lazzaretto M.S. D, Bentley H, et al. Dose-dependent effects of smoked cannabis on Capsaicin-induced pain

and hyperalgesia in healthy volunteers. *Anesthesiol J Am Soc Anesthesiol*. 2007 Nov 1;107(5):785–96.

26. Subramaniam VN, Menezes AR, DeSchutter A, Lavie CJ. The cardiovascular effects of marijuana: Are the potential adverse effects worth the high? *Mo Med*. 2019;116(2):146–53.

27. Kendall DA, Yudowski GA. Cannabinoid receptors in the central nervous system: Their signaling and roles in disease. *Front Cell Neurosci*. 2017 Jan 4;10:294.

28. Gill EW, Paton WDM, Pertwee RG. Preliminary experiments on the chemistry and pharmacology of cannabis. *Nature*. 1970 Oct 1;228:134–6.

29. Merkus FWHM. Cannabivarin and tetrahydrocannabivarin, two new constituents of hashish. *Nature*. 1971;232(5312):579–80.

30. Thomas A, Stevenson LA, Wease KN, Price MR, Baillie G, Ross RA, et al. Evidence that the plant cannabinoid Delta9-tetrahydrocannabivarin is a cannabinoid CB1 and CB2 receptor antagonist. *Br J Pharmacol*. 2005 Dec;146(7):917–26.

31. Wargent ET, Zaibi MS, Silvestri C, Hislop DC, Stocker CJ, Stott CG, et al. The cannabinoid Δ9-tetrahydrocannabivarin (THCV) ameliorates insulin sensitivity in two mouse models of obesity. *Nutr Diabetes*. 2013;3(5):e68–e68.

32. Deiana S, Watanabe A, Yamasaki Y, Amada N, Arthur M, Fleming S, et al. Plasma and brain pharmacokinetic profile of cannabidiol (CBD), cannabidivarine (CBDV), Δ9-tetrahydrocannabivarin (THCV) and cannabigerol (CBG) in rats and mice following oral and intraperitoneal administration and CBD action on obsessive–compulsive behavi. *Psychopharmacology (Berl)*. 2012;219(3):859–73.

33. Bátkai S, Mukhopadhyay P, Horváth B, Rajesh M, Gao RY, Mahadevan A, et al. Δ8-Tetrahydrocannabivarin prevents hepatic ischaemia/reperfusion injury by decreasing oxidative stress and inflammatory responses through cannabinoid CB2 receptors. *Br J Pharmacol*. 2012 Apr;165(8):2450–61.

34. Hillard CJ. The Endocannabinoid signaling system in the CNS: A primer. *Int Rev Neurobiol*. 2015/11/06. 2015;125:1–47.

35. Lu H-C, Mackie K. An introduction to the endogenous cannabinoid system. *Biol Psychiatry*. 2015/10/30. 2016 Apr 1;79(7):516–25.

36. Serrano A, Parsons LH. Endocannabinoid influence in drug reinforcement, dependence and addiction-related behaviors. *Pharmacol Ther*. 2011/07/18. 2011 Dec;132(3):215–41.

37. Maccarrone M, Gasperi V, Catani MV, Diep TA, Dainese E, Hansen HS, et al. The

Endocannabinoid system and its relevance for nutrition. *Annu Rev Nutr*. 2010 Jul 1;30(1):423–40.

38. Aggarwal SK. Cannabinergic pain medicine: a concise clinical primer and survey of randomized-controlled trial results. *Clin J Pain*. 2013 Feb;29(2):162—171.

39. Hermanson DJ, Marnett LJ. Cannabinoids, endocannabinoids, and cancer. *Cancer Metastasis Rev*. 2011 Dec;30(3–4):599–612.

40. Pertwee RG. The diverse CB1 and CB2 receptor pharmacology of three plant cannabinoids: delta9-tetrahydrocannabinol, cannabidiol and delta9-tetrahydrocannabivarin. *Br J Pharmacol*. 2007/09/10. 2008 Jan;153(2):199–215.

41. Battista N, Di Tommaso M, Bari M, Maccarrone M. The endocannabinoid system: An overview. *Front Behav Neurosci*. 2012 Mar 14;6:9.

42. Pertwee RG, Howlett AC, Abood ME, Alexander SPH, Di Marzo V, Elphick MR, et al. International union of basic and clinical pharmacology. LXXIX. Cannabinoid receptors and their ligands: Beyond CB_1 and CB_2. *Pharmacol Rev*. 2010 Dec;62(4):588–631.

43. Kraft B. Is there any clinically relevant cannabinoid-induced analgesia? *Pharmacology*. 2012;89(5–6):237–46.

44. Di Marzo V, Piscitelli F, Mechoulam R. Cannabinoids and endocannabinoids in metabolic disorders with focus on diabetes BT-diabetes-perspectives in drug therapy. In: Schwanstecher M, editor. Berlin, Heidelberg: Springer Berlin Heidelberg; 2011. p. 75–104.

45. Quarta C, Mazza R, Obici S, Pasquali R, Pagotto U. Energy balance regulation by endocannabinoids at central and peripheral levels. *Trends Mol Med*. 2011;17(9):518–26.

46. Ma Y-L, Weston SE, Whalley BJ, Stephens GJ. The phytocannabinoid Delta(9)-tetrahydrocannabivarin modulates inhibitory neurotransmission in the cerebellum. *Br J Pharmacol*. 2008/03/03. 2008 May;154(1):204–15.

47. O'Sullivan SE. An update on PPAR activation by cannabinoids. *Br J Pharmacol*. 2016/05/19. 2016 Jun;173(12):1899–910.

48. Janssens A, Silvestri C, Martella A, Vanoevelen JM, Di Marzo V, Voets T. Δ9-tetrahydrocannabivarin impairs epithelial calcium transport through inhibition of TRPV5 and TRPV6. *Pharmacol Res*. 2018;136:83–9.

49. Cascio MG, Zamberletti E, Marini P, Parolaro D, Pertwee RG. The phytocannabinoid, Δ9-tetrahydrocannabivarin, can act through 5-HT1A receptors to produce antipsychotic effects.

Br J Pharmacol. 2015 Mar 1;172(5):1305–18.

50. Anavi-Goffer S, Baillie G, Irving AJ, Gertsch J, Greig IR, Pertwee RG, et al. Modulation of L-α-lysophosphatidylinositol/GPR55 mitogen-activated protein kinase (MAPK) signaling by cannabinoids. *J Biol Chem*. 2011/10/25. 2012 Jan 2;287(1):91–104.

51. Guindon J, Hohmann AG. The endocannabinoid system and pain. *CNS Neurol Disord Drug Targets*. 2009 Dec;8(6):403–21.

52. Wright K, Rooney N, Feeney M, Tate J, Robertson D, Welham M, et al. Differential expression of cannabinoid receptors in the human colon: Cannabinoids promote epithelial wound healing. *Gastroenterology*. 2005;129(2):437–53.

53. Senin LL, Al-Massadi O, Folgueira C, Castelao C, Pardo M, Barja-Fernandez S, et al. The gastric CB1 receptor modulates ghrelin production through the mTOR pathway to regulate food intake. *PLoS One*. 2013 Nov 26;8(11):e80339–e80339.

54. Pertwee RG. Cannabinoids and the gastrointestinal tract. *Gut*. 2001 Jun;48(6):859–67.

55. Mackie K. Signaling via CNS cannabinoid receptors. *Mol Cell Endocrinol*. 2008/02/06. 2008 Apr 16;286(1-2 Suppl 1):S60–5.

56. Wright KL, Duncan M, Sharkey KA. Cannabinoid CB2 receptors in the gastrointestinal tract: A regulatory system in states of inflammation. *Br J Pharmacol*. 2007/10/01. 2008 Jan;153(2):263–70.

57. Bouaboula M, Rinaldi M, Carayon P, Carillon C, Delpech B, Shire D, et al. Cannabinoid-receptor expression in human leukocytes. *Eur J Biochem*. 1993 May 1;214(1):173–80.

58. Galiègue S, Mary S, Marchand J, Dussossoy D, Carrière D, Carayon P, et al. Expression of central and peripheral cannabinoid receptors in human immune tissues and leukocyte subpopulations. *Eur J Biochem*. 1995 Aug 1;232(1):54–61.

59. Ihenetu K, Molleman A, Parsons ME, Whelan CJ. Inhibition of interleukin-8 release in the human colonic epithelial cell line HT-29 by cannabinoids. *Eur J Pharmacol*. 2003;458(1):207–15.

60. DiPatrizio N V. Endocannabinoids in the gut. *Cannabis cannabinoid Res*. 2016/02/24. 2016 Feb;1(1):67–77.

61. Romano B, Pagano E, Orlando P, Capasso R, Cascio MG, Pertwee R, et al. Pure Δ9-tetrahydrocannabivarin and a Cannabis sativa extract with high content in Δ9-tetrahydrocannabivarin inhibit nitrite production in murine peritoneal macrophages.

Pharmacol Res. 2016;113:199–208.

62. Russo EB. Cannabinoids in the management of difficulty to treat pain. *Ther Clin Risk Manag*. 2008 Feb;4(1):245–59.

63. Dariš B, Tancer Verboten M, Knez Ž, Ferk P. Cannabinoids in Cancer Treatment: Therapeutic potential and legislation. *Bosn J basic Med Sci*. 2019 Feb 12;19(1):14–23.

64. Anand P, Whiteside G, Fowler CJ, Hohmann AG. Targeting CB2 receptors and the endocannabinoid system for the treatment of pain. *Brain Res Rev*. 2008/12/25. 2009 Apr;60(1):255–66.

65. Dhopeshwarkar A, Mackie K. CB2 cannabinoid receptors as a therapeutic target-What does the future hold? *Mol Pharmacol*. 2014/08/08. 2014 Oct;86(4):430–7.

66. Konishi T, Lentsch AB. Hepatic ischemia/reperfusion: Mechanisms of tissue injury, repair, and regeneration. *Gene Expr*. 2017/09/11. 2017 Nov 27;17(4):277–87.

67. Jaeschke H. Reactive oxygen and ischemia/reperfusion injury of the liver. *Chem Biol Interact*. 1991;79(2):115–36.

68. Lu D, Dopart R, Kendall DA. Controlled downregulation of the cannabinoid CB1 receptor provides a promising approach for the treatment of obesity and obesity-derived type 2 diabetes. *Cell Stress Chaperones*. 2016 Jan;21(1):1–7.

69. Buggy Y, Cornelius V, Wilton L, Shakir SAW. Risk of Depressive Episodes with Rimonabant. *Drug Saf*. 2011;34(6):501–9.

70. Silvestri C, Paris D, Martella A, Melck D, Guadagnino I, Cawthorne M, et al. Two non-psychoactive cannabinoids reduce intracellular lipid levels and inhibit hepatosteatosis. *J Hepatol*. 2015;62(6):1382–90.

71. Vanoevelen J, Janssens A, Huitema LFA, Hammond CL, Metz JR, Flik G, et al. Trpv5/6 is vital for epithelial calcium uptake and bone formation. *FASEB J*. 2011 Sep 1;25(9):3197–207.

72. Hoenderop JGJ, Nilius B, Bindels RJM. Calcium Absorption Across Epithelia. *Physiol Rev*. 2005 Jan 1;85(1):373–422.

73. Scaldaferri F, Fiocchi C. Inflammatory bowel disease: Progress and current concepts of etiopathogenesis. *J Dig Dis*. 2007 Nov 1;8(4):171–8.

74. Talley J, Abreu T, Achkar P, Bernstein N, Dubinsky C, Hanauer B, et al. An evidence-

based systematic review on medical therapies for inflammatory bowel disease. *Am J Gastroenterol*. 2011;106.

75. Ha F, Khalil H. Crohn's disease: A clinical update. *Therap Adv Gastroenterol*. 2015 Nov;8(6):352–9.

76. Ungaro R, Mehandru S, Allen PB, Peyrin L, Colombel F. Ulcerative colitis. *Lancet (London, England)*. 2016/12/01. 2017 Apr 29;389(10080):1756–70.

77. Shale M, Ghosh S. How intestinal epithelial cells tolerise dendritic cells and its relevance to inflammatory bowel disease. *Gut*. 2009 Sep 1;58(9):1291 LP – 1299.

78. Huang Y, Chen Z. Inflammatory bowel disease related innate immunity and adaptive immunity. *Am J Transl Res*. 2016 Jun 15;8(6):2490–7.

79. McGuckin A, Eri R, Simms A, Florin J, Radford G. Intestinal barrier dysfunction in inflammatory bowel diseases. *Inflamm Bowel Dis*. 2008 Jul 11;15(1):100–13.

80. Sokol L, Luster D. The chemokine system in innate immunity. *Cold Spring Harb Perspect Biol*. 2015 Jan 29;7(5):a016303.

81. Roda G, Sartini A, Zambon E, Calafiore A, Marocchi M, Caponi A, et al. Intestinal epithelial cells in inflammatory bowel diseases. *World J Gastroenterol*. 2010 Sep 14;16(34):4264–71.

82. Thim L. Trefoil peptides: From structure to function. *Cell Mol Life Sci C*. 1997;53(11):888–903.

83. Atuma C, Strugala V, Allen A, Holm L. The adherent gastrointestinal mucus gel layer: Thickness and physical state in vivo. *Am J Physiol Liver Physiol*. 2001 May 1;280(5):G922–9.

84. Holleran G, Lopetuso L, Petito V, Graziani C, Ianiro G, McNamara D, et al. The innate and adaptive immune system as targets for biologic therapies in inflammatory bowel disease. *Int J Mol Sci*. 2017 Sep 21;18(10):2020.

85. Uehara A, Fujimoto Y, Fukase K, Takada H. Various human epithelial cells express functional Toll-like receptors, NOD1 and NOD2 to produce anti-microbial peptides, but not proinflammatory cytokines. *Mol Immunol*. 2007;44(12):3100–11.

86. Laukoetter MG, Nava P, Nusrat A. Role of the intestinal barrier in inflammatory bowel disease. *World J Gastroenterol*. 2008 Jan 21;14(3):401–7.

87. Fasano A. Intestinal permeability and its regulation by zonulin: Diagnostic and therapeutic

implications. *Clin Gastroenterol Hepatol*. 2012/08/16. 2012 Oct;10(10):1096–100.

88. Bruewer M, Luegering A, Kucharzik T, Parkos CA, Madara L, Hopkins M, et al. Proinflammatory cytokines disrupt epithelial barrier function by apoptosis-independent mechanisms. *J Immunol*. 2003 Dec 1;171(11):6164 LP – 6172.

89. Gassler N, Rohr C, Schneider A, Kartenbeck J, Bach A, Obermüller N, et al. Inflammatory bowel disease is associated with changes of enterocytic junctions. *Am J Physiol Liver Physiol*. 2001 Jul 1;281(1):G216–28.

90. Arseneau O, Tamagawa H, Pizarro T, Cominelli F. Innate and adaptive immune responses related to IBD pathogenesis. *Curr Gastroenterol Rep*. 2007;9(6):508–12.

91. Yang J, Zhang L, Yu C, Yang F, Wang H. Monocyte and macrophage differentiation: Circulation inflammatory monocyte as biomarker for inflammatory diseases. *Biomark Res*. 2014 Jan 7;2(1):1.

92. Novak N, Koch S, Allam P, Bieber T. Dendritic cells: Bridging innate and adaptive immunity in atopic dermatitis. *J Allergy Clin Immunol*. 2010;125(1):50–9.

93. Niess JH. Role of mucosal dendritic cells in inflammatory bowel disease. *World J Gastroenterol*. 2008 Sep 7;14(33):5138–48.

94. Niess JH, Reinecker H-C. Dendritic cells in the recognition of intestinal microbiota. *Cell Microbiol*. 2006 Apr 1;8(4):558–64.

95. Ramasundara M, Leach ST, Lemberg DA, Day AS. Defensins and inflammation: The role of defensins in inflammatory bowel disease. *J Gastroenterol Hepatol*. 2009 Feb 1;24(2):202–8.

96. Voss E, Wehkamp J, Wehkamp K, Stange EF, Schröder JM, Harder J. NOD2/CARD15 mediates induction of the antimicrobial peptide human beta-defensin-2. *J Biol Chem*. 2006;281(4):2005–11.

97. Wehkamp J, Harder J, Weichenthal M, Schwab M, Schäffeler E, Schlee M, et al. NOD2 (CARD15) mutations in Crohn's disease are associated with diminished mucosal α-defensin expression. *Gut*. 2004 Nov 1;53(11):1658 LP – 1664.

98. Xavier RJ, Podolsky DK. Unravelling the pathogenesis of inflammatory bowel disease. *Nature*. 2007;448(7152):427–34.

99. Corthay A. How do regulatory T cells work? *Scand J Immunol*. 2009 Oct;70(4):326–36.

100. Sallusto F, Lanzavecchia A. The instructive role of dendritic cells on T-cell responses. *Arthritis Res*. 2002/05/09. 2002;4 Suppl 3(Suppl 3):S127–32.

101. Mora JR, Bono MR, Manjunath N, Weninger W, Cavanagh LL, Rosemblatt M, et al. Selective imprinting of gut-homing T cells by Peyer's patch dendritic cells. *Nature*. 2003;424(6944):88–93.

102. Koizumi M, King N, Lobb R, Benjamin C, Podolsky DK. Expression of vascular adhesion molecules in inflammatory bowel disease. *Gastroenterology*. 1992;103(3):840–7.

103. Kayama H, Takeda K. Regulation of intestinal homeostasis by innate and adaptive immunity. *Int Immunol*. 2012 Sep 7;24(11):673–80.

104. Sakuraba A, Sato T, Kamada N, Kitazume M, Sugita A, Hibi T. Th1/Th17 immune response is induced by mesenteric lymph node dendritic cells in Crohn's disease. *Gastroenterology*. 2009;137(5):1736–45.

105. Raphael I, Nalawade S, Eagar TN, Forsthuber TG. T cell subsets and their signature cytokines in autoimmune and inflammatory diseases. *Cytokine*. 2015;74(1):5–17.

106. Romagnani S. Lymphokine production by human T Cells in disease states. *Annu Rev Immunol*. 1994 Apr 1;12(1):227–57.

107. Kmieć Z, Cyman M, Ślebioda TJ. Cells of the innate and adaptive immunity and their interactions in inflammatory bowel disease. *Adv Med Sci*. 2017;62(1):1–16.

108. Mizoguchi A, Mizoguchi E, Takedatsu H, Blumberg RS, Bhan AK. Chronic intestinal inflammatory condition generates IL-10-producing regulatory B Cell subset characterized by CD1d upregulation. *Immunity*. 2002;16(2):219–30.

109. Li Z, Li D, Tsun A, Li B. FOXP3+ regulatory T cells and their functional regulation. *Cell Mol Immunol*. 2015;12(5):558–65.

110. Kobayashi T, Okamoto S, Hisamatsu T, Kamada N, Chinen H, Saito R, et al. IL23 differentially regulates the Th1/Th17 balance in ulcerative colitis and Crohn's disease. *Gut*. 2008 Dec 1;57(12):1682 LP – 1689.

111. Sanchez-Munoz F, Dominguez-Lopez A, Yamamoto-Furusho J-K. Role of cytokines in inflammatory bowel disease. *World J Gastroenterol*. 2008 Jul 21;14(27):4280–8.

112. Podolsky DK. Inflammatory bowel disease. *N Engl J Med*. 2002 Aug 8;347(6):417–29.

113. Spiceland CM, Lodhia N. Endoscopy in inflammatory bowel disease: Role in diagnosis, management, and treatment. *World J Gastroenterol*. 2018 Sep 21;24(35):4014–20.

114. Fakhoury M, Coussa-Charley M, Al-Salami H, Prakash IK and S. Use of artificial cell microcapsule containing thalidomide for treating TNBS-induced Crohn's disease in mice. Vol. 11, Current Drug Delivery. 2014. p. 146–53.

115. Zhou G, Song Y, Yang W, Guo Y, Fang L, Chen Y, et al. ASCA, ANCA, ALCA and many more: Are they useful in the diagnosis of inflammatory bowel disease? *Dig Dis*. 2016;34(1–2):90–7.

116. Burger D, Travis S. Conventional medical management of inflammatory bowel disease. *Gastroenterology*. 2011;140(6):1827-1837.e2.

117. Fakhoury M, Negrulj R, Mooranian A, Al-Salami H. Inflammatory bowel disease: clinical aspects and treatments. *J Inflamm Res*. 2014 Jun 23;7:113–20.

118. Poggioli G, Laureti S, Campieri M, Pierangeli F, Gionchetti P, Ugolini F, et al. Infliximab in the treatment of Crohn's disease. *Ther Clin Risk Manag*. 2007 Jun;3(2):301–8.

119. Wang Q, Wen Z, Cao Q. Risk of tuberculosis during infliximab therapy for inflammatory bowel disease, rheumatoid arthritis, and spondyloarthropathy: A meta-analysis. *Exp Ther Med*. 2016/07/26. 2016 Sep;12(3):1693–704.

120. Peyrin-Biroulet L, Reinisch W, Colombel J-F, Mantzaris GJ, Kornbluth A, Diamond R, et al. Clinical disease activity, C-reactive protein normalisation and mucosal healing in Crohn's disease in the SONIC trial. *Gut*. 2014;63(1):88–95.

121. Chen P, Zhou G, Lin J, Li L, Zeng Z, Chen M, et al. Serum biomarkers for inflammatory bowel disease. *Front Med*. 2020;7:123.

122. Sharma V, Mandavdhare HS, Lamoria S, Singh H, Kumar A. Serial C-reactive protein measurements in patients treated for suspected abdominal tuberculosis. *Dig Liver Dis*. 2018;50(6):559–62.

123. Chambers RE, Stross P, Barry RE, T WJ. Serum amyloid A protein compared with C-reactive protein, alpha 1-antichymotrypsin and alpha 1-acid glycoprotein as a monitor of inflammatory bowel disease. *Eur J Clin Invest*. 1987 Oct 1;17(5):460–7.

124. Rump JA, Schölmerich J, Gross V, Roth M, Helfesrieder R, Rautmann A, et al. A new type of perinuclear anti-neutrophil cytoplasmic antibody (p-ANCA) in active ulcerative colitis but not in Crohn's disease. *Immunobiology*. 1990;181(4–5):406–13.

125. Beaven SW, Abreu MT. Biomarkers in inflammatory bowel disease. *Curr Opin Gastroenterol*. 2004;20(4):318–27.

126. O 2, Bruckner D, Gordon LK, Misra R, Wei B, Eggena ME, et al. Colonic bacteria express an ulcerative colitis pANCA-related protein epitope. *Infect Immun*. 2000;68(3):1542–8.

127. Prideaux L, Kamm MA, De Cruz P, van Langenberg DR, Ng SC, Dotan I. Inflammatory bowel disease serology in Asia and the West. *World J Gastroenterol WJG*. 2013;19(37):6207.

128. Norouzinia M, Chaleshi V, Alizadeh AHM, Zali MR. Biomarkers in inflammatory bowel diseases: insight into diagnosis, prognosis and treatment. *Gastroenterol Hepatol from Bed to Bench*. 2017;10(3):155.

129. Main J, McKenzie H, Yeaman GR, Kerr MA, Robson D, Pennington CR, et al. Antibody to Saccharomyces cerevisiae (bakers' yeast) in Crohn's disease. *BMJ Br Med J*. 1988;297(6656):1105.

130. Barker N, van Oudenaarden A, Clevers H. Identifying the stem cell of the intestinal crypt: Strategies and pitfalls. *Cell Stem Cell*. 2012;11(4):452–60.

131. Wallach TE, Bayrer JR. Intestinal organoids: New frontiers in the study of intestinal disease and physiology. *J Pediatr Gastroenterol Nutr*. 2017 Feb;64(2):180–5.

132. Okita K, Ichisaka T, Yamanaka S. Generation of germline-competent induced pluripotent stem cells. *Nature*. 2007;448(7151):313–7.

133. Min S, Kim S, Cho S-W. Gastrointestinal tract modeling using organoids engineered with cellular and microbiota niches. *Exp Mol Med*. 2020;52(2):227–37.

134. Umar S. Intestinal stem cells. *Curr Gastroenterol Rep*. 2010 Oct;12(5):340–8.

135. Onozato D, Akagawa T, Kida Y, Ogawa I, Hashita T, Iwao T, et al. Application of Human Induced Pluripotent Stem Cell-Derived Intestinal Organoids as a Model of Epithelial Damage and Fibrosis in Inflammatory Bowel Disease. *Biol Pharm Bull*. 2020;43(7):1088–95.

136. Workman MJ, Gleeson JP, Troisi EJ, Estrada HQ, Kerns SJ, Hinojosa CD, et al. Enhanced Utilization of Induced Pluripotent Stem Cell–Derived Human Intestinal Organoids Using Microengineered Chips. *Cell Mol Gastroenterol Hepatol*. 2018;5(4):669-677.e2.

137. Jonsson MKB, van Veen TAB, Synnergren J, Becker B. Towards creating the perfect in vitro cell model. *Stem Cells Int*. 2016/02/03. 2016;2016:3459730.

138. Dahlgren D, Lennernäs H. Intestinal permeability and drug absorption: Predictive

experimental, computational and in vivo approaches. *Pharmaceutics*. 2019 Aug 13;11(8):411.

139. Awortwe C, Fasinu PS, Rosenkranz B. Application of Caco-2 cell line in herb-drug interaction studies: Current approaches and challenges. *J Pharm Pharm Sci*. 2014;17(1):1–19.

140. Sun D, Lennernas H, Welage LS, Barnett JL, Landowski CP, Foster D, et al. Comparison of human duodenum and Caco-2 gene expression profiles for 12,000 gene sequences tags and correlation with permeability of 26 drugs. *Pharm Res*. 2002;19(10):1400–16.

141. Sun H, Chow ECY, Liu S, Du Y, Pang KS. The Caco-2 cell monolayer: Usefulness and Limitations. *Expert Opin Drug Metab Toxicol*. 2008 Apr 1;4(4):395–411.

142. Rios AC, Clevers H. Imaging organoids: A bright future ahead. *Nat Methods*. 2018;15(1):24–6.

143. Zachos NC, Kovbasnjuk O, Foulke-Abel J, In J, Blutt SE, de Jonge HR, et al. Human enteroids/colonoids and intestinal organoids functionally recapitulate normal intestinal physiology and pathophysiology. *J Biol Chem*. 2015/12/16. 2016 Feb 19;291(8):3759–66.

144. Asha S, Vidyavathi M. Role of human liver microsomes in in vitro metabolism of drugs-A Review. *Appl Biochem Biotechnol*. 2010;160(6):1699–722.

145. Miyazawa M, Nakanishi K. Biotransformation of (−)-menthone by human liver microsomes. *Biosci Biotechnol Biochem*. 2006 May 23;70(5):1259–61.

146. Finn RD, McLaughlin LA, Ronseaux S, Rosewell I, Houston JB, Henderson CJ, et al. Defining the in vivo role for cytochrome b5 in cytochrome P450 function through the conditional hepatic deletion of microsomal cytochrome b5. *J Biol Chem*. 2008/09/19. 2008 Nov 14;283(46):31385–93.

147. Araya Z, Wikvall K. 6-alpha-hydroxylation of taurochenodeoxycholic acid and lithocholic acid by CYP3A4 in human liver microsomes. *Biochim Biophys Acta*. 1999;1438(1):47–54.

148. Brandon EFA, Raap CD, Meijerman I, Beijnen JH, Schellens JHM. An update on in vitro test methods in human hepatic drug biotransformation research: Pros and cons. *Toxicol Appl Pharmacol*. 2003;189(3):233–46.

149. Wong Z-YZ and YN. Enzyme kinetics for clinically relevant CYP inhibition. Vol. 6, Current Drug Metabolism. 2005. p. 241–57.

150. Pelkonen O, Turpeinen M. In vitro–in vivo extrapolation of hepatic clearance: Biological

tools, scaling factors, model assumptions and correct concentrations. *Xenobiotica*. 2007 Nov 1;37(10–11):1066–89.

151. Mendel CM, Mendel DB. "Non-specific" binding. The problem, and a solution. *Biochem J*. 1985 May 15;228(1):269–72.

152. Giuliano C, Jairaj M, Zafiu CM, Laufer R. Direct determination of unbound intrinsic drug clearance in the microsomal stability assay. *Drug Metab Dispos*. 2005 Sep 1;33(9):1319 LP – 1324.

153. Bowman CM, Benet LZ. An examination of protein binding and protein-facilitated uptake relating to in vitro-in vivo extrapolation. *Eur J Pharm Sci*. 2018/08/08. 2018 Oct 15;123:502–14.

154. Gonzalez D, Schmidt S, Derendorf H. Importance of relating efficacy measures to unbound drug concentrations for anti-infective agents. *Clin Microbiol Rev*. 2013 Apr;26(2):274–88.

155. Roberts JA, Pea F, Lipman J. The Clinical Relevance of Plasma Protein Binding Changes. *Clin Pharmacokinet*. 2013;52(1):1–8.

156. Lin JH, Cocchetto DM, Duggan DE. Protein Binding as a Primary Determinant of the Clinical Pharmacokinetic Properties of Non-Steroidal Anti-Inflammatory Drugs. *Clin Pharmacokinet*. 1987;12(6):402–32.

157. Sethi PK, Muralidhara S, Bruckner J V, White CA. Measurement of plasma protein and lipoprotein binding of pyrethroids. *J Pharmacol Toxicol Methods*. 2014;70(1):106–11.

158. Borchardt RT. Hidalgo, I. J., Raub, T. J., and Borchardt, R. T.: Characterization of the Human Colon Carcinoma Cell Line (Caco-2) as a Model System for Intestinal Epithelial Permeability. *AAPS J*. 2011;13(3):323–7.

159. Lathrop JT, Jeffery DA, Shea YR, Scholl PF, Chan MM. US Food and Drug Administration Perspectives on Clinical Mass Spectrometry. *Clin Chem*. 2016 Jan 1;62(1):41–7.

160. Obach RS, Reed-Hagen AE. Measurement of michaelis constants for cytochrome P450-mediated biotransformation reactions using a substrate depletion approach. *Drug Metab Dispos*. 2002 Jul 1;30(7):831 LP – 837.

161. Lin C, Alcorn ESK and J. The comparison of rat and human intestinal and hepatic glucuronidation of enterolactone derived from flaxseed lignans. Vol. 3, The Natural Products Journal. 2013. p. 159–71.

162. Hubatsch I, Ragnarsson EGE, Artursson P. Determination of drug permeability and prediction of drug absorption in Caco-2 monolayers. *Nat Protoc*. 2007;2(9):2111–9.

163. Haines-Saah RJ, Fischer B. Youth Cannabis use and Legalization in Canada - Reconsidering the Fears, Myths and Facts Three Years In. *J Can Acad Child Adolesc Psychiatry*. 2021/08/01. 2021 Aug;30(3):191–6.

164. Rowland M. Protein Binding and Drug Clearance. *Clin Pharmacokinet*. 1984;9(1):10–7.

165. de Boer T, Meijering H. Equilibrium Dialysis, Ultracentrifugation, and Ultrafiltration in LC-MS Bioanalysis. Sample Preparation in LC-MS Bioanalysis. 2019. p. 45–51. (Wiley Online Books).

166. Bohnert T, Gan L-S. Plasma protein binding: From discovery to development. *J Pharm Sci*. 2013;102(9):2953–94.

167. Vuong S. Development of Liquid Chromatography-Tandem Mass Spectrometry Methods of Cannabinoids for Pediatric Patient Samples. University of Saskatchewan; 2020.

168. Lemaire M, Urien S, Albengres E, Riant P, Zini R, Tillement J-P. Lipoprotein binding of drugs. Drug-protein binding. Praeger Publishers, NY, USA; 1986. p. 93–108.

169. KLAUSNER HA, WILCOX HG, DINGELL J V. The use of zonal ultracentrifugation in the investigation of the binding of delta 9-Tetrahydrocannabinol by plasma lipoproteins. *Drug Metab Dispos*. 1975 Jul 1;3(4):314 LP – 319.

170. Jones HM, Houston JB. Substrate depletion approach for determining in vitro metabolic clearance: time dependencies in hepatocytes and microsomal incubations. *Drug Metab Dispos*. 2004 Sep 1;32(9):973 LP – 982.

171. Obach RS. Prediction of human clearance of twenty-nine drugs from hepatic microsomal intrinsic clearance data: An examination of in vitro half-life approach and nonspecific binding to microsomes. *Drug Metab Dispos*. 1999 Nov 1;27(11):1350 LP – 1359.

172. ElSohly MA, DeWit H, Wachtel SR, Feng S, Murphy TP. Δ9-Tetrahydrocannabivarin as a marker for the ingestion of Marijuana versus Marinol®: Results of a clinical study. *J Anal Toxicol*. 2001 Oct 1;25(7):565–71.

173. Taylor S, Harker A. Modification of the ultrafiltration technique to overcome solubility and non-specific binding challenges associated with the measurement of plasma protein binding of corticosteroids. *J Pharm Biomed Anal*. 2006;41(1):299–303.

174. Brian Houston J. Utility of in vitro drug metabolism data in predicting in vivo metabolic clearance. *Biochem Pharmacol*. 1994;47(9):1469–79.
175. Patilea-Vrana GI, Unadkat JD. Quantifying hepatic enzyme kinetics of (-)-Δ9-Tetrahydrocannabinol (THC) and its psychoactive metabolite, 11-OH-THC, through in vitro modeling. *Drug Metab Dispos*. 2019 Jul 1;47(7):743 LP – 752.

176. Beers JL, Fu D, Jackson KD. Cytochrome P450–Catalyzed metabolism of Cannabidiol to the active metabolite 7-hydroxy-CBD. *Drug Metab Dispos*. 2021 Oct 1;49(10):882 LP – 891.

177. Zientek MA, Goosen TC, Tseng E, Lin J, Bauman JN, Walker GS, et al. In vitro kinetic characterization of Axitinib metabolism. *Drug Metab Dispos*. 2016 Jan 1;44(1):102 LP – 114.

178. Strober W. Trypan Blue Exclusion Test of Cell Viability. *Curr Protoc Immunol*. 2015 Nov 1;111(1):A3.B.1-A3.B.3.

179. Gustafsson SB, Lindgren T, Jonsson M, Jacobsson SOP. Cannabinoid receptor-independent cytotoxic effects of cannabinoids in human colorectal carcinoma cells: Synergism with 5-fluorouracil. *Cancer Chemother Pharmacol*. 2009;63(4):691–701.

180. Guzmán M. Cannabinoids: potential anticancer agents. *Nat Rev Cancer*. 2003;3(10):745–55.

181. Rieder SA, Chauhan A, Singh U, Nagarkatti M, Nagarkatti P. Cannabinoid-induced apoptosis in immune cells as a pathway to immunosuppression. *Immunobiology*. 2010;215(8):598–605.

182. Nallathambi R, Mazuz M, Ion A, Selvaraj G, Weininger S, Fridlender M, et al. Anti-inflammatory activity in colon models is derived from Δ9-Tetrahydrocannabinolic acid that interacts with additional compounds in Cannabis extracts. *Cannabis Cannabinoid Res*. 2017 Jul 1;2(1):167–82.

183. Chen X, Unadkat JD, Mao Q. Tetrahydrocannabinol and its major metabolites are not (or are poor) substrates or inhibitors of human P-glycoprotein [ATP-binding cassette (ABC) B1] and breast cancer resistance protein (ABCG2). *Drug Metab Dispos*. 2021 Oct 1;49(10):910 LP – 918.

184. Sambuy Y, De Angelis I, Ranaldi G, Scarino ML, Stammati A, Zucco F. The Caco-2 cell line as a model of the intestinal barrier: Influence of cell and culture-related factors on Caco-2 cell functional characteristics. *Cell Biol Toxicol*. 2005;21(1):1–26.

185. Zihni C, Mills C, Matter K, Balda MS. Tight junctions: From simple barriers to

multifunctional molecular gates. *Nat Rev Mol Cell Biol*. 2016;17(9):564–80.

186. Srinivasan B, Kolli AR, Esch MB, Abaci HE, Shuler ML, Hickman JJ. TEER measurement techniques for in vitro barrier model systems. *J Lab Autom*. 2015/01/13. 2015 Apr;20(2):107–26.

187. Thomas T, Gopikrishna V, Kandaswamy D. Comparative evaluation of maintenance of cell viability of an experimental transport media "coconut water" with Hank's balanced salt solution and milk, for transportation of an avulsed tooth: An in vitro cell culture study. *J Conserv Dent*. 2008;11:22–9.

188. Tetko I V, Tanchuk VY, Villa AEP. Prediction of n-Octanol/Water Partition Coefficients from PHYSPROP Database Using Artificial Neural Networks and E-State Indices. *J Chem Inf Comput Sci*. 2001 Sep 1;41(5):1407–21.

189. Hidalgo IJ, Li J. Carrier-mediated transport and efflux mechanisms in Caco-2 cells. *Adv Drug Deliv Rev*. 1996;22(1):53–66.

190. El-Kattan A. Oral Absorption, intestinal metabolism and human oral bioavailability. In: Paxton MVE-J, editor. Rijeka: IntechOpen; 2012. p. Ch. 1.

191. Tetko I V, Tanchuk VY, Kasheva TN, Villa AEP. Estimation of Aqueous Solubility of Chemical Compounds Using E-State Indices. *J Chem Inf Comput Sci*. 2001 Nov 1;41(6):1488–93.

192. Blume HH, Schug BS. The biopharmaceutics classification system (BCS): Class III drugs — Better candidates for BA/BE waiver? *Eur J Pharm Sci*. 1999;9(2):117–21.

193. Martin YC. A practitioner's perspective of the role of quantitative structure-Activity analysis in medicinal chemistry. *J Med Chem*. 1981 Mar 1;24(3):229–37.

194. Artursson P, Palm K, Luthman K. Caco-2 monolayers in experimental and theoretical predictions of drug transport. *Adv Drug Deliv Rev*. 2001;46 1-3:27–43.

195. Palmgrén JJ, Mönkkönen J, Korjamo T, Hassinen A, Auriola S. Drug adsorption to plastic containers and retention of drugs in cultured cells under in vitro conditions. *Eur J Pharm Biopharm*. 2006;64 3:369–78.

196. Fukazawa T, Yamazaki Y, Miyamoto Y. Reduction of non-specific adsorption of drugs to plastic containers used in bioassays or analyses. *J Pharmacol Toxicol Methods*. 2010;61(3):329–33.

197. Bertani B, Ruiz N. Function and biogenesis of lipopolysaccharides. *EcoSal Plus*. 2018;8(1).

198. Beurel E, Jope RS. Lipopolysaccharide-induced interleukin-6 production is controlled by glycogen synthase kinase-3 and STAT3 in the brain. *J Neuroinflammation*. 2009;6(1):9.

199. Hwang J-S, Kwon M-Y, Kim K-H, Lee Y, Lyoo IK, Kim JE, et al. Lipopolysaccharide (LPS)-stimulated iNOS induction is increased by glucosamine under normal glucose conditions but is inhibited by glucosamine under high glucose conditions in macrophage cells. *J Biol Chem*. 2017;292(5):1724–36.

200. Rincon M. Interleukin-6: from an inflammatory marker to a target for inflammatory diseases. *Trends Immunol*. 2012;33(11):571–7.

201. Rumbo M, Courjault-Gautier F, Sierro F, Sirard J, Felley-Bosco E. Polarized distribution of inducible nitric oxide synthase regulates activity in intestinal epithelial cells. *FEBS J*. 2005;272(2):444–53.

202. McCoy KL. Interaction between cannabinoid system and toll-like receptors controls inflammation. *Mediators Inflamm*. 2016;2016.

203. Kamdar K, Nguyen V, DePaolo RW. Toll-like receptor signaling and regulation of intestinal immunity. *Virulence*. 2013;4(3):207–12.

204. Zhang Y-G, Wu S, Xia Y, Sun J. Salmonella-infected crypt-derived intestinal organoid culture system for host–bacterial interactions. *Physiol Rep*. 2014 Sep 1;2(9):e12147.

205. Atreya R, Neurath MF. Involvement of IL-6 in the pathogenesis of inflammatory bowel disease and colon cancer. *Clin Rev Allergy Immunol*. 2005;28(3):187–95.

206. Vermeire S, Van Assche G, Rutgeerts P. C-reactive protein as a marker for inflammatory bowel disease. *Inflamm Bowel Dis*. 2004;10(5):661–5.

207. Li VSW. Modelling intestinal inflammation and infection using 'mini-gut' organoids. *Nat Rev Gastroenterol Hepatol*. 2021;18(2):89–90.

208. Fengming Y, Jianbing W. Biomarkers of inflammatory bowel disease. *Dis Markers*. 2014;2014.

209. Hayashi A, Sato T, Kamada N, Mikami Y, Matsuoka K, Hisamatsu T, et al. A single strain of Clostridium butyricum induces intestinal IL-10-producing macrophages to suppress acute experimental colitis in mice. *Cell Host Microbe*. 2013;13(6):711–22.

210. Biagioli M, Carino A, Cipriani S, Francisci D, Marchianò S, Scarpelli P, et al. The bile acid receptor GPBAR1 regulates the M1/M2 phenotype of intestinal macrophages and

activation of GPBAR1 rescues mice from murine colitis. *J Immunol*. 2017;199(2):718–33.

211. Angus HCK, Butt AG, Schultz M, Kemp RA. Intestinal organoids as a tool for inflammatory bowel disease research. *Front Med*. 2020;6:334.

212. Jarry A, Bossard C, Bou-Hanna C, Masson D, Espaze E, Denis MG, et al. Mucosal IL-10 and TGF-β play crucial roles in preventing LPS-driven, IFN-γ–mediated epithelial damage in human colon explants. *J Clin Invest*. 2008;118(3):1132–42.

213. Kwon O-K, Lee M-Y, Yuk J-E, Oh S-R, Chin Y-W, Lee H-K, et al. Anti-inflammatory effects of methanol extracts of the root of Lilium lancifolium on LPS-stimulated Raw264. 7 cells. *J Ethnopharmacol*. 2010;130(1):28–34.

214. Cho E, Shin J-S, Noh Y-S, Cho Y-W, Hong S-J, Park J-H, et al. Anti-inflammatory effects of methanol extract of *Patrinia scabiosaefolia* in mice with ulcerative colitis. *J Ethnopharmacol*. 2011;136(3):428–35.

215. Sanchez-Dominguez CN, Gallardo-Blanco HL, Salinas-Santander MA, Ortiz-Lopez R. Uridine 5'-diphospho-glucronosyltrasferase: Its role in pharmacogenomics and human disease. *Exp Ther Med*. 2018;16(1):3–11.

216. Williams JA, Hurst SI, Bauman J, Jones BC, Hyland R, Gibbs JP, et al. Reaction phenotyping in drug discovery: moving forward with confidence? *Curr Drug Metab*. 2003;4(6):527–34.

217. Kumar AR, Patilea-Vrana GI, Anoshchenko O, Unadkat JD. Characterizing and quantifying extrahepatic metabolism of (−)-Δ9-Tetrahydrocannabinol (THC) and its psychoactive metabolite,(±)-11-hydroxy-Δ9-THC (11-OH-THC). *Drug Metab Dispos*. 2022;50(6):734–40.

218. Volpe DA. Application of method suitability for drug permeability classification. *AAPS J*. 2010;12(4):670–8.

219. Stuyt E. The problem with the current high potency THC marijuana from the perspective of an addiction psychiatrist. *Mo Med*. 2018;115(6):482.